



International Energy Agency

**Energy Conservation in Buildings
and Community Systems Programme**

Annex 20 Air Flow Patterns within Buildings

**Room Air and
Contaminant Flow,
Evaluation of
Computational Methods**

Subtask-1 Summary Report

Ann 20 1993:1

Room Air and Contaminant Flow, Evaluation of Computational Methods

Subtask-1 Summary Report

Editor:
A.D. Lemaire

Contributors:
Q. Chen
M. Ewert
J. Heikkinen
C. Inard
A. Moser
P.V. Nielsen
G. Whittle

December 1993

This report documents results of cooperative work performed under the IEA Programme for Energy Conservation in Buildings and Community Systems, Annex 20: Air Flow Patterns within Buildings.

Preface

International Energy Agency

The International Energy Agency (IEA) was established in 1974 within the framework of the Organisation for Economic Co-operation and Development (OECD) to implement an International Energy Programme. A basic aim of the IEA is to foster co-operation among the twenty-one IEA Participating Countries to increase energy security through energy conservation, development of alternative energy sources and energy research development and demonstration (RD&D). This is achieved in part through a programme of collaborative RD&D consisting of forty-two Implementing Agreements, containing a total of over eighty separate energy RD&D projects. This publication forms one element of this programme.

Energy Conservation in Buildings and Community Systems

The IEA sponsors research and development in a number of areas related to energy. In one of these areas, energy conservation in buildings, the IEA is sponsoring various exercises to predict more accurately the energy use of buildings, including comparison of existing computer programs, building monitoring, comparison of calculation methods, as well as air quality and studies of occupancy. Seventeen countries have elected to participate in this area and have designated contracting parties to the Implementing Agreement covering collaborative research in this area. The designation by governments of a number of private organisations, as well as universities and government laboratories, as contracting parties, has provided a broader range of expertise to tackle the projects in the different technology areas than would have been the case if participation was restricted to governments. The importance of associating industry with government sponsored energy research and development is recognized in the IEA, and every effort is made to encourage this trend.

The Executive Committee

Overall control of the programme is maintained by an Executive Committee, which not only monitors existing projects but identifies new areas where collaborative effort may be beneficial. The Executive Committee ensures that all projects fit into a pre-determined strategy, without unnecessary overlap or duplication but with effective liaison and communication. The Executive Committee has initiated the following projects to date (completed projects are identified by *).

- Annex 1: Load energy determination of buildings (*)
- Annex 2: Ekistics & advanced community energy systems (*)
- Annex 3: Energy conservation in residential buildings (*)
- Annex 4: Glasgow commercial building monitoring (*)
- Annex 5: Air infiltration and ventilation centre
- Annex 6: Energy systems and design of communities (*)
- Annex 7: Local government energy planning (*)
- Annex 8: Inhabitants behaviour with regard to ventilation (*)
- Annex 9: Minimum ventilation rates (*)
- Annex 10: Building HVAC system simulation (*)
- Annex 11: Energy auditing (*)
- Annex 12: Windows and fenestration (*)
- Annex 13: Energy management in hospitals (*)
- Annex 14: Condensation and energy (*)
- Annex 15: Energy efficiency of schools (*)
- Annex 16: BEMS 1 - User interfaces and system integration
- Annex 17: BEMS 2 - Evaluation and emulation techniques
- Annex 18: Demand controlled ventilating systems
- Annex 19: Low slope roofs systems
- Annex 20: Air flow patterns within buildings
- Annex 21: Calculation of energy & environmental performance of buildings
- Annex 22: Energy efficient communities
- Annex 23: Multizone air flow modelling
- Annex 24: Heat, air & moisture transport in new and retrofitted insulated envelope parts
- Annex 25: Real time simulation of HVAC systems and fault detection

Annex 20: Air Flow Patterns within Buildings

A task-sharing Annex to the International Energy Agency's Implementing Agreement for a Program of Research and Development on Energy Conservation in Buildings and Community Systems.

Objectives: To evaluate the performance of single- and multi-zone air and contaminant flow simulation techniques and to establish their viability as design tools.

Start: May 1, 1988

Duration: 3 1/2 years

Completion: November 1, 1991

Subtasks: The work is organized in two parallel subtasks

1. Room air and contaminant flow
2. Multi-zone air and contaminant flow and measurement techniques

Participating Countries: Belgium, Canada, Denmark, Finland, France, Germany, Italy, The Netherlands, Norway, Sweden, Switzerland, United Kingdom, and the United States of America.

Operating Agent: The Swiss Federal Office of Energy (BEW). Contractor: The Energy Systems Laboratory of the Swiss Federal Institute of Technology (ETH), Zurich, Switzerland. Executive OA: Dr. Alfred Moser.

Subtask leader 1 (single room): Ir. Tony Lemaire, TNO Building and Construction Research, P.O. Box 29, NL-2600 AA Delft, The Netherlands.

Subtask leader (multi-zone): Dr. Claude-Alain Roulet, LESO-PB, EPFL - Ecublens, CH-1015 Lausanne, Switzerland.

Specific Objectives of Subtask 1

- . To evaluate the performance of 3-dimensional complex and simplified air flow models in predicting flow patterns, energy transport, and indoor air quality
- . to show how to improve air flow models
- . to evaluate applicability as design tools
- . to produce guidelines for selection and use of models
- . to acquire experimental data for evaluation of models.

Specific Objectives of Subtask 2

- . to develop new algorithms for specific problems, as flow through large openings, inhabitant behaviour, air-flow-driven contaminants, or multi-room ventilation efficiency
- . to develop new, or improve existing measurement techniques
- . to collect and test input data sets of experimental data (reference cases for code validation)

First edition, September 1992

Second edition, December 1993 (final version)

ISBN 90-6743-298-9

Cover: Atelier P.G. Ulmer, CH-8200 Schaffhausen

FOREWORD

This report is a summary of the work performed in subtask 1 of IEA Annex 20: 'Air Flow Patterns within Buildings'. It consolidates the information from the technical reports and papers produced within the subtask in one single volume. Its main purpose is to serve as an entry to those documents. The report is an official 'Annex Product Report' and focuses on the evaluation of computational methods.

To a great extent the report consists of extracts from Annex-20 subtask 1 technical reports and papers, in some cases compiled and complemented by the editor. In particular, chapter 3 on the evaluation of the computational methods, is based on the work done by Whittle. Some parts have been written by selected participants. The report was reviewed by representatives of each participating country focusing on their specific contributions. A general review on the technical contents was performed by Heikkinen and a review on the english language by Whittle.

Main contributors to this report are (in alphabetical order):

- . Q. Chen, who in section 2.3.3 described his "database model"
- . M. Ewert, who in section 2.1.3 described the Laser Doppler Anemometry
- . J. Heikkinen, who reviewed the report on technical contents
- . C. Inard, who described "zonal models" in section 2.3.3
- . A. Moser, who contributed to almost the whole part of chapter 1 "Introduction" and chapter 4 "Conclusions and recommendations" by means of his paper "The message of Annex 20"
- . P.V. Nielsen, who contributed to section 2.3.1. on "design models based on self-similar jet flow"
- . G. Whittle, who contributed to almost the whole part of chapter 3 by means of his report on "Evaluation of cases B, D, E, F and 2D".

Coordination, editing and final responsibility was in hands of A.D. Lemaire, subtask 1 leader.

Acknowledgements

The work reported here is based on measurements and computations carried out by many researchers. Appendix A lists the main contributors and their organisations. The operating agent for Annex 20 is Dr. Alfred Moser, ETH Zurich, Switzerland.

Financial support for the production of this report was provided by NOVEM, The Netherlands.

LIST OF SYMBOLS

The most frequently used symbols are listed. Multiple definitions of some symbols occur. Their meaning follows from the context.

a_o	effective supply area of diffuser	m^2
Ar	Archimedes number defined by $g \theta h / T u_o^2$	-
c_p	fluid specific heat at constant pressure	$J kg^{-1} K^{-1}$
C	concentration of contaminant	$m^3 m^{-3}$
C_1, C_2, C_3	empirical constants in source term for ϵ equation	-
C_μ	constant in μ_t expression	-
D	coefficient of molecular diffusion	$m^2 s^{-1}$
g	gravitational acceleration scalar	$m s^{-2}$
g_i	gravitational acceleration component in x_i direction	$m s^{-2}$
h	enthalpy	$J kg^{-1}$
h	height of inlet slot	m
H	height of (test) room	m
k	kinetic energy of turbulence	$m^2 s^{-2}$
l_{th}	throw of jet according to equation 2.5	m
L	length of (test) room	m
p	pressure	$N m^{-2}$
t	time	s
T	temperature level	K
u_m	maximum velocity in occupied zone	$m s^{-1}$
u_o	supply velocity of diffuser or inlet slot	$m s^{-1}$
u_r	velocity in radial direction of supply jet	$m s^{-1}$
u_x	maximum velocity in wall jet at distance x from opening	$m s^{-1}$
U_m	mean air speed	$m s^{-1}$
U_t	turbulent velocity	$m s^{-1}$
U^*	modified air speed defined by $(U_m^2 + U_t^2)^{0.5}$	$m s^{-1}$
V_i	velocity component in x_i -direction	$m s^{-1}$
x_i	cartesian coordinate direction	m
x_o	distance to virtual origin of wall jet	m
x_o	penetration depth of non-isothermal jet according to figure 2.6	m
X	length-coordinate in test room defined in figure 2.1	m
Y	height-coordinate in test room defined in figure 2.1	m
Z	width-coordinate in test room defined in figure 2.1	m

Greek symbols

β	fluid coefficient of thermal expansion	K^{-1}
ϵ	dissipation rate of kinetic energy	$m^2 s^{-3}$
ϕ	field variable in transport equation 2.1	-
λ	fluid thermal conductivity	$W m^{-1} K^{-1}$
μ	fluid molecular dynamic viscosity	$kg m^{-1} s^{-1}$
μ_t	turbulent (eddy) viscosity	$kg m^{-1} s^{-1}$
ρ	fluid density	$kg m^{-3}$
σ_\dagger	turbulent Prandtl number for ϕ	-
θ	angle in radial direction of supply jet	rad
θ	temperature difference between exhaust and inlet	K

CONTENTS

	Page
1. INTRODUCTION	1
1.1 The reasons for IEA Annex 20	1
1.2 Objectives of IEA Annex 20	2
1.2.1 <i>General objectives</i>	2
1.2.2 <i>Objectives of subtask 1</i>	2
1.3 Approach and project organization	3
1.3.1 <i>General approach and organization</i>	3
1.3.2 <i>Approach of subtask 1</i>	4
1.4 Work plan and survey of performed work	4
2. AIR FLOW SIMULATION AND MEASUREMENT TECHNIQUES	7
2.1 Experimental equipment	7
2.1.1 <i>Configuration of the basic test room</i>	7
2.1.2 <i>Scale model experiments</i>	9
2.1.3 <i>Measuring equipment</i>	10
2.2 Computational fluid dynamics models	12
2.2.1 <i>Air flow computer codes</i>	12
2.2.2 <i>Mathematical and numerical models</i>	12
2.2.3 <i>Modelling of boundary conditions</i>	16
2.3 Simplified air flow models	19
2.3.1 <i>Design models based on self-similar jet flow</i>	19
2.3.2 <i>Zonal models</i>	21
2.3.3 <i>Database model</i>	23
3. EVALUATION OF PERFORMANCE OF MODELS IN PREDICTION OF FLOW PARAMETERS	25
3.1 Introduction	25
3.2 Specification of test cases	25
3.2.1 <i>Two-dimensional test cases</i>	26
3.2.2 <i>Three-dimensional test cases</i>	27
3.3 Results and discussion	30
3.3.1 <i>Measurements, simulations and data analysis</i>	30
3.3.2 <i>Two-dimensional test cases</i>	34
3.3.3 <i>Test case B (forced convection, isothermal)</i>	40
3.3.4 <i>Test case E (mixed convection, summer cooling)</i>	50
3.3.5 <i>Test case D (free convection with radiator)</i>	57
3.3.6 <i>Test case F (forced convection with contaminant)</i>	62
3.3.7 <i>Test case G (displacement ventilation)</i>	65
3.4 Application of existing computational fluid dynamics models	68
3.4.1 <i>Flow asymmetries</i>	68
3.4.2 <i>Representation of boundary conditions at the supply opening</i>	68
3.4.3 <i>Wall functions</i>	70
3.4.4 <i>Turbulence models</i>	70
3.4.5 <i>Difference scheme</i>	71
3.4.6 <i>Grid refinement</i>	71
3.4.7 <i>Computer resources</i>	72

	Page
4. CONCLUSIONS AND RECOMMENDATIONS FOR FUTURE WORK	74
4.1 Application of simulation models as design tools	74
4.2 Performance of models in prediction of flow parameters	74
4.3 Technical problems of CFD models	75
4.4 General conclusions	76
4.5 Recommendations for future work	77

REFERENCES	78
-------------------	-----------

APPENDICES:

- A. List of contributing investigators, organisations and countries
- B. Names and addresses of participating organisations

1. INTRODUCTION

1.1 The reasons for IEA Annex 20.

"It should become possible to predict air flow patterns within buildings by numerical simulation!"

This was concluded by a small group of ventilation experts who met in September 1987 in Ittingen, Switzerland. New commercial codes appeared on the market, and research codes were developed at universities and research labs. The workshop participants expected that some expensive laboratory tests could be avoided if air flows in rooms, infiltration in rooms, and exchange with the outside atmosphere could be predicted numerically with a certain degree of confidence. New tools would enable the designer to evaluate different variations of a ventilation concept on a computer. Contamination transport within buildings or rooms could be modelled and the effectiveness of ventilation assessed in a systematic way.

The idea to start a new "IEA Energy Conservation in Buildings and Community Systems" Annex was born: Many promising simulation models existed and specialists had started to apply them to real buildings [1]. Experienced engineers voiced scepticism, while their younger colleagues looked for the "best" computer programs. It was the right time to survey and evaluate existing methods on an international basis.

Annex 20, "Air Flow Patterns within Buildings", provided the framework to bring the experts together, to compile information and to undertake validation exercises. For single- and multi-zone air flow, experimental datasets were required as benchmark cases. Therefore experiments had to be specified for the project. Soon the scope of the Annex was extended to include the evaluation and documentation of advanced measurement techniques for multi-zone air flow and the development of new algorithms to model special flow mechanisms.

The experienced user of air flow codes will appreciate the benefits of numerical simulation:

- Information is available on all points of the flow field
- Any desired variable of the physical model can be output and plotted: Air velocity and its fluctuations (turbulence), temperature, concentrations of contaminants and humidity, "local age" (an indicator of the freshness of the air), and comfort parameters (thermal comfort and "risk of draught"). Also heat transfer to and from window and radiator surfaces.
- Sensitivity tests and parameter variations are easy to do, and computed trends should be even more reliable than absolute values of variables.

The objective of the Annex is expressed in one short sentence, but its relevance was immediately recognized by all countries of the IEA Implementing Agreement. Thirteen nations decided to participate in Annex 20.

One reason for this wide participation certainly was the strong impact the work has on energy conservation. The trend to air-tight buildings with improved thermal insulation calls for controlled air exchange. The energy required to exchange the air grows with the temperature difference between fresh outside air and supply air to the rooms. In mechanical systems, a substantial portion of the energy is used to move the air through the ducting and the rest for cooling or heating and other conditioning. The former is a function of the air change rate, the latter of temperatures and heat recovery, if installed.

This energy consumption is of growing significance in relation to the heat loss through the envelope of well insulated buildings. The designer of these new-generation buildings wants to know how air flows before the house is built.

1.2 Objectives of IEA Annex 20

1.2.1 General objectives

Formal participation in this task-sharing Annex is based on the legal text [2] that defines project objectives, tasks, and responsibilities. The document states:

"Research attention has recently been given to the patterns of air circulation within rooms and through buildings, to ensure that fresh air supply and pollutant removal requirements are effectively obtained without undue use of energy resources."

"Recent developments in measurement techniques and computer hardware open new possibilities to study this phenomenon, while several advanced computer based simulation methods have been produced in an attempt to describe this flow".

"The objectives of this task are: to evaluate the performance of single- and multi-zone air and contaminant flow simulation techniques and to establish their viability as design tools. The task is divided into two subtasks:

- (a) Subtask 1 - Room air and contaminant flow;
- (b) Subtask 2 - Multi-zone air and contaminant flow, including related measurement techniques."

1.2.2 Objectives of subtask 1

The objectives of subtask 1 were:

- to evaluate the performance of three-dimensional complex and simplified air flow models in predicting air flow patterns, energy transport, and indoor air quality,
- to show how to improve air flow models,
- to evaluate their applicability as design tools,
- to produce guidelines for selection and use of models,
- to acquire experimental data for evaluation of models.

The following products were expected:

- A report on the evaluation of the performance of 3-dimensional, 2-dimensional and simplified air flow models in predicting air flow patterns, energy transport, and indoor air quality and of their viability as design tools.
- Guidelines on the use of the models: evaluation of the range of applicability of the different codes.
- Experimental data sets for future evaluation of simulation models. Data will be made available by the AIVC in a data base in a standardized format.

1.3 Approach and project organization

1.3.1 General approach and organization

The organization and structure of the project was kept as simple as possible. The following agreements were made:

- (1) Two parallel subtasks for the full project term, because the methods are different for single- and multi-zone air movement.
- (2) Each subtask has a subtask leader responsible for the scientific product of the task.
- (3) The technical work within each subtask is structured in "Research Items" (RI.), each with a "RI-Description (RID)". The RID states objectives, methods, completion date, and the principle investigator (PI) and is looked upon as a formal commitment of the PI to perform the described work. In principle, results of "Research Items" are written in reports with the same title as the RI. The reports are work reports intended for Annex 20 members or publications accessible to 'the scientific world'.
- (4) The project has a preparation phase, main performance, and reporting phase. Observer status is restricted to the preparation phase.
- (5) Expert meetings are held twice a year (8 total).

Wide publicity of the work was sought by the publication of a newsletter (Flow Flash) and by inviting interested persons of participating countries, - in addition to the active experts, - to the Annex meetings. The experts were encouraged to publish their own work during the course of the project as Annex reports, in journals, or at conferences. Reports and publications were advertised in a "list of Annex Documentation", that was updated periodically. The list holds over 100 titles and abstracts and records of final publications are also fed into AIRBASE (AIVC-database). Table 1.1 lists the participating countries along with their subtask commitments and cities where they organized meetings.

TABLE 1.1 Participating countries and meeting sites.

Country	Commitment:		Expert Meeting:	
	1	Subtask 2	City and date	
Belgium		full	Lommel	Nov. 89
Canada	full	c	Ottawa	Sep. 91
Denmark	full		Aalborg	May 89
Finland	full			
France	full	full	Nice	Oct. 90
Germany	full		Aachen	Apr. 91
Italy	full			
Netherlands	full STL	full		
Norway (to April 90)	full		Oslo	June 90
Sweden	full	c		
Switzerland	full	full STL	Winterthur	May 88
United Kingdom	c	full	Warwick	Nov. 88
USA	c	full		
Totals	13	10	6	8

full = full commitment, c = contribution, STL = subtask leader

1.3.2 Approach of subtask 1

In subtask 1 the basic approach was to solve "identical problems" in different participating countries by "different methods" and different facilities. The results have been collected, analyzed and compared [3]. This approach did not only allow each country to assess the performance of the employed method, but also provided a methodology and experimental data sets to evaluate simulation models of the future.

Special problems encountered during this evaluation process were studied in separate Research Items: Modification of turbulence models for low Reynold numbers and thermal buoyancy [4], [5], [6], simulation of air supply devices [7], [8], [38], [43] or the specification of temperature boundary conditions that account for radiation [11].

Simplified methods have also been evaluated and in some cases even developed [9]. These methods have a particular appeal to the design engineer, because he can apply them with little investment of resources and specialized training.

Complex and simplified simulation methods have been evaluated by applying them to five different benchmark cases, each representative of a particular basic air flow phenomenon, such as forced or natural convection. Most attention (four cases) was paid to mixing flows, because they are the most used. One case, however, represents a displacement flow. Measurements and simulations have been carried out simultaneously by different groups. To compare the numerical performance of simulation methods, simple two dimensional flow fields have also been calculated.

1.4 Work plan and survey of performed work

The approach of the research was reflected in the following work plan with a project duration of 3.5 years.

1. Preparation phase (9 months):
 - survey of programs
 - selection of test cases.
2. Main phase (24 months):
 - specification of testcases
 - measurements in identical testrooms
 - simulation exercises with field models and simplified models
 - additional measurements
 - evaluation of experiments and simulated cases
 - improvement of simulation models.
3. Reporting phase (9 months).

A list of completed Research Items with the Principle Investigator(s) is shown in table 1.2.

Highlights of the performed work have been presented at the 12th AIVC Conference [10]. Table 1.3 shows an overview of papers/posters contributed by subtask-1 experts to this conference. The table shows that efforts have concentrated on problem areas (air supply) and on detailed measurements of flow quantities that are important to occupant comfort (turbulence intensity and concentrations of contaminants). The development and verification of simplified methods are also reported.

TABLE 1.2 List of completed Research Items with the Principle Investigator(s)

NO.	RESEARCH ITEM	PRINCIPAL INVESTIGATOR
1.01	Low Reynolds number effects in single-room air flow	A. Moser, Q. Chen (CH)
1.02	Selection of air terminal device	P. Nielsen (DK)
1.03	Test rooms, identical testrooms	T. Lemaire (NL)
1.04	Selection of radiator	T. Lemaire (NL)
1.05	Simplified models for room air distribution	P. Nielsen (DK)
1.06	Identify measuring values	P. Ollaro (I)
1.07	Survey of computer codes and data requirements	M. Liddament (UK)
1.08	Survey of existing measured data	M. Liddament (UK)
1.10	Survey of other computer codes	N. Sald (C)
1.11	Representation of boundary conditions at supply openings	P. Nielsen (DK)
1.12	Modelling of boundary conditions near the radiator	T. Lemaire (NL)
1.13	Specification of testcase B (forced convection, Isothermal)	J. Helkkinen (SF)
1.14	Specification of testcase E (mixed convection, summer cooling)	J. Helkkinen (SF)
1.15	Specification of testcase d (free convection with radiator)	T. Lemaire (NL)
1.16	Measurement of testcase B	DK,S2,SF
1.17	Measurement of testcase E	N,S2,SF
1.18	Measurement of testcase D	NL
1.19	Simulation of testcase B	C,CH,D1,D2,DK,F,N,NL,S1,SF
1.20	Simulation of testcase E	C,CH,D1,D2,N,NL,S1,SF
1.21	Simulation of testcase D	CH,D1,D2,NL,SF
1.22	Evaluation of cases B, E, D	G. Whittle (UK)
1.23	Simplified model with database of computed flow fields	Q. Chen (CH)
1.24	Modelling of the air inlet device	J. Helkkinen (SF)
1.26	Simulation of testcase D with zonal models	C. Inard, D. Buty (F)
1.31	Specification of testcase F (isothermal case with contaminants)	E. Skaaret (N)
1.32	Measurement of testcase F	DK, NL
1.33	Simulation of testcase F	C,F,NL,SF,S
1.34	Additional measurements in testcase B, D, E or F	All
1.35	Evaluation of cases B, D, E and F	G. Whittle (UK)
1.36	Measurement of testcase B in scale model with water	J. Fontaine, F. Biolley (F)
1.40	Preparation of the evaluation report	G. Whittle (UK)
1.41	Preparation of user guidelines	M. Liddament (UK)
1.42	Interaction with AIVC database	M. Liddament (UK)
1.43	Turbulence parameters at supply opening (measurements)	M. Zeller, M. Ewert (D2)
1.45	Specification of simple testcases: 2D1 (Isothermal) (isothermal) and 2D2 (mixed convection)	P. Nielsen (DK), U. Renz (D2)
1.46	Simulation of simple testcases 2D1, 2D2	C,CH,D,DK,NL,S,SF
1.47	Specification of testcase G (displacement ventilation)	T. Lemaire (NL)
1.48	Simulation of testcase G	NL,S
1.49	Measurement of testcase G	NL,S
1.50	Velocity distribution in rooms with displacement ventilation and low level diffusers	P. Nielsen (DK)

TABLE 1.3 Papers and posters presented at 12th AIVC Conference by Annex 20, Subtask-1 investigators.

PROBLEM	MEASUREMENT	SIMULATION
Air supply device	Ewert, Heikkinen	Chen, Ewert, Heikkinen, Skovgaard
Room flow field		
- turbulence	Sandberg, Zhang	
- concentration	Helselberg	
- scaling & Low Reynolds		Moser, Skovgaard
- water scale-model	Biolley	Fontaine
Simplified methods		
- jet models		Nielsen
- zonal model		Inard
Evaluation	Whittle	Whittle

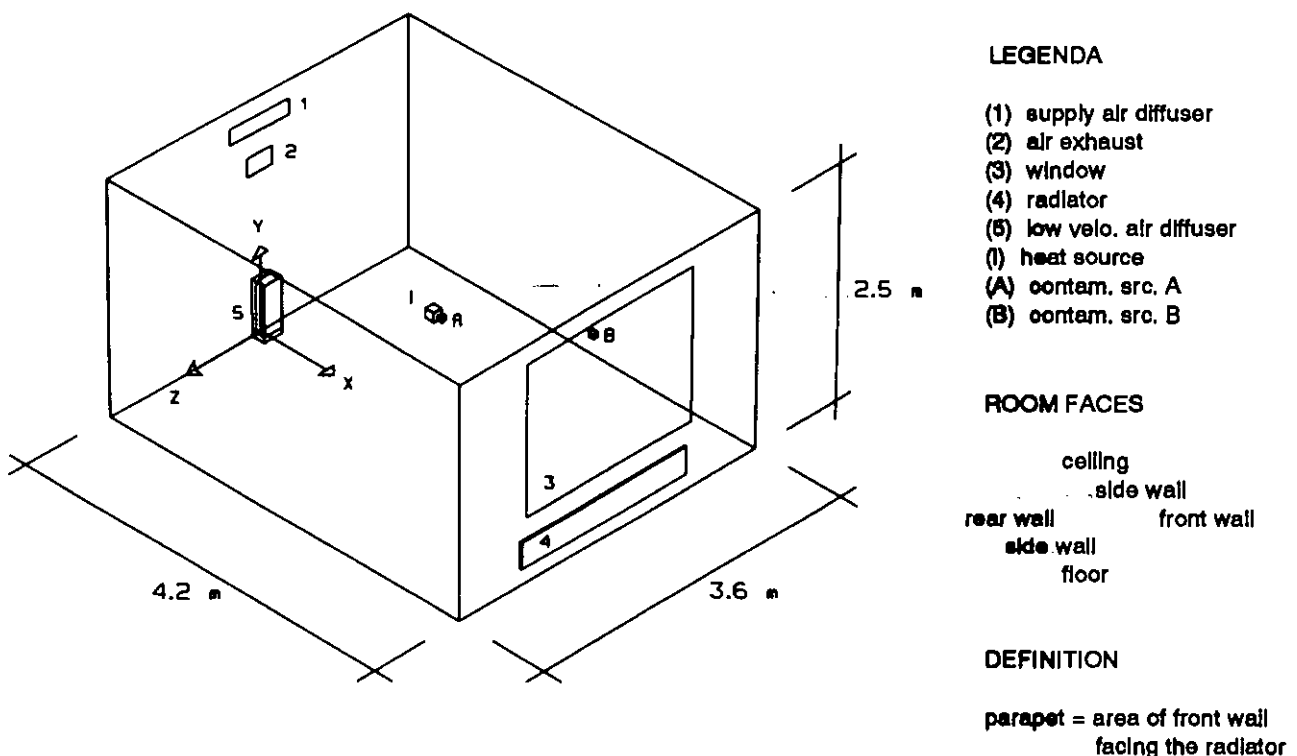


FIGURE 2.1 Configuration of the test room for all test cases (Note: for case G location and dimensions of air exhaust and window(s) slightly different)

2. AIR FLOW SIMULATION AND MEASUREMENT TECHNIQUES

2.1 Experimental equipment

2.1.1 Configuration of the basic test room

Geometry and items

The test room configuration to be used for the measurements and numerical simulation of the identical problems is described by Lemaire [82]. The choice of the configuration was based on common features between the test facilities of several participants. Unfortunately it was not possible to find common test room dimensions for all participants, so small differences exist in the dimensions of individual test rooms.

Figure 2.1 shows the configuration of the test room with its dimensions and the co-ordinate system. The room is sized 4.2m x 3.6m x 2.5m height (Denmark: 2.4m height). The walls of the room consist of at least 0.10m thick insulation and a wooden sheet (not necessary black) on the inner side.

The room configuration depends on the studied test case and is given in table 2.1. Further specification of the test cases is given in chapter 3.

TABLE 2.1 The configuration of each test case.

		case B forced conv.	case D free conv.	case E mixed conv.	case F contaminants	case G displ. vent.
(1)	supply air diffuser	X		X	X	
(2)	air exhaust	X		X	X	X
(3)	window	X	X	X	X	X
(4)	radiator		X			
(5)	low velocity air diffuser					X
(I)	heat source					X
(A)	cont. src. A				X	X
(B)	cont. src. B					X

All items of the possible room configurations are listed below.

- (1) A *supply air diffuser* of HESCO type KS (no. KS4W205K390) consisting of 4 horizontal rows of 21 nozzles (diameter 12mm, length 15mm) each. The nozzles are on a 0.71m x 0.17m rectangle and are set to a 40° discharge angle to the horizontal - as seen on a vertical plane through the centre of the room in the streamwise direction. The diffuser is mounted in the rear (opposite) wall at a distance of 0.20m to the ceiling.
- (2) An *air exhaust opening* (extract) sized 0.30m x 0.20 m in the rear wall located at a distance of 1.70m from the floor. For test case G: sized 0.60m x 0.25m at 0.15m from ceiling.
- (3) A *single-glazed window* sized 2.00m x 1.60m height in the front wall placed at a distance of 0.70 m from the floor. For test case G: 3 single glazed windows each sized 0.83m x 135m height.
- (4) A *single plane radiator* sized 2.0m x 0.30 m height and rated at 0.862kW situated beneath the window at a distance of 0.05 m from the front wall and 0.10 m from the floor.

- (5) A low velocity air diffuser (Stratos FMH.02) placed on the floor against the rear wall.
- (I) An electric bulb simulating a heat source of 100W located at $(X,Y,Z) = (2.1, 1.25, 0.0)$ m.
- (A) A neutral contaminant source A located at $(X,Y,Z) = (2.2, 1.25, 0.0)$ m injected through a porous spherical device of 30mm diameter.
- (B) A neutral contaminant source B located at $(X,Y,Z) = (4.0, 2.0, 0.0)$ m injected through a porous spherical device of 50mm diameter.

All configurations are symmetrical with respect to the vertical plane $Z = 0$ m. Note the lack of infiltration cracks and a window sill.

Location of measuring points

For case B, D and E a total number of 560 points for velocity and temperature measurements was specified. Table 2.2a identifies the co-ordinates of these standard measuring locations. The choice of the locations was based on the expected flow patterns (mixed ventilation). However the requirement to measure 560 points proved to be demanding. Some contributors concentrated their attention in measuring detailed flow structure in the jet, whilst others were able to measure throughout the space and mostly, but not universally at all agreed positions. In order to maintain at least some agreement, it was decided during the project that all participants should measure velocity and temperature profiles along the horizontal lines $(Y,Z) = (1.0, 0.0)$ m and $(X,Y) = (2.2, 1.0)$ m and the vertical line $(X,Z) = (2.2, 0.0)$ m.

For case G, velocity and temperature profiles along vertical lines were measured. (See table 2.2b) On each vertical line some 13 positions were sampled. The locations were chosen from the expected flow pattern for displacement ventilation.

For case F and G concentration measurements in several vertical and horizontal planes were specified. In reality only concentrations in the vertical symmetry plane $Z = 0.0$ m were measured. Table 2.3 shows the locations of the measuring points. The locations were concentrated around the contamination source A where large gradients were expected, at the front wall to see how far the jet would penetrate in the room and at the boundary surfaces.

TABLE 2.2a Case B,D,E:
velocity and temperature
measurement locations

X (m)	Y (m)	Z (m)
0.1	0.05	-1.7
0.6	0.1	-1.2
1.4	0.2	-1.6
2.2	0.5	0.0
3.0	1.0	0.6
3.6	1.5	1.2
4.0	2.0	1.7
4.1	2.3	
	2.4	
	2.45	

TABLE 2.2b Case G:
velocity and temperature
measurement locations

X (m)	Z (m)
0.2	-1.7
0.4	-1.2
0.6	-0.6
1.2	0.0
1.6	0.6
1.8	1.2
2.2	1.7
2.4	
2.8	
3.2	
3.6	
4.0	
4.1	

TABLE 2.3 Case F,G:
concentration
measurement locations

X (m)	Y(NL) (m)	Y(DK) (m)
0.08	0.10	0.08
0.40	0.35	0.30
1.00	0.65	0.60
1.50	0.95	0.90
1.90	1.15	1.10
2.20	1.35	1.50
2.50	1.55	1.80
2.90	1.85	2.10
3.40	2.15	2.35
3.90	2.45	
4.08		

2.1.2 Scale model experiments

While other participants made full scale measurements, Biolley et al. [12] represented the test room by a water scale model (scale 1/6). The parameters were determined according to Reynolds similarity. The method was flexible and well adapted to flow visualizations. For quantitative analyses, mean and turbulent velocity measurements were performed by Laser Doppler anemometry. (See also section 2.1.3 for LDA-technique)

The altuglass scale model and the hydraulic bench are sketched in figure 2.2. The scale model was placed in a 2.25m x 1.75m x 1.0m closed experimental tank (1, fig.2.2a). The front face of the tank was in glass and the bottom in altuglass. A pump (2) sucked the water out of the model and transferred it into a 3m³ buffer tank (3). A flowmeter (4) monitored the pump flow rate. The air diffuser (1, fig.2.2b) was modelled either as a scaled HESCO diffuser, as a slot (0.71m x 0.016m) or as a basic rectangle (0.18m x 0.062m). By conservation of mass, water came from the surrounding of the model (2) and entered through the diffuser. Before entering the flow was homogenized by a divergent-convergent system (3) equipped with grids. For flow visualization a dye (fluorescein) could be added (4) and properly mixed with the water sucked into the divergent-convergent zone.

Based on Reynolds similarity (using the same Reynolds number in the model and the original) the following scaling relations were applied: length 1/6, time 1/2.4, velocity 1/2.5, flow rate 1/90, renewal time 2.4/1.

Velocities were measured on the lines $(Y,Z) = (1, 0)m$, $(X,Z) = (2.2, 0)m$ and $(X,Y) = (2.2, 1) m$. Some measurement points on the faces of a box ($0m \leq X \leq 1m$, $2m \leq Y \leq 2.5m$ and $-0.5m \leq Z \leq 0.5m$) surrounding the inlet were added.

Longitudinal (u) and vertical (v) components were obtained by LDA measurements through the front face of the experimental tank; longitudinal (u) and transversal (w) components through the bottom face. Statistical mean velocities u_m and standard deviations σ were computed from N values of instantaneous velocities ($N = 3072$). After u_m and σ were computed, all values u with $|u - u_m| > 6\sigma$ were eliminated and new values of u_m and σ were computed from the remaining data.

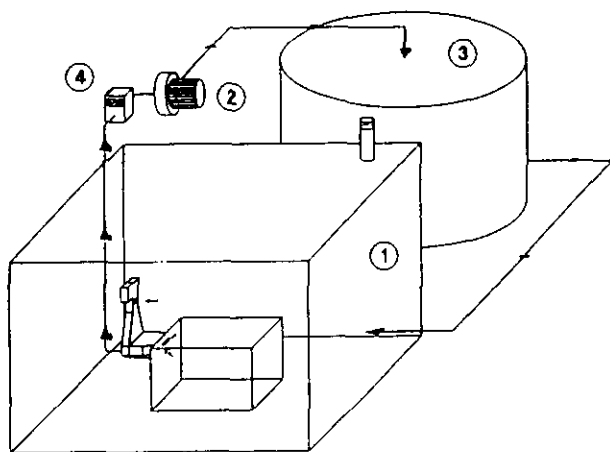


FIGURE 2.2a Sketch of the hydraulic bench

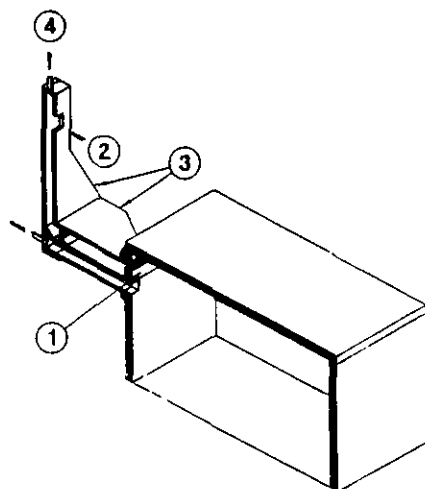


FIGURE 2.2b Test room model (scale 1/6)

2.1.3 Measuring equipment

Thermal anemometry

The measuring instrumentation used was mainly based on thermal anemometry using hot-wire and omnidirectional hot-film probes from Disa-Dantec, TSI and B&K. Modified constant-current anemometers [13] were also used. Most of these instruments are designed to measure thermal comfort according to requirements of ISO 7726 standard [104]. The required accuracy is $\pm |0.05 + 0.05v_a|$ m/s, where v_a is the mean air velocity in the range 0.05 to 1.0 m/s.

Blomqvist [14,15] in test cases B, E and G used constant temperature thermistor anemometers developed at NSIBR. Temperatures were measured using thermocouples connected to a data acquisition system. At each position 300 samples of velocity and temperature were taken over a period of 15 minutes.

Heikkinen [16] used constant temperature thermistor anemometers developed at the Helsinki University of Technology for measurement of cases B, and E. A total of 40 probes were used. A time period of four days was needed for the measurement of all 560 points in the room. In case E the supply air temperature and window temperature were controlled to within a band of 0.4°C.

Fossdal [17] used TSI 1620 omnidirectional anemometers and Cu/Con thermocouples connected to a data acquisition system. Ten sets of anemometers and thermocouples were mounted on the instrumentation column between the heights of 0.05m and 2.47m.

Lemaire et al. [18,19,20] in test cases B, D and G used modified thermal anemometers developed by the TNO Research Institute for Environmental Hygiene. The instrument works as a thermocouple with each weld being surrounded by a small (5mm diameter) grey sphere. One of the spheres is electrically heated and the other one is used as a reference. Velocities below 0.06m/s could not be measured, because of the free convection caused by the heated sphere of the anemometer. Air and surface temperatures were measured with Cu-Con thermocouples. Positioning of the anemometers in the room was automated using a movable rack.

Concentration measurements

Heiselberg [21,22] used the tracer gas CO₂ as a contaminant mixed with the carrier gases N₂ and He in order to give the required flow rate and different contaminant densities. The contamination source consisted of a ping pong ball (diameter 30mm) with 6 evenly distributed holes with a diameter of 1mm each. Concentrations were measured in the supply, in the exhaust and on 10 points along a vertical measuring column in the room at the same time. The room average concentration was determined by measuring the concentration in the room after a final mixing of the room air after air and contaminant supply were shut off. Concentrations were measured with a BINOS infrared analyzer.

Lemaire et al. [23] used a mixture of N₂O (tracer gas) and air as contaminant. The mixture was injected through a porous sphere. Flow rates of approx. 0.50ml/s N₂O and 87.5ml/s air were used. Positioning of the measuring points in the room was automated using a movable rack with mounted PVC-tubes. The tubes were connected to a Miran infrared analyzer which was placed outside the room.

Observation of air flow directions

Heikkinen [16] observed the air flow directions by introducing a small amount of smoke into the flow. The smoke was generated using "air current tubes" from Drägerwerk, Germany. The flow

may have been affected by the observer who had to stay in the room during the test.

Laser Doppler Anemometry

Ewert et al. [24,25] performed measurements of local velocity components near the supply air diffuser in the test room (isothermal conditions) using Laser Doppler Anemometry (LDA). The data collected at one position with a one component Argon-Ion-Laser-System is stochastic and time dependent. The laser and data processing system were located outside the test room. Only the optical sensor, connected with the laser and Burst Spectrum Analyzer (BSA) by way of a fibre optic cable, and the traversing device were placed inside. The measurement setup for a dual beam system is shown in figure 2.3.

The laser beams (wave length 514.5nm) passed through a beam splitter, bragg cell for frequency shifting of one beam (shifting 40Mhz) and optic elements to couple the beams into a fibre optic cable. After passing the front lens of the LDA sensor with a separation of 73mm, the two beams crossed at a focus at 600mm forming the measuring volume. In a dual beam system, crossing of two coherent laser beams creates a fringe pattern from the interference of the wave fronts. A measurement was made when particles in the air flow scattered light in all directions while going through the beam crossing. The scattered light was collected at 180° backscatter with the front lens and then focused through the fibre onto the photodetector. The frequency of the scattered light was Doppler shifted and referred to as the Doppler frequency of the flow. After shifting to lower frequencies the particle velocity was calculated from the Doppler frequency in a Burst Spectrum Analyzer (BSA) and sent to a Personal Computer to store the data for additional evaluations.

The BSA received data only if a particle was passing the measuring volume. For that reason signals of the time dependent velocity were stochastic. The data rate and validation of the system depended on the particle concentration, convection velocity of the air flow, laser power and optical system parameters. With the system used maximum data rates of 800Hz in the inlet jet (1.2m/s) and 200Hz below the inlet jet (0.1m/s) could be found. As scattering particles, an oil aerosol with a mean diameter of 0.5 μm was used generated by a seeding generator with compressed air.

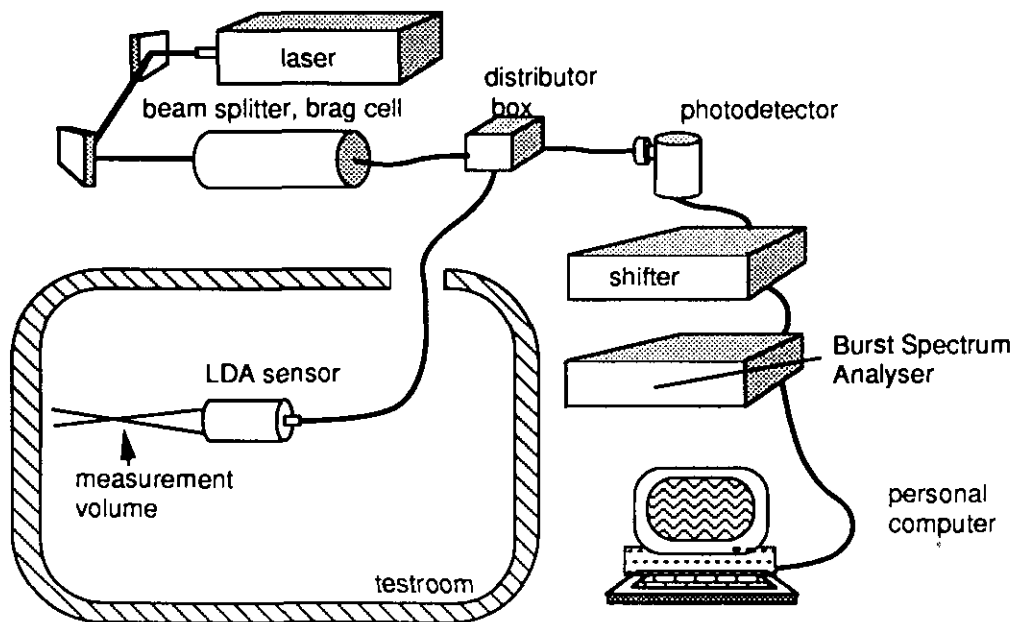


FIGURE 2.3 LDA-measurements set up

2.2 Computational fluid dynamics models

2.2.1 Air flow computer codes

Available codes for the prediction of the air flow pattern, the temperature field and the distribution of contaminants within a room are listed in [26]. Some general CFD-codes used in North America and elsewhere may be found in [27]. A critical review of computational fluid dynamics procedures was prepared for the ASHRAE by Baker and Kelso [28].

Some commonly used computer codes, including those applied by the Annex 20 participants, are listed in table 2.4. "FloVENT" is used by IEA Solar Task 12, Project A.3, 'Atrium model development'. All codes listed use finite volume discretization with the exception of three, which employ the finite element (FE) method.

TABLE 2.4 Computer codes for air flow simulation

Name	Origin of Code	Type	Method	Annex-20 users	Remarks
ARIA	Abacus	UK	C	FV	
ASTEC	Harwell	UK	C	FV	
CALC-BFC	Chalmers	S	R	FV	Sweden
CHAMPION	TUD	NL	R	FV	
EOL-3D	INRS	F	R	FV	France
EXACT3	NIST	USA	R	FV	Canada
FEAT		UK	C	FE	
FIDAP	FDI	USA	C	FE	
FIRE	AVL	A	C	FV	
FLOTRAN	Compuflow		C	FE	
FloVENT	FLOMERICS	UK	C	FV	SHC Task 12
FLOW-3D	Harwell	UK	C	FV	
FLUENT	Fluent Inc.	USA	C	FV	Germany, Finland
JASMINE	BRE-FRS	UK	R	FV	fire, smoke
KAMELEON	SINTEF	N	R	FV	Norway
PHOENICS	CHAM	UK	C	FV	Switzerland
SIMULAR AIR	AVL	A	C	FV	Germany
STAR-CD	CD	UK	C	FV	
TEACH-3D	Aalborg	DK	R	FV	Denmark
TEMPEST	Battelle	USA	R	FV	
WISH-3D	TNO	NL	R	FV	Netherlands, Finland

Note: R = research codes, C = commercial codes, FV = finite volume, FE = finite element.

Common features of the codes used by the Annex 20 participants are: finite volume formulation, utilization of a pressure correction method and turbulence modelling with the k-ε model.

2.2.2 Mathematical and numerical models

Liddament [26] has outlined recent developments in building air flow analyses using computational fluid dynamics and has focused on some difficulties associated with this complex field of study. This paragraph will only focus on the mathematical and numerical models implemented in the CFD-codes used by the Annex-20 participants.

The transport equations

The aim of the numerical prediction is to solve the governing set of partial differential equations of viscous flow. The equations consist of the continuity, momentum (Navier-Stokes) and energy

equations. The distribution of neutral contaminants requires an additional equation, which can be solved after the flow field is predicted. The air is considered an ideal gas and an incompressible fluid. In most cases the Boussinesq approximation is used to account for air density variations due to temperature gradients. With this approximation the air density is taken as a constant and the buoyancy force is represented by including a gravitational term in the momentum equations.

The above mentioned equations suffice to describe laminar flows. More generally, the behaviour of room ventilation is dominated by turbulence generated by relatively high supply air velocities and large temperature differences. This type of flow cannot even in principle be described exactly, since almost all the physical properties (such as velocity components V_i , pressure p , enthalpy h and density ρ , etc.) fluctuate and interact with each other. Since engineers are mainly interested in mean values, they use so-called turbulence transport models, which simulate only the gross features of the turbulent flows. The models are based on good physical insight and can be applied to complicated flows encountered in reality. The basic governing equations remain almost the same as for laminar flows. The unknown quantities are replaced by their statistically time averaged values and a turbulent diffusivity is added to the laminar diffusivity (viscosity, conductivity) in the equations. In the k - ϵ model the turbulent diffusivity is expressed in terms of the kinetic energy of turbulence k , and the dissipation rate of kinetic energy of turbulence, ϵ (Launder and Spalding [29]). This results in two extra equations for k and ϵ of a similar form as the previous equations. Simultaneous solution with the continuity, momentum and energy equations is required.

All governing equations can be expressed in a common form:

$$\underbrace{\frac{\partial(\rho\phi)}{\partial t}}_I + \underbrace{\frac{\partial(\rho V_i \phi)}{\partial x_i}}_{II} - \underbrace{\frac{\partial}{\partial x_i} (\Gamma_{\phi, \text{eff}} \frac{\partial \phi}{\partial x_i})}_{III} = \underbrace{S_{\phi}}_{IV} \quad (2.1)$$

where ϕ , $\Gamma_{\phi, \text{eff}}$ and S_{ϕ} are given in table 2.5. (Note: in room air flow simulation the air temperature T equals h/c_p .)

The transport equation expresses a balance between the four terms:

- I transient term: accumulation of ϕ during timestep t ;
- II convective term: transport of ϕ by convection;
- III diffusive term: transport of ϕ by diffusion;
- IV source term: local production of ϕ .

Near wall treatment

Originally the k - ϵ model was developed for high Reynolds number or high turbulence flow. In rooms, however, low turbulence regions occur especially close to the solid boundaries. In order to deal with this problem the standard k - ϵ model is corrected near the wall with so called wall functions or a "low Reynolds modification" is applied throughout the entire flow field. A review of literature was done by Moser [4].

Usually the wall function is achieved by first defining a viscous sublayer above which flow is assumed to be fully turbulent. Within this sublayer, the mean velocity parallel to the wall or boundary is assumed to vary linearly with distance from the wall while, beyond this region, it is assumed to vary linearly with the logarithmic distance. Variations in k , local turbulent shear stress and ϵ are then made consistent with these velocity functions. Within the viscous sublayer, turbulent shear stress is zero and ϵ is constant. In order to reflect fluid temperature distribution a near wall temperature model is also required. The wall function is strictly valid for forced convection boundary layers, although in reality it is also applied to mixed and free convection

TABLE 2.5 Values of ϕ , $\Gamma_{\phi,eff}$ and S_{ϕ} terms for a cartesian co-ordinate system.
 (Note: values of emperical constants may differ among the participants)

ϕ	$\Gamma_{\phi,eff}$	S_{ϕ}
1	0	0 (continuity)
V_i	$\mu_t + \mu$	$-\partial p/\partial x_i - \rho\beta/c_p g_i (h-h_0)$
k	$\mu_t + \mu/\sigma_k$	$G - \rho\varepsilon + G_B$
ε	$\mu_t + \mu/\sigma_{\varepsilon}$	$(C_1 G - C_2 \rho\varepsilon + C_3 G_B) \varepsilon/k$
h	$\lambda/c_p + \mu/\sigma_h$	S_h
C	$\rho D + \mu/\sigma_C$	S_C

$G = \mu_t (\partial V_i/\partial x_i + \partial V_i/\partial x_i)$	$G_B = \beta/c_p g_i \mu/\sigma_h \partial(h-h_0)/\partial x_i$	$\mu_t = \rho C_{\mu} k^2/\varepsilon$
$C_1 = 1.44$ $C_2 = 1.92$ $C_3 = 1.44$	$\sigma_k = 1.0$ $\sigma_{\varepsilon} = 1.3$ $\sigma_h = 0.9$ $\sigma_C = 1.0$	$c_{\mu} = 0.09$

V_i = velocity comp. in x_i -dir (m/s)	ρ = fluid density (kg/m ³)
p = pressure (Pa)	μ_t = dynamic viscosity (Ns/m ²)
k = kinetic energy of turbulence (J/kg)	μ = turbulent viscosity (Ns/m ²)
ε = dissipation rate of kinetic energy (J/kg s)	λ = coef. of heat conductivity (W/mK)
h = enthalpy (J/kg)	D = coef. of molecular diffusion (m ² /s)
C = concentration (m ³ /m ³)	c_p = specific heat (J/kgK)
x_i = cartesian coordinate direction	σ_{ϕ} = turb. Prandtl number for ϕ
t = time (s)	β = coef. of thermal expansion (K ⁻¹)
g_i = gravity component (m/s ²)	C_{μ} , C_1 , C_2 , C_3 = emperical constants

boundary layers.

Chen, Moser et al. [5] recommend to apply low-Reynolds-number corrections to the simulation of free and mixed convection in rooms. Using the Lam and Bremhorst [30] model to compute air flow and heat transfer in a cavity with natural convection, they found better agreement with experimental data. In the low-Reynolds-number approach, the k- ε model is retained, but three functions f_1 , f_2 and f_{μ} are introduced which are continuous and valid throughout the entire flow region. Within the turbulent regime, the value of each of these functions is unity, reflecting the fact that viscous forces within this region are negligible. However, as the laminar sublayer is approached, the value of these functions vary in order to reflect the increasing influence of viscous forces within this zone. With the low-Reynolds-number models an additional 20 to 30 gridlines are required for the near wall region. (See e.g. [82]). This significantly increases the computing costs and limits the practical applications of the models.

The numerical method

The numerical method starts from the general form (2.1). Several methods are available: finite element, boundary element, finite volume etc. See e.g. [31] for a description of these methods. All Annex-20 participants applied the finite volume method with SIMPLE-like algorithms to steady state flows on a cartesian co-ordinate system. Therefore this method is briefly explained as follows.

- (1) The calculation domain is divided into a finite number of grid cells (or control volumes). Within each cell V_p each variable ϕ is represented by a single value ϕ_p on a gridnode P. Very often a staggered grid is employed in order to obtain a consistent connection

between the pressure gradient and the velocities. This implies that the velocities are calculated at the boundaries of the volumes of the original grid.

- (2) The equations are discretized over the control volumes so that the integral balance of ϕ over the volume surrounding each node is satisfied. In this way a non-linear equation set is generated for each variable ϕ with the form:

$$A_p \phi_p = \sum_{nb} a_{nb} \phi_{nb} + S_c \quad (2.2)$$

where nb denotes all neighbours. Negative coefficients are to be avoided in order to ensure convergence.

- (3) Several algorithms may be applied to solve the set (2.2). Probably the most frequently applied is the SIMPLE-algorithm proposed by Patankar and Spalding [32]. This algorithm introduces the so-called pressure correction p' . An equation for p' is obtained by substitution of the momentum equations into the continuity equation. Within each iteration the momentum and p' equations are solved and the velocity fields and pressures updated according to pressure corrections several times until satisfactory continuity is obtained. The transport equations which influence the flow field (e.g. temperature field, turbulence etc.) are then solved.
- (4) For each iteration the coefficients A_p , a_{nb} and source term S_c are updated, and step (3) is performed, until convergence to the non-linear set (2.2) is achieved.

Recent developments

Until recently staggered grids were necessary to avoid 'checkboard-oscillations' in velocities and pressure. In 1983 Rhie and Chow [33] introduced a new algorithm for a non-staggered grid, which is now implemented in e.g. the FLOW-3D or Fluent code.

In case of non-rectangular spaces, coordinate transformations can be applied to map the physical space onto a rectangular grid. In this way the implementation of boundary conditions remains relatively easy whilst maintaining the same discretization procedure. The source term S_c , however, becomes much more complicated. (Burns [34]). Alternatively, the equations can be represented directly in physical space. This results in a unstructured equation matrix. Both methods require larger amounts of memory either to deal with the distorted grid and transformation equations or to store the unstructured matrix.

The Annex-20 participants applied Hybrid, Upwind, Power Law or Quick difference schemes. First order upwind schemes can cause poor accuracy and unrealistic flow representation if the grid is not aligned with the main flow direction. In order to solve this problem new schemes have been proposed as e.g. the Skew scheme (Raithby [35]). An alternative method is local grid refinement at locations of interests in which a series of control volumes are subdivided into smaller units.

To overcome convergence problems occurring with high buoyant flows, strongly coupled solutions are being introduced. Thompson et al [36] and Vanka et al [37] describe such a non-segregated technique in which the velocities and pressures are simultaneously updated, resulting in tight coupling between equations. However, substantial computer memory is required, since more sets of equations are held in memory at the same time. To further assist rapid convergence a "multigrid" discretisation system is introduced in which part of the analysis is undertaken on a coarse grid and the results are applied to successively finer grids.

2.2.3 Modelling of boundary conditions

The flow pattern within a room is determined by conditions at the boundaries and by the characteristics of source terms. It is therefore necessary to represent as accurately as possible such terms and to ensure that flow adjacent to boundaries follows boundary layer theory. In Annex 20 collective guidance was given on options for modelling boundary conditions such as the supply air diffuser [38] or the radiator [39].

Representation of boundary conditions at the supply air diffuser

The air supply is characterized by geometry, inlet velocity, volume flow rate and turbulence characteristics. These parameters can be obtained by test or from manufacturers data for various room configurations. For test case B (forced convection, isothermal) the air movement in the room is expected to be controlled by the momentum flow in the jet created around the inlet below the ceiling. It is therefore essential that both the inlet velocity and volume flow rate are accurately represented. This may require a very fine grid near the diffuser, which (without local grid refinement) extends throughout the whole room resulting in an excessive number of grid nodes. The HESCO diffuser (see figure 2.4a), in particular, is difficult to model directly, because the 84 tiny nozzles are distributed over a fairly large area and are directed upwards in an angle of 40°. The following inlet models were used.

Simple rectangular slot model. The complex diffuser is replaced by one or more simple rectangular slots. Total effective area a_0 and total volume flow rate Q_0 are the same as those of the 84 round nozzles. The inlet velocity u_0 is directed upwards in an angle of 40°. The momentum flow created around the diffuser is preserved. The following combinations of location, aspect-ratio and number of slots were used. (See figure 2.4).

Basic model. This one-slot model is used by all Annex-20 participants. The slot has the same aspect ratio as the real diffuser and is located in the middle of the diffuser. The slot is sized 180mm x 62mm height and its centre is located 285mm from the ceiling. Turbulence intensity Tu was set at 10% and the dissipation rate corresponds to developed channel flow. See [40].

Wide slot. Making the slot wider is believed to result in more mixing in the early stages of jet development, because the perimeter of the jet is greater than in the basic model and corresponds more closely to reality. Heikkinen [7] uses a slot of 437mm x 26mm height and Fürst [41,42] a slot of 0.71m (actual width of diffuser) by 0.0126m height. The slot area and turbulence inlet conditions are the same as in the basic model.

Multiple slots. Chen [8] uses configurations with 12 slots and 84 slots as shown in figure 2.4 with the same turbulence conditions as in the basic model.

Momentum method. In the momentum method boundary conditions for the continuity equation and momentum equations are set separately so that the inlet area can be chosen freely. Volume flow rate Q_0 and momentum $Q_0 u_0$ of supplied air belonging to the actual diffuser are specified for an opening with the same dimensions as the area occupied by the nozzles (gross area). The momentum method can be regarded as setting infinite nozzles/slots as shown in figure 2.4. Chen [8] applies the method in the PHOENICS code. Here the flow rate in the inlet is characterised with a fraction of the effective over gross area of the diffuser. The fraction indicates the area of the grid cells within the inlet available for the supply air. Heikkinen [7] modified the WISH-code by incorporating a mass sink in the first layer of grid cells in front of the opening. Different diffusers can be simulated by giving different supply momentum and its initial directions.

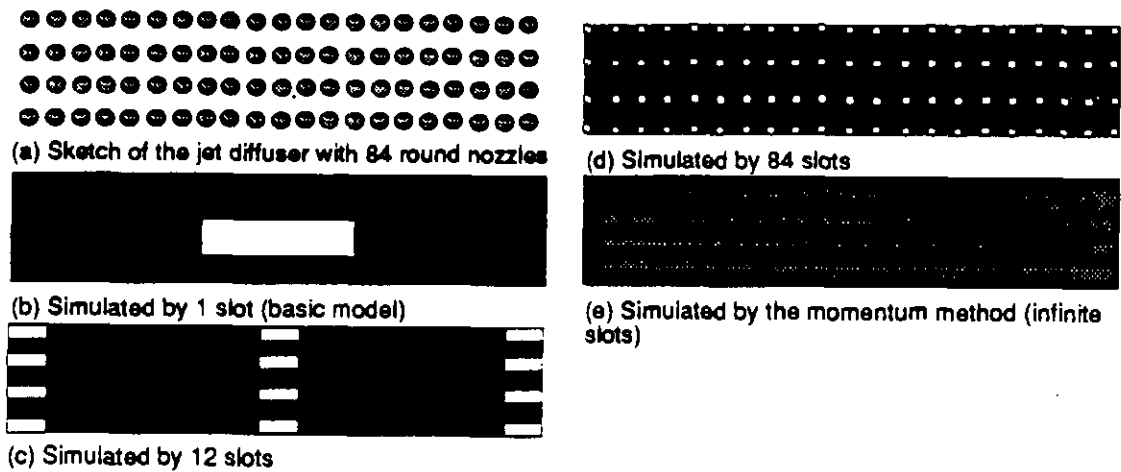


FIGURE 2.4 The diffuser (a) simulated with the simple-rectangular slot model (b),(c),(d) and the momentum method (e)

Box model. In the box model boundary conditions for the variables $\phi = u, v, w, k, \varepsilon, T$ and C are specified on the faces of an imaginary box surrounding the supply opening and located up against the ceiling. Boundary conditions are of "zero flux" or "prescribed value" type. The boundary values are calculated analytically for self-preserving jets or are measured at the actual diffuser.

2D-wall jet profiles are discussed by Nielsen [38]. The front face of the box should be located at sufficient distance x_a from the inlet in an area with a fully developed wall jet. This reduces the gradients of ϕ and thus the required number of grid nodes. On the other hand x_a should only be a small fraction of the room length L because the flow in the outer part of the wall jet is strongly influenced by the recirculating flow. The height y_b of the vertical faces should be adequate for the momentum flow to be established in the wall jet. Values of y_b/δ_x of 0.75 to 1.0 are recommended, where the width δ_x is defined as the vertical distance from the ceiling to the location in the wall jet where the velocity is half the maximum velocity. Jet profiles can be applied in non-isothermal flow, provided that the buoyancy forces are small in comparison with the momentum forces.

Measured boundary values are applied by Ewert et al. [24] and Heikkinen [7] for case B (forced convection, isothermal) on a box sized 1.0m x 1.0m x 0.4m height. Heikkinen specifies measured velocities and calculated turbulence values applicable to a two-dimensional wall jet. Ewert specifies measured velocities and measured as well as calculated k and ε profiles. The profiles are calculated from the measured time averaged velocity V at a distance $y = L$ from the ceiling for a turbulence intensity $Tu = 0.1$ with:

$$k = 1.5(VTu)^2 ; \varepsilon = c_D^{0.75} k^{1.5} / L ; c_D = 0.09 \quad (2.3)$$

Prescribed velocity model. With this model, as discussed by Nielsen [38], only the u and w velocity profiles (velocities in x - and z -direction respectively) are prescribed in the volume of the similar imaginary box as used in the 'box model'. Inlet profiles of all variables ϕ are also given as boundary conditions at the opening, but on a low number of grid nodes. The volume flow, energy supply and contaminant supply should be correctly given at the inlet. The remaining variables (v, k, ε) within the box are computed by the computer-code, based on the specified u and w field. The idea is to minimize the required data. As with the 'box model' the data is calculated analytically for self preserving jets or taken from measurements.

Jet profiles are applied by Skovgaard et al.[43] within the box volume and by Lemaire et al.[44] and Fontaine [12] on the vertical faces of the box only. They use formulas derived by Skovgaard et al.[45] from tests on the HESCO-diffuser. (See section 2.3.1). The box is sized 1.0m x 1.0m x 0.2m height. The model is applied to test case B (forced convection, isothermal) by both participants and to test case E (mixed convection summer cooling) by Lemaire only. In the 'mixed convection' case 'zero gravity' is prescribed, instead of temperature profiles, which were unknown. It is assumed that the buoyancy forces in the box are low compared to the momentum forces.

Measured data is used by Heikkinen [7]. He specifies only the u-velocity profile on a small plane at a distance of 1.0m from the inlet. The width of the plane is 0.6m and the height 0.13m where the velocity is about 35% of the maximum value. His idea was to test if the flow field produced by the basic model could be easily revised.

Representation of boundary conditions near the radiator

A number of models for the simulation of the thermal behaviour of the radiator near the wall exists. Only the models proposed by Lemaire [46] or used by the participants are discussed here.

Closed box model. The radiator is replaced by a rectangular closed box. The boundary conditions on the faces of the box and on the parapet can be:

- *prescribed (uniform) temperature*, calculated with a flow-radiation program or from a simple thermal network model (monozone model). Correct convective heat transfer coefficients can be determined with correct wall functions, a low-Reynolds-number model (Chen [47], Vogl et al.[48]) or semi-empirical formulas (Fürst [49]).
- *prescribed (uniform) convective heat fluxes*, as suggested by Lemaire and Inard [50] from a comparison between several zone-models. The model was used by Lemaire [51], and Heikkinen et al.[52], because at the 5th expert meeting (Oslo) several participants reported severe problems using prescribed temperatures.

Convective heat source. A simple alternative is to replace the radiator by a uniform convective heat source. The heat source encloses the radiator and the space between the radiator and the parapet, but imposes no physical obstacle for the flow. The total convective heat flow is determined in advance or during the simulation process using a simple thermal network. The model reduces the number of grid nodes, but seems to be less accurate than the 'closed box' model. The model was not used in Annex-20.

Thermal boundary conditions at the wall surfaces

The walls of the 'basic test room' are assumed to be adiabatic during the experiments (test case D and E). This boundary condition is not valid for the flow simulations, because of the radiative heat transfer between the walls, window and radiator. *The wall surface temperatures must be estimated beforehand with:* (1) a simple thermal network or zonal model [11], (2) a stand-alone radiation program or (3) a coupled flow-radiation program.

The last two options are preferable, because they calculate local surface temperatures. A coupled program can also take into account variations in local convective heat transfer influencing the surface temperatures.

Modelling of contaminant sources

Contaminant sources can be modelled by a solid box with prescribed contaminant flows at the faces of the box or by a permeable source in one or more grid cells. The last model was preferred by all participants who performed test case F or G..

2.3 Simplified air flow models

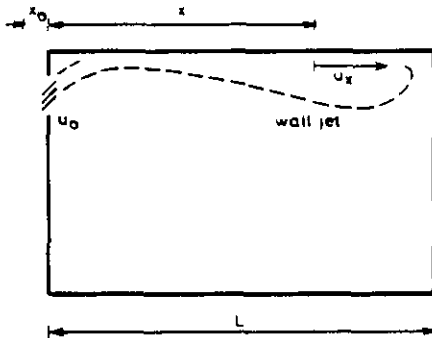
Simplified air flow models can be applied with little investment of resources and specialized training and are very attractive to the design engineer. For this reason the Annex-20 research focused also on this kind of models.

2.3.1 Design models based on self-similar jet flow

These models are based on the theory of self-similar jet flow. They are used in the design procedure to control the air distribution in the room in such a way that the maximum velocity u_{m} in the occupied zone is up to 0.15 m/s. Nielsen [53] discusses the limitations and possibilities of the methods in comparison with CFD-codes and shows the necessary boundary conditions. The evaluation of the models is supported by the measurements made in test rooms in different countries as discussed in chapter 3.

Design according to throw of isothermal jet (isothermal flow)

Figure 2.5 shows an example of a jet flow in a room with a sidewall mounted grille. The flow below the ceiling is a self-similar wall jet which is independent of the downstream room geometry, which means that it is independent of room height H and length L . Equations (2.4) and (2.5) describe the velocity decay u_x/u_o in the wall jet and the throw l_{Th} .



$$\frac{u_x}{u_o} = K_a \frac{\sqrt{a_o}}{x + x_o} \quad (2.4)$$

$$l_{\text{Th}} = \frac{u_o K_a \sqrt{a_o}}{u_{\text{Th}}} - x_o \quad (2.5)$$

FIGURE 2.5 Wall jet in a ventilated room

Here u_o and u_x are supply velocity and maximum velocity in the wall jet at the distance x from the opening, respectively. a_o is the effective supply area of the diffuser and x_o is the distance to the virtual origin of the wall jet. K_a is a constant which varies from 2 to 10. x_o is about zero, dependent on the actual diffuser and diffuser location. K_a , a_o and x_o may depend on the Reynolds number in case of low turbulent flow. The throw l_{Th} is defined as the distance from the opening to a location where the maximum velocity u_x is equal to a given reference value u_{Th} . The maximum velocity in the occupied zone u_{m} up to 0.15 m/s is generally achieved when the throw l_{Th} is equal to room length L and the reference velocity u_{Th} is equal to 0.2 m/s or 0.25 m/s.

Normally a throw equal to the room length L is recommended for the situation shown in figure 2.5. More generally the throw is the half length between two diffusers with opposite position or the length between diffuser and wall. Other definitions of l_{Th} may be used to compensate for different diffuser designs and different room geometry. A throw of $L + H - 1.8$ m is for example used when the room is high and it expresses formally that the maximum velocity in the wall jet is supposed to be equal to u_{Th} when it passes through the occupied zone.

The characteristics of the HESCO diffuser, determined by preliminary measurements [53] of the velocity decay, are: $x_o = 0.45$ m, $a_o = 0.00855$ m² and $K_a = 4.8$. The design velocity u_o is 2.09

m/s, corresponding with a specific airflow rate of $1.78h^{-1}$. Skovgaard et al.[45] describe the jet as a combination of a three-dimensional wall jet and a radial impinging jet, using the following set of equations.

$$\frac{u_r}{u_o} = K(\theta) \frac{\sqrt{a_o}}{r + x_o} \quad (2.6)$$

$$\begin{aligned} u_x &= u_r \cos\theta \\ u_z &= u_r \sin\theta \end{aligned}$$

$$K(\theta) = 4.2 - 0.975\theta - 8.206\theta^2 + 7.838\theta^3 - 2.828\theta^4 \quad (2.7) \quad \delta_{\eta}(x) = 0.08(x + 0.45) \text{ m} \quad (2.8)$$

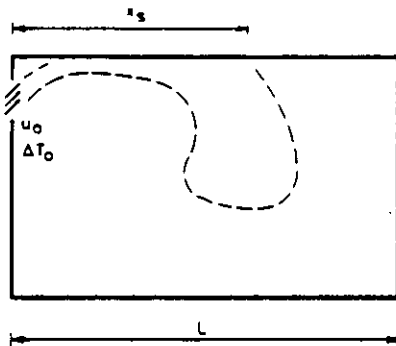
Here u_r and θ are resp. the velocity (m/s) and angle (rad) in the radial direction.

Maximum velocity in the occupied zone (isothermal flow)

For the configuration of test case B the maximum velocity u_{mm} in the occupied zone will be located close to the floor at a distance of $\sim 2/3L$ from the supply opening. Experiments with isothermal flow show that u_{mm} is a simple function of a reference velocity u_L which is the velocity in an undisturbed wall jet at the length L from the actual diffuser. For a two-dimensional wall jet $u_{mm}/u_L \sim 0.7$ and for a semi-radial jet u_{mm}/u_L varies between 0.3 and 0.7. Since u_L follows from (2.4) with $x = L$, the value of u_{mm} can be calculated if u_{mm}/u_L is known. Experiments show that $u_{mm}/u_L \sim 0.45$ for test case B.

Penetration depth of non-isothermal jet

In case of a low supply temperature the wall jet can separate from the ceiling at a distance x_b from the diffuser and may fall down into the occupied zone as shown in figure 2.6. A short penetration depth is undesirable because the jet may have a high velocity and a low temperature when it enters the occupied zone. Calculation of the penetration depth x_b is thus a part of the design procedure of the air distribution system. The equation for x_b follows from an analysis of the forces acting on a thermal jet [54] and is given in the figure. The relation between the specific heat load Q and the design variables is also shown, see [53].



$$\frac{x_b}{\sqrt{a_o}} = 0.19 K_{ba} K_a \left(\frac{1}{Ar}\right)^{0.5} \quad (2.9)$$

$$Q \sim u_{mm}^3 / K_a \quad (2.10)$$

FIGURE 2.6 Penetration depth x_b of a thermal jet in a room

Here Ar is the Archimedes number (see eq. 3.1) and K_{ba} is a constant dependent on parameters outside the wall jet, such as room dimensions, location of thermal load, etc. K_{ba} is $\sim 1.5 - 1.6$ (test case E), and depends on the location of the heat source. An air distribution system which can handle a high heat load is desirable. Equation (2.10) shows the strong influence of u_{mm} and the advantage of tolerating a high maximum velocity in the occupied zone. Therefore it is important that the design procedure is able to lay down a system which gives a velocity u_{mm} close to 0.15 m/s or similar design velocity. The equation also shows the advantage of a low K_a -value, which corresponds to a high initial diffusion and is partly achieved by a semi-radial or radial flow in the wall jet below the ceiling. The supply air diffuser in the subtask 1 work does have a high initial diffusion, and a semi-radial wall jet is generated in the ceiling regions, see reference [45].

2.3.2 Zonal models

Zonal models are a promising way to predict air movement in a room with respect to comfort and gradient of temperature because they require extremely low computer time and may be therefore rather easily included in multizone air movement models.

In Annex 20, subtask 1 the ability of zonal models to predict the thermal behaviour of air have been studied by Inard et al. [9,56]. They developed a five zone and a two zone simplified model with the support of test case D (natural convection with a radiator) and according to the monozone simulation procedure presented by Lemaire [46].

The basic assumption of zonal models is to split the air volume of a heated room into several zones coupled via mass and enthalpy flows. The arbitrary division of the indoor air volume into elementary zones requires at first a knowledge of the different kind of flow we are supposed to find in a real case. Furthermore, writing continuity and energy balance equations in each zone is not sufficient to ensure the closure of the problem. So, the identification of one or various enthalpy flows relative to the selected flow pattern is a necessary task. This one has to be realized by theoretical or experimental studies dealing with each classic configuration.

The five zone model

The indoor air volume is split into five zones connected to the following air mass flow rates: air leaving the radiator (T_{p1}), thermal plume (T_p), upper zone (T_u), central zone (T_{roa}) and lower zone (T_l). The convective network is shown in figure 2.7.

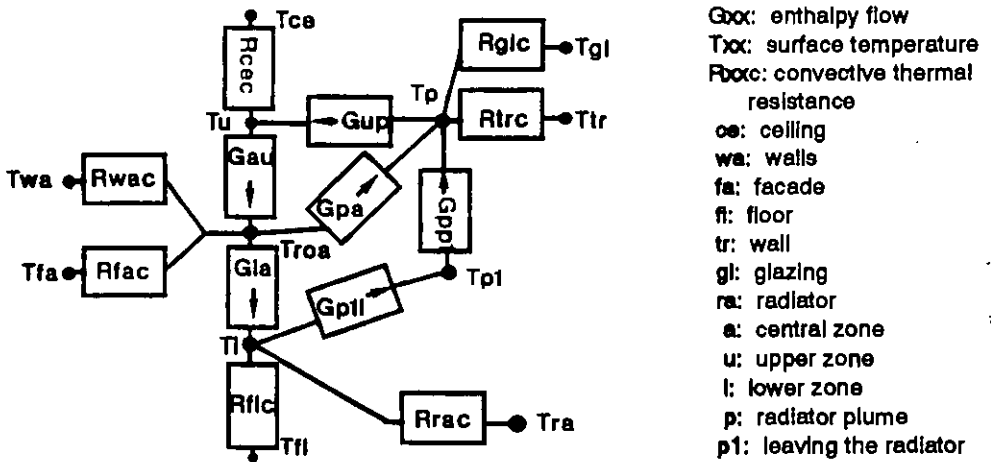


FIGURE 2.7 Convective network of test room with five zones

From the expression of air mass flow rate in the plume from the radiators [57] and assuming that the radiator is located at 0.1m from the floor, we write:

$$G_{pp1} = 9.10^{-3} C_p \left[\left(\frac{T_{ra} - T_l}{R_{rac}} \right) / L_{ra} \right]^{1/3} (H_{ra} + 0.1 - z_0) L_{ra} \quad (2.11)$$

$$G_{up} = 9.10^{-3} C_p \left[\left(\frac{T_{ra} - T_l}{R_{rac}} - \frac{T_p - T_{gl}}{R_{glc}} - \frac{T_p - T_{tr}}{R_{trc}} \right) / L_{ra} \right]^{1/3} (\text{height} - z_0) L_{ra} \quad (2.12)$$

where L_{ra} and H_{ra} are respectively the length and the height of the radiator. z_0 is the virtual origin of the radiator plume. The remaining enthalpy flows are calculated from G_{pp1} and G_{up} ,

based on mass balances, and the air temperatures are calculated from the zone energy balance equations which can be derived from the network.

The two zone model

In this model, the convective scheme (fig.2.8) is based on the studies carried out by Howarth [58]. The room is divided into two zones, an upper one and a lower one separated by a neutral plane, across which the net vertical air mass flow rate is equal to zero.

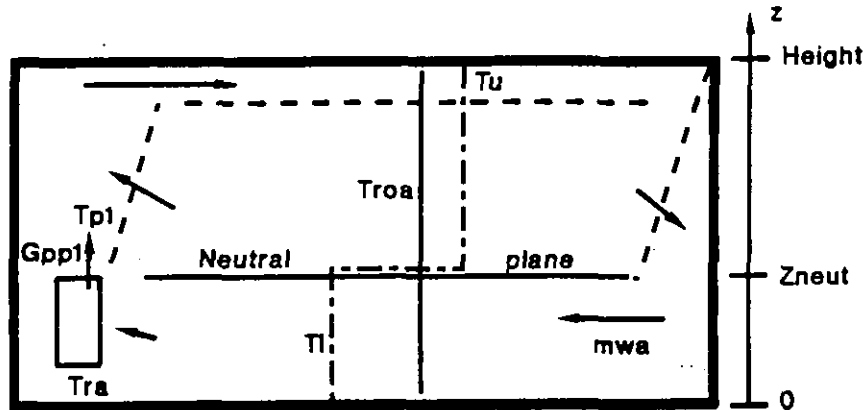


FIGURE 2.8 Convective scheme of a two zone model

The main difference with the five zone model is that the plume behaviour is entirely described by only one equation. This equation is a thermal balance for the upper zone, the central zone and the thermal plume of the five zone model. Splitting the room air volume results in the unknown temperatures: mean air leaving the radiator (T_{p1}), upper zone mean air temperature (T_u), lower zone mean air temperature (T_l) and average air temperature of the room (T_{roa}). In order to determine these temperatures, there must be four equations to close the system.

The first equation is a balance equation between the convective heat output of the radiator and the convective heat losses at the surfaces. The second equation gives the departure temperature of the plume leaving the radiator. The third equation assumes that the radiator plume is discharged almost immediately in the upper region. Thus, this zone is in equilibrium at the departing plume temperature modified by the heat losses to the glazing, the ceiling and the wall. We get this equation from the five zone model balance equations assuming that $T_p = T_{p1}$ and $T_{roa} = T_u$. Finally, the average air temperature is computed as a mean value over the height, with z_{neut} the height of the neutral plane. It is the altitude where the uprising mass flow rate in the plume is equal to the downward mass flow rate in the cold boundary layers along the walls (m_{wa}). The four equations are given below.

$$\frac{(T_{ra} - T_l)}{R_{rac}} = \frac{(T_u - T_{ce})}{R_{cec}} + \frac{(T_l - T_{fl})}{R_{cfl}} + \frac{(T_{p1} - T_{tr})}{R_{trc}} + \frac{(T_{p1} - T_{g1})}{R_{glc}} + \phi_{conv_{wa}} \quad (2.13)$$

$$G_{pp1} (T_{p1} - T_l) = \frac{(T_{ra} - T_l)}{R_{rac}} \quad (2.14)$$

$$G_{pp1} (T_u - T_{p1}) + \frac{(T_{p1} - T_{g1})}{R_{glc}} + \frac{(T_u - T_{ce})}{R_{cec}} + \frac{(T_{p1} - T_{tr})}{R_{trc}} = 0 \quad (2.15)$$

$$T_{roa} \text{ Height} = T_l z_{neut} + T_u (\text{Height} - z_{neut}) \quad (2.16)$$

2.3.3 Database model

This simplified method has been developed recently by Chen et al.[59,60]. The method allows design engineers, consulting engineers and HVAC students to assess indoor airflow patterns, indoor air quality, and draught risk without doing a costly experiment or running an expensive and complicated flow field simulation code. For this purpose a pre-calculated airflow database has been set up. The database includes a number of precalculated indoor airflow patterns and the corresponding air quality and draught risk maps for given spaces under different types of ventilation systems. The given spaces and ventilation systems are selected to be within the range of common interest of design and consulting engineers. The most important information in the database is compiled as a handbook, which provides engineers with the general information and typical results of any design case. In addition, a magnetic tape or disk is used to store all the data of the database together with a simple computer program. The tape can be used on a work station to allow an engineer to obtain more detailed information of the cases he is interested in. The database is constructed in a functional way and can be easily used by an engineer who has little knowledge of flow modelling. The database will also be used for educational purposes giving HVAC students a more comprehensive concept of indoor airflow. The database provides information about the field distributions of air velocity, temperature, turbulence, and contaminant concentration due to contaminant sources at different locations.

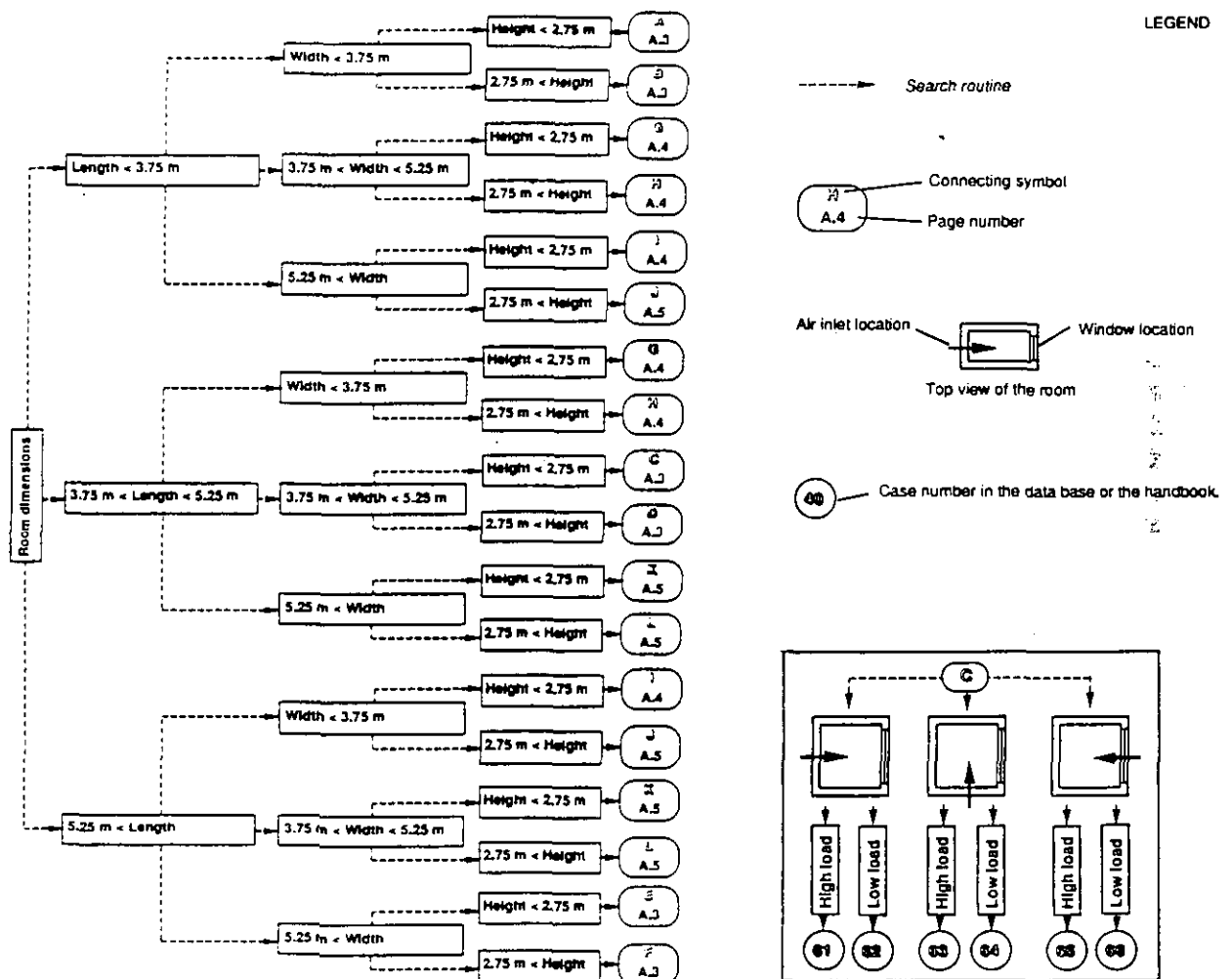


FIGURE 2.9 The case search routine for the displacement ventilation system.

The present structure of the database is as follows. Each type of ventilation system constitutes its own domain of cases, cooling and heating situations creating further sub-domains. For every sub-domain, there exist parameters of primary importance, such as geometry (length, width and height), space loads and locations of air inlet openings, etc. Each combination of the parameters represents a case for which the whole information is given. Since there are certainly differences between a specific design case and the corresponding case in the database, it is necessary to estimate the error caused by the differences. General rules for interpolating the results from the database to a specific case are discussed in [61],[62].

For every sub-domain there exist also parameters of secondary importance, e.g. window size, lighting location, furniture location and air supply parameters (shape, dimension and location of diffuser, flow rate and air temperature supplied). The influence of these parameters is evaluated by sensitivity studies.

The database is established by numerical simulation of room airflow, solving the full three-dimensional, time-averaged Navier-Stokes equations and using a turbulence model (low-Reynolds-number $k-\epsilon$ model with buoyancy), which was tested and validated against experiments in previous studies. The current database has been established for a well-mixed and a displacement ventilation system [60]. The case search routine for the displacement ventilation system is shown in fig. 2.9. The results of a typical pre-calculated case in the database are shown as an example in fig. 2.10 (only velocities).

Case No. 61
 1 - Inlet; 2 - Outlet; 3 - Window; 4 - Bookshelf A; 5 - Bookshelf B;
 6 - Table A; 7 - Table B; 8 - Filing cabinet A; 9 - Filing cabinet B;
 10 - Occupant A; 11 - Occupant B; 12 - Computer A; 13 - Computer B.

Room size: length 4.5 m; width 4.5 m; height 2.5 m; wall temperature 22.3 °C; all the walls and the ceiling with the same pollutant source C; the floor with pollutant source C.

Inlet: width 0.6 m; height 0.6 m; inflow 5 ach; air temperature 19.0 °C; air velocity 0.195 m/s, flow turbulence intensity 40%.

Outlet: width 0.6 m; height 0.33 m; top frame to the ceiling 0.17 m; width 2.9 m; height 1.1 m; top frame to the ceiling 0.4 m; convective heat source 150 W.

Bookshelf: length 1.4 m; thickness 0.4 m; height 1.5 m; both with same amount of pollutant source B.

Table: length 1.6 m; width 1.05 m; height 0.62 m; distance to the window 0.4 m.

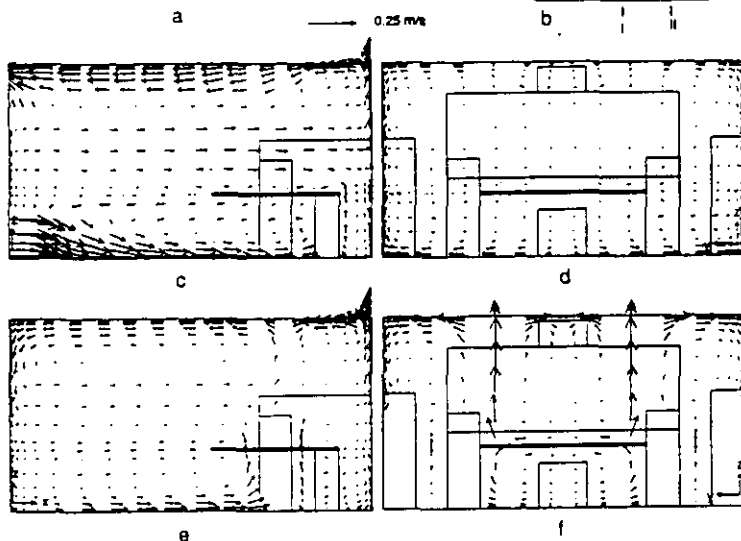
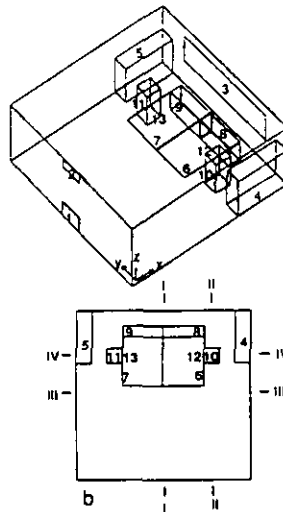
Cabinet: length 1.05 m; width 0.3 m; height 0.8 m

Occupant: length 0.4 m; width 0.4 m; height 1.25 m; heat source 60 W; one of them with pollutant source A.

Computer: (no blockage, on the tables, in front of the occupants); heat source 120 W.

The amount of each pollutant source is 1.0 air or 0.01 m³/s.

Similar cases:
 With different length: Case 13, Case 21, Case 73, Case 81.
 With different width: Case 13, Case 21, Case 73, Case 81.
 With different height: Case 67.
 With different inlet and window location: Case 63, Case 65.
 With different load: Case 62.



(a) descriptions of Case 61; (b) sketch of the case; (c) velocity in section I-I; (d) velocity in section II-II; (e); velocity in section III-III; (f) velocity in section IV-IV.

FIGURE 2.10
 An example of a typical pre-calculated case in the database.

3. EVALUATION OF PERFORMANCE OF MODELS IN PREDICTION OF FLOW PARAMETERS

3.1 Introduction

The ability to accurately predict air movement and temperature distribution in spaces offers the potential for design engineers to evaluate and optimize room air distribution systems at an early stage, leading to improved thermal comfort and ventilation effectiveness. The computer models which are used for detailed analyses are based on computational fluid dynamics (see section 2.2) and employ sophisticated numerical algorithms to satisfy the basic laws of physics. The programs are such that they are more complex and more difficult to use than those with which design engineers may be more familiar (see section 2.3). Specialised skills are required to get the best from the codes, and, as with most new techniques, a greater confidence is needed before their use can be expected to become more routine. It is the latter point concerning confidence in use which is addressed by IEA Annex 20, Subtask 1.

In subtask 1 of the Annex, which deals with single-zone spaces, laboratory experiments in similar test rooms and computer simulations have been carried out at a number of sites in Europe and North America. The data comprises information on air flow patterns and on point-by-point values of mean velocity, velocity fluctuation (turbulent velocity), temperature and contaminant concentration throughout a space.

This chapter reviews the data, highlights some of the features which the comparisons of measured and computed room air distribution have yielded and co-ordinates results reported by individual researchers. The contents of this chapter are mainly based on R.I. 1.22, 1.35 and 1.40 "Evaluation of cases B, D, E and F" as carried out by Whittle [3,63]

Besides giving a unified perspective on data from different sites to quantify the general degree of agreement, the evaluation exercise also has the potential for:

- establishing benchmarks for the validation and evaluation of computer codes for room air movement;
- highlighting advantages/limitations of the simulation methods used;
- assessing overall confidence level in computer simulations;
- indicating accuracy and repeatability of measurements and simulations;
- guiding research on simplified models of air movement and identifying problem areas where attention should be focused.

3.2 Specification of test cases

Five full test configurations and one simulation-only test case have been considered. These comprised forced convection, isothermal flow (case B) [64]; free convection with a radiator (case D) [11], mixed convection, summer cooling (case E) [65], forced convection with contaminant concentration in an isothermal flow (case F) [66], displacement ventilation flow (case G) [67] and a two-dimensional isothermal and summer cooling test case (case 2D) [68].

3.2.1 Two-dimensional test cases

The two-dimensional test case is only simulated, but its results can be compared with available experimental data. The test case represents both isothermal flow at a Reynolds number of 5,000 (2D1), and summer cooling at a range of Archimedes number (2D2). The configuration is shown in figure 3.1. The room is specified by ratios of $L/H = 3$, $h/H = 0.056$, $t/H = 0.16$, where 'L' is the room length, 'h' the inlet slot height, 't' the exhaust height and H the room height (3.0m).

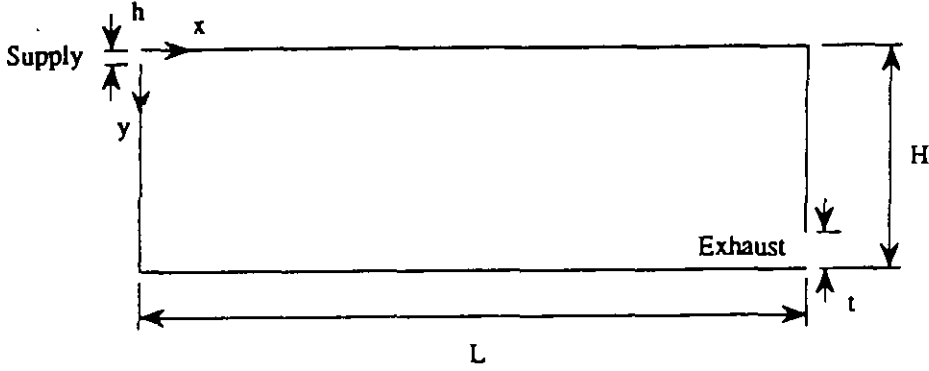


FIGURE 3.1 2D Test case configuration

Test case 2D1: isothermal

At the inlet the Reynolds number is 5,000 and the turbulence intensity 4%. For a real room with height 3.0m this corresponds with inlet velocity $u_o = 0.455\text{m/s}$ and inlet temperature $T_o = 20^\circ\text{C}$. The test case is extended with transport of contaminants with a uniform mass flux of contaminants along the floor. Experimental data for Reynolds number 5,000 has been reported previously [69]. The aim is to compare the simulated results with this data. In particular profiles on two vertical lines $x = H$ and $x = 2H$ and on two horizontal lines $y = h/2$ and $y = H - h/2$.

Test case 2D2: non-isothermal

The aim of this test case is to predict flow with a strong buoyant effect. A constant heat flux is added along the floor. The critical factor is the influence of the Archimedes number on jet penetration. The simulations are repeated for increasing Archimedes number (= increasing heat flux) until the CFD code predicts a flow with a reduced penetration depth x_o (see section 2.3.1).

The Archimedes number is defined as:

$$Ar = g \theta h / T u_o^2 \quad (3.1)$$

where h = inlet slot height (m), g = gravitational acceleration (m/s^2); u_o = inlet velocity (m/s), T = temperature level (K), θ = temperature difference between exhaust and inlet ($^\circ\text{C}$).

The penetration depth x_o depends in some cases on the initial conditions. Different values of x_o can be obtained by increasing or decreasing the Archimedes number until the same experimental conditions are reached. Each participant should predict the penetration depth as a function of Archimedes number. The maximum velocity u_m in the occupied zone can also be given as a function of the Archimedes number. The reduction of x_o is expected to occur for Ar between 0.2 and 0.12. For room height $H = 3.0\text{m}$ the Archimedes number $Ar = 0.02$ corresponds to $\theta = 0.74^\circ\text{C}$ for $u_o = 0.455\text{m/s}$ and $T = 20^\circ\text{C}$.

3.2.2 Three-dimensional test cases

Figures 3.2 and 3.3 show the geometry and basic configuration of the test room and the test conditions. The configuration of the basic test room and the measuring equipment were discussed in par. 2.1. Graphical presentation and format of data files [70] were also specified.

The supply air diffuser provides a real challenge to simulation codes and practitioners. The participants were free to represent boundary conditions at the diffuser in their own way. For a better comparison between the simulated results, it was decided that each participant would also apply the 'one-slot basic model' of the diffuser for the test cases B2, E2 and F2. The models are discussed in section 2.2.3.

The walls are assumed to be 'adiabatic' during the experiments. In simulations the participants were free to choose their own thermal boundary conditions at the walls, floor and ceiling. Some guidelines were provided as discussed in section 2.3.3.

Each test case is summarized below.

Test case B (forced convection, isothermal flow)

Test case B represents forced convection (at isothermal conditions) at three different air flow rates.

Case: B1 flow rate: $0.0158\text{m}^3/\text{s}$ (1.5 ach^{-1}).

Case: B2 flow rate: $0.0315\text{m}^3/\text{s}$ (3.0 ach^{-1}).

Case: B3 flow rate: $0.0630\text{m}^3/\text{s}$ (6.0 ach^{-1}).

Case B1 represents a low Reynolds number case. The supply air velocity in the HESCO-diffuser is about 2m/s . At this velocity some indications of low Reynolds number effects can be seen from the preliminary experiments [71]. Secondly the air flow rate is around the minimum value required to ventilate an office room. The throw of the jet is about $3/4$ of the room length.

Case B2 is regarded as the basic case. The air flow rate is around the usual value in office rooms. The supply air velocity is about 4m/s .

Case B3 represents a high Reynolds number case. The velocity measurements can be done with good accuracy, because of the high velocities. The case is therefore important for the comparison of measured and calculated results.

Test case D (free convection with radiator)

Test case D represents free convection with a radiator located beneath a cold window, with three corresponding radiator and window surface temperatures.

Case: D1 radiator surface temperature: 46°C ,
window surface temperatures: 10°C .

Case: D2 radiator surface temperature: 55°C
window surface temperature: 5°C

Case: D3 radiator surface temperature: 65°C
window surface temperature: 0°C

LEGENDA

- (1) supply air diffuser
- (2) air exhaust
- (3) window
- (4) radiator
- (5) low velo. air diffuser
- (I) heat source
- (A) contam. src. A
- (B) contam. src. B

ROOM FACES

- ceiling
- side wall
- rear wall
- side wall
- front wall
- floor

DEFINITION

parapet = area of front wall facing the radiator

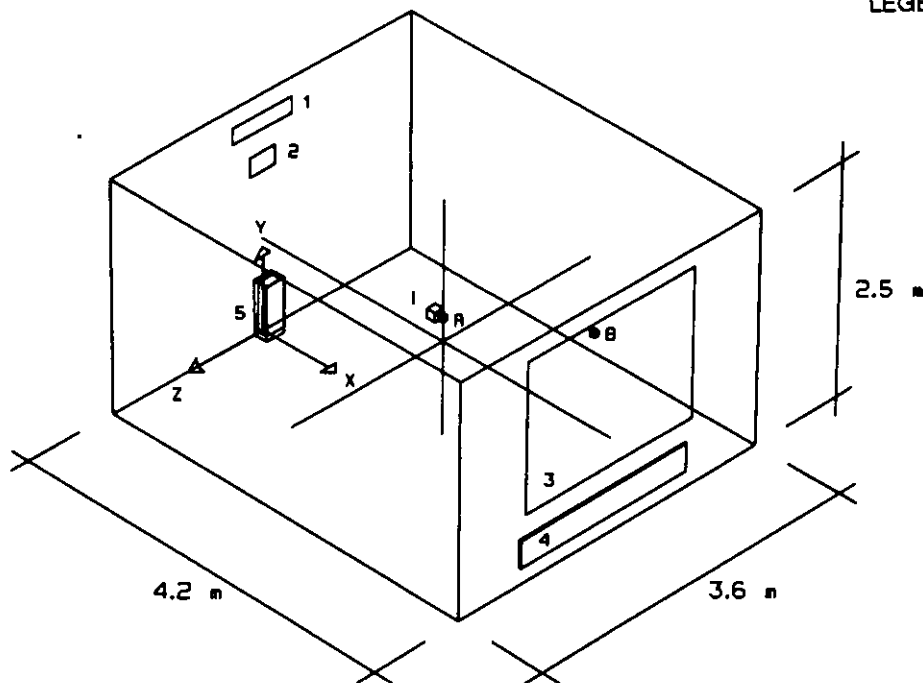
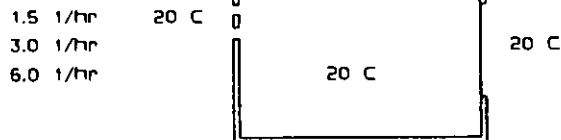
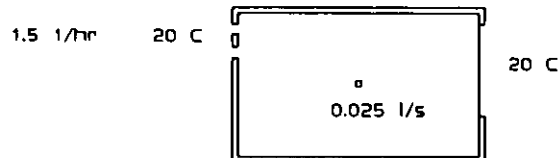


FIGURE 3.2 Geometry and configuration of the basic test room and location of measuring lines A, B and C.

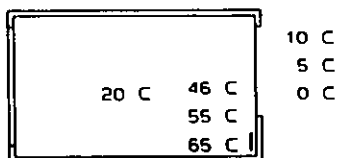
CASE B: Forced Convection, Isothermal



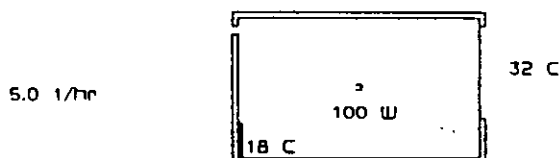
CASE F: Forced Conv., Isothermal with Contaminants



CASE D: Free Convection with Radiator



CASE G: Displacement Ventilation



CASE E: Mixed Convection, Summer Cooling

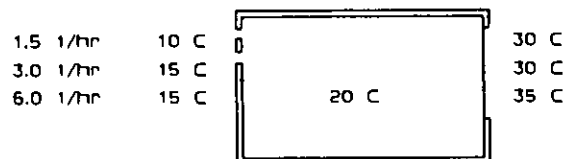


FIGURE 3.3 Survey of specified test cases.

The expected room temperature is about 20°C. In simulations, if no radiation model is used, surface temperatures of 19°C for the front wall (excl. parapet) and 20°C for the remaining walls were proposed. The participants were free to use their own modelling of the radiator-parapet, though some guidelines were provided as discussed in section 2.2.3.

Case D1 represents a situation with double glazing and ambient temperature ~ -10°C. The required heat load is about 19W/m² floor area

Case D2 represents a situation with single glazing and ambient temperature ~ 0°C. The required heat load is about 28W/m² floor area.

Case D3 represents a situation with single glazing and ambient temperature ~ -10°C. The required heat load is about 38W/m² floor area.

Test case E (mixed convection, summer cooling)

Test case E represents mixed convection under summer cooling conditions at three different supply air flow rates.

Case: E1 flow rate: 0.0158 m³/s (1.5 ach⁻¹),
supply air temperature: 10°C,
window surface temperature: 30°C.

Case: E2 flow rate: 0.0315 m³/s (3.0 ach⁻¹),
supply air temperature: 15°C,
window surface temperature: 30°C.

Case: E3 flow rate: 0.0630 m³/s (6.0 ach⁻¹),
supply air temperature: 15°C,
window surface temperature: 35°C.)

The expected room temperature is around 20 - 22°C. In simulations, if no radiation model is used, surface temperatures of 22°C for the front wall (excl. parapet) and 21°C for the remaining walls were proposed.

Case E1 represents a high Archimedes number case. The supply air jet may detach and cause discomfort in the occupied zone. This situation may occur if outdoor inlets are used in exhaust air ventilation. The case may be difficult to simulate. The required cooling load is quite small, about 15W/m² floor area.

Case E2 has an air flow rate around the usual value in office rooms. The cooling load is not much higher than in case E1.

Case E3 represents a low Archimedes number case. The cooling load is, about 30W/m² floor area, which is quite normal for office rooms..

Test case F (forced convection with contaminants)

Test case F represents contaminant concentration in forced convection (at isothermal conditions) with three different densities of contaminant. The contaminant is released at the centre of the room. The air flow rate and contaminant flow rates are 0.0158m³/s (1.5 ach⁻¹) and 0.025 litre/s, respectively.

- Case: F1 contaminant density 0.8 kg/m³
- Case: F2 contaminant density 1.2 kg/m³
- Case: F3 contaminant density 1.8 kg/m³

The tests are based on case B1 but with the addition of a contaminant released in the centre of the room.

Test case G (displacement ventilation)

Test case G represents displacement ventilation under average summer cooling conditions with one person in the middle of the room generating heat and contaminants. A second contaminant source is located in the upper corner near the window.

- Case: G1 flow rate: 0.0525m³/s (5.0 ach⁻¹)
 supply air temperature: 18°C
 window surface temperature: 32°C
 heat source: 100 W electric bulb
 contaminant release: 0.025litre/s each
 contaminant density: 1.2 kg/m³

The cooling load is about 20W/m² floor area.

In order to get a better representation of the heat generation by a person, a case G2 was specified with a black painted cylinder (height 1m, diam. 0.4m) located on the floor in the middle of the room. This case, however, remains to be studied.

3.3 Results and discussion

3.3.1 Measurements, simulations and data analysis

Measurements

Results were obtained from participants generally according to a prescribed format [72,73]. A full data set for test cases B, D and E comprised 560 points at which mean air speed (U_m), turbulent velocity (U_t) and temperature (T) were measured or predicted. In the case of contaminant concentration (case F), then, of course, concentration was also specified. In addition, data on the velocity decay of the supply air jet and the jet penetration length related to Archimedes number were obtained from some participants for test cases B and 2D, and E, respectively.

The specification of 560 points meant that those undertaking simulations were required to limit the data supplied. As expected, simulations were carried out with many thousands of calculation nodes. However, for those undertaking measurements, the requirements of the 560 specified points proved to be demanding. Some contributors concentrated their attention in measuring the detailed flow structure in the jet, whilst others were able to measure throughout the space and mostly, but not universally, at all the agreed positions.

The measuring equipment and the location of measuring points are discussed in section 2.1. As a subset of these locations, an occupied zone is defined up to a height of 1.8m and to within 0.6m of walls [74,75]. Occupied zone data is of interest to designers in assessing thermal comfort and ventilation effectiveness.

Simulations

The computer codes were all of finite volume formulation and all utilised a pressure-correction method. (See section 2.2) The codes were: CALC-BFC, EOL3D, EXACT3, FLUENT, KAMELEON, PHOENICS, SIMULAR-AIR, WISH3D and TEACH derivatives. A number of zonal models were also used, operated by INSA/CSTB, France. (See section 2.3)

CFD simulations were carried out with the different codes identified above, with collective guidance given on options for modelling boundary conditions such as the supply terminal and the radiator as discussed in section 2.2.3. For the supply terminal, a number of inlet models were defined.

The code operators were free to generate meshes which they felt were appropriate, bearing in mind the need to resolve certain features of the flow such as the supply air jet and boundary layers, whilst also recognising practical limitations associated with computing resources, code capabilities and project time-scale. Some contributors investigated different options such as specifying boundary conditions, influence of mesh resolution and alternative differencing schemes. The difference schemes used include Upwind (UDS), Hybrid (HDS), Power Law (PLDS) and QUICK. All CFD simulations were carried out with turbulence represented using the two-equation k-epsilon model. Most turbulence models incorporated the buoyancy-extension to represent the generation or suppression of turbulence energy due to temperature gradient, and some models incorporate low Reynolds number variants [76,77] based on Lam and Bremhorst [30] or Jones and Launder [78].

Almost all simulations were carried out in one half of the room, assuming symmetry.

Table 3.1, 3.2 and 3.3 identify individual simulations. More detailed information on the methods used in these studies can be found in participants' individual reports listed in the references section.

Data analysis

The fundamental quantities which are calculated and compared are the mean air speed (U_m), air temperature (T) and contaminant concentration. However, the mean air speed from measurements using an omni-directional probe is the time-averaged value of instantaneous air speed, whilst in simulations it is the magnitude of the mean velocity. These are not identical physical quantities since averaging is performed differently. To ensure consistency between measurements and simulations [64] a modified air speed has been defined, where the modified air speed is,

$$U^* = (U_m^2 + U_t^2)^{0.5} \quad (3.2)$$

The turbulent velocity (U_t) from measurements is the standard deviation of velocity (given by an omnidirectional probe), but in simulations it is $(2k)^{1/2}$ where 'k' is the turbulent kinetic energy per unit mass. The modified speed has been presented only for the averaged comfort parameters and for some statistical comparisons. In practice, the modified air speed is very similar to mean air speed.

Measurement and simulation data are considered in the following ways.

Flow patterns. A comparison of flow patterns provide a first and qualitative indication of whether agreement exists between data sets. Indications are given in the figures of flow patterns and contours of velocity and temperature for selected cases. These are reproduced from participants' reports. In the case of measured data, speed contours are shown rather than

TABLE 3.1 Test case references: case B.

Ref.	Code	Inlet model	Diff. scheme	Grid XxYxZ	Radiator model	High or low Re	Full or half room
B1001DK	TEACH3D	basic	HDS	32x31x16	-	high	half
B2001DK	TEACH3D	basic	HDS	32x31x16	-	high	half
B3001DK	TEACH3D	basic	HDS	32x31x16	-	high	half
B1004DK	TEACH3D	pres.vel.	HDS	32x31x16	-	high	half
B2004DK	TEACH3D	pres.vel.	HDS	32x31x16	-	high	half
B3004DK	TEACH3D	pres.vel.	HDS	32x31x16	-	high	half
B1_CTH_C	CALC-BFC		HDS	22x25x24	-	high	half
B2_CTH_C	CALC-BFC		HDS	22x25x24	-	high	half
B3_CTH_C	CALC-BFC		HDS	22x25x24	-	high	half
B1FRG	FLUENT		PLS	24x26x15	-	high	half
B2FRG	FLUENT		PLS	24x26x15	-	high	half
B3FRG	FLUENT		PLS	24x26x15	-	high	half
B1CO3SF1	WISH3D	basic	UDS	20x21x15	-	high	half
B2CO3SF1	WISH3D	basic	UDS	20x21x15	-	high	half
B2CO4SF1	WISH3D	basic	UDS	30x30x20	-	high	half
B3CO3SF1	WISH3D	basic	UDS	20x21x15	-	high	half
B2CD	EXACT3	basic	HDS	32x36x23	-	high	half
B1POOINL	WISH3D	pres.vel.	UDS	20x22x21	-	high	half
B2POOINL	WISH3D	pres.vel.	UDS	20x22x21	-	high	half
B2POO2NL	WISH3D	pres.vel.	UDS	40x44x21	-	high	half
B3POOINL	WISH3D	pres.vel.	UDS	20x22x21	-	high	half
B2B00INL	WISH3D	basic	UDS	20x22x14	-	high	half
B2B002NL	WISH3D	basic	UDS	30x33x21	-	high	half
B1CH	PHOENICS		UDS	28x29x15	-	low	half
B2CH	PHOENICS		UDS	28x29x15	-	low	half
B3CH	PHOENICS		UDS	28x29x15	-	low	half
B1GER	SIMULAR-AIR			18x21x12	-	high	half
B2GER	SIMULAR-AIR			18x21x12	-	high	half
B3GER	SIMULAR-AIR			18x21x12	-	high	half
B1CO1SF1	WISH3D		UDS	25x28x14	-	high	half
B2CO1SF1	WISH3D		UDS	25x28x14	-	high	half
B3CO1SF1	WISH3D		UDS	25x28x14	-	high	half
B20F	EOL3D	pres vel.	-	32x36x26	-	high	half
B2N2	KAMELEON	basic	PLS	20x22x18	-	high	half

vector plots.

Key comfort parameters. The thermal comfort of occupants and air movement in the room can be assessed by consideration of comfort parameters such as average air speed, turbulence, and air temperature, and the maximum and minimum air temperatures in the occupied zone. The measured data shown is that for the whole of the occupied zone whilst the simulation data was generated mainly for half the zone (by specifying a symmetry boundary along the middle of the room).

Statistical correlations and RMS differences. Some early analysis was carried out using a statistically-based point-by-point comparison of data using calculations of linear correlation coefficient and RMS error.

The sample linear correlation coefficient (SCC) and root mean square of the difference (RMS) was calculated between each pair of data sets for the modified air speed, the turbulent velocity and the air temperature. Thus, the results from participant A were compared with those of

TABLE 3.2 Test case references: case D, E, F, and G.

Ref.	Code	Inlet model	Diff. scheme	Grid XxYxZ	Radiator model	High or low Re	Full or half room
D1Q001NL	WISH3D	-	UDS	27x29x18	heat flux	high	half
D2Q001NL	WISH3D	-	UDS	27x29x18	heat flux	high	half
D3Q001NL	WISH3D	-	UDS	27x29x18	heat flux	high	half
D1FRG	FLUENT	-	PLS			low	half
D2FRG	FLUENT	-	PLS			low	half
D3FRG	FLUENT	-	PLS			low	half
D1CO2SF1	WISH3D	-	UDS	26x26x15	heat flux	high	half
D2CO2SF1	WISH3D	-	UDS	26x26x15	heat flux	high	half
D3CO2SF1	WISH3D	-	UDS	26x26x15	heat flux	high	half
D1GER	SIMULAR-AIR			18x17x12	wall func	high	half
D2GER	SIMULAR-AIR			18x17x12	wall func	high	half
D3GER	SIMULAR-AIR			18x17x12	wall func	high	half
D2COSF1	WISH3D	-	UDS	27x30x16	-	high	half
E1CO2SF1	WISH3D	basic	UDS	20x21x15	-	high	half
E2CO2SF1	WISH3D	basic	UDS	20x21x15	-	high	half
E3CO2SF1	WISH3D	basic	UDS	20x21x15	-	high	half
E2CD	EXACT3	basic	HDS	32x36x23	-	high	half
E1GER	SIMULAR-AIR			16x21x12	-	high	half
E2GER	SIMULAR-AIR			18x21x12	-	high	half
E3GER	SIMULAR-AIR			18x21x12	-	high	half
E2CO1SF1	WISH3D	basic	UDS	20x21x15	-	high	half
E2N2	KAMELEON	basic	PLS	20x22x18	-	high	half
E1P001NL	WISH3D	pres.vel.	UDS	26x22x21	-	high	half
E2P001NL	WISH3D	pres.vel.	UDS	26x22x21	-	high	half
E3P001NL	WISH3D	pres.vel.	UDS	26x22x21	-	high	half
E2B001NL	WISH3D	basic	UDS	20x22x14	-	high	half
E2B002NL	WISH3D	basic	UDS	30x33x21	-	high	half
E1FRG	FLUENT		PLS			high	half
E2FRG	FLUENT		PLS			high	half
E2FRGXQ	FLUENT		QUICK			high	half
E3FRG	FLUENT		PLS			high	half
F2C01SF1	WISH3D	basic	UDS	26x28x16	-	high	half
F2P001NL	WISH3D	pres.vel.	HDS	20x22x21	-	high	half
G1P001NL	WISH3D	-	HDS	33x34x25	-	high	half

participant B for the corresponding measuring points.

In practice, correlation coefficients and RMS difference were relatively large both comparing measured to measured and calculated to calculated data. The nature of room air movement, which is characterised by large amplitude and low frequency velocity fluctuations, is such that point-by-point comparisons do not yield meaningful results. Therefore, analyses using this approach was discontinued.

Profiles/graphs. Velocity decay with distance from the diffuser, variation of maximum (or mean) velocity in the room and penetration length of the jet in summer cooling have been identified as a critical factors in quantifying agreement. Examples of some of these graphs are shown in this report.

3.3.2 Two-dimensional test cases

Very detailed computations are possible for this particular test case, and useful data has been generated. A survey of performed simulations is given in table 3.3

TABLE 3.3 Test case references: two-dimensional cases 2D1 and 2D2

Ref.	Case	Investigator	Code	Diff. scheme	Grid XxYxZ	Additional profiles	High or low Re	Full or half room
[79] C	D1D2	Sald	EXACT3	HDS	37x34x15	-	high	half
[80] CH	D1D2	Chen	PHOENIX-84	UDS		temp.	low	-
[81] D2	D1D2	Vogl et al.	FLUENT	PLDS/ QUICK	56x62x1	-	high	-
[77] DK	D1	Skovgaard et al.	TEAM	PLDS	38x78x1	-	low	-
[83] NL	D1D2	Lemaire	WISH3D	UDS	36x30x1	conc.	high	-
[84] SF	D1D2	Heikkinen et al.	FLUENT/ WISH3D	PLDS/ QUICK	45x26x1	conc.	high	-

Test case 2D1: isothermal

Vogl et al. [81] Figure 3.3 shows predicted velocity field u/u_0 and distribution of turbulent intensity $\sqrt{u^2}/u_0$ which agree well with others. A comparison is shown with predictions from Skovgaard et al. (fig.3.4) with a low-Reynolds-model. Figure 3.5 shows comparisons at section $X/H = 1.0$ of power law and QUICK differencing, with simulations by Chen and with measurements. The general trends of velocity and turbulent intensity are represented reasonably well by all simulation approaches but some discrepancies exist in certain areas. In general, the simulations by Vogl and Renz, along with most others, do not predict recirculation in the corners, and under-predict turbulence levels particularly near the floor.

Heikkinen et al. [84]. Results with WISH3D and FLUENT with PLDS-scheme show that the flow pattern is well predicted apart from the lack of recirculation in the upper corner at the wall containing the exhaust. A good correspondence of velocity decay and velocity fluctuation is obtained up to $X/H = 2.0$, beyond which the predicted velocity decay is more rapid. Figure 3.6 shows a comparisons of velocity profile at $X/H = 2.0$ between WISH, FLUENT (PLDS and QUICK) and measurement. The maximum velocity near the floor occurs at the same position in x-direction as measurements indicated, but the value is 8% lower. The velocity fluctuation is less well predicted near the floor.

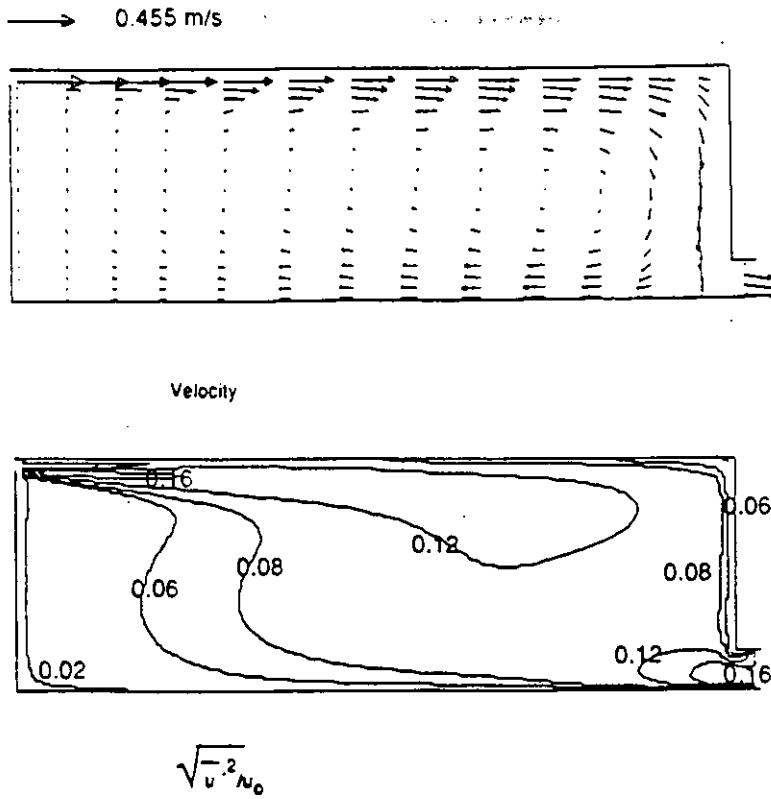


FIGURE 3.3 Test case 2D1: Vogl et al. (high Reynolds model)
Velocity field u/u_0 and turbulent intensity $\sqrt{u'^2}/u_0$ (from $\sqrt{k} = 1.1 \sqrt{u'^2}$)

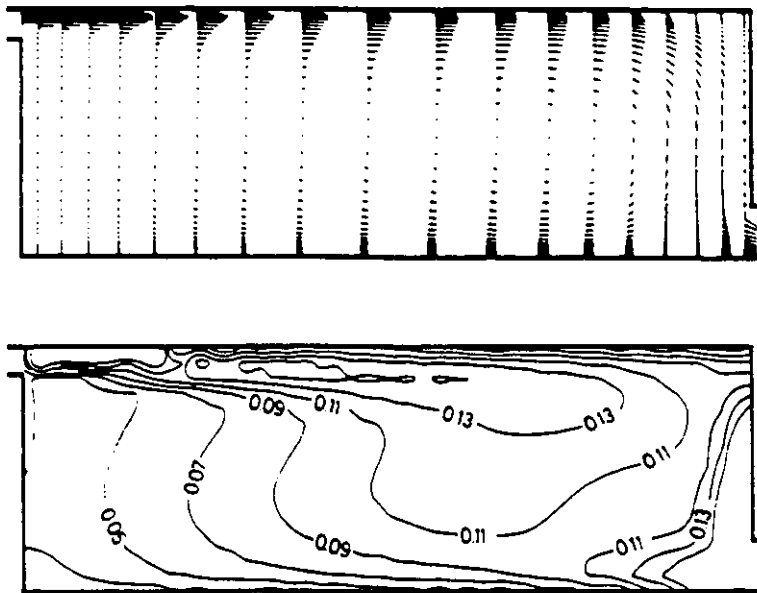


FIGURE 3.4 Test case 2D1: Skovgaard et al. (low Reynolds model)
Velocity field u/u_0 and turbulent intensity $\sqrt{u'^2}/u_0$ (from $\sqrt{k} = 1.1 \sqrt{u'^2}$)

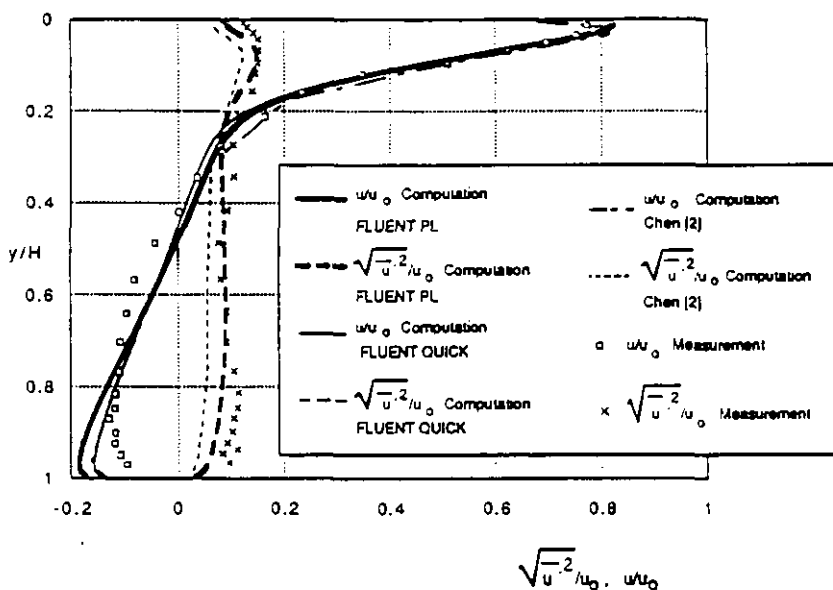


FIGURE 3.5
 Test case 2D1: Vogl et al.
 Comparison between the
 computed (FLUENT
 QUICK, FLUENT PLDS,
 Chen) and measured
 (Nielsen) mean velocity
 and turbulent intensity in
 section $x/H = 1.0$

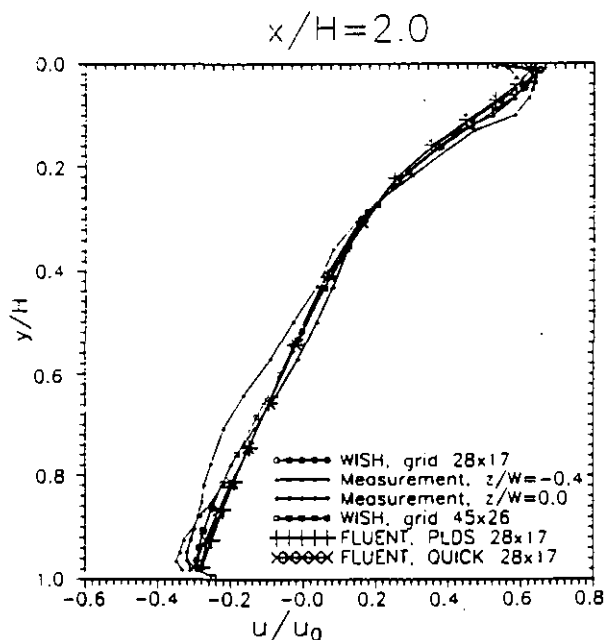


FIGURE 3.6
 Test case 2D1: Heikkinen
 et al.
 Comparison between
 computed and measured
 mean velocity in section
 $x/H = 2.0$

The best result for velocity near the floor level was found using QUICK on a coarse grid where the velocity was within 6% of measurement. Finer grids resulted in an over-estimate of wall friction due to the wall function used.

Lemaire [83]. The prediction of velocity decay corresponded quite well with measurements except that the measured recirculation in the corners was not predicted (fig. 3.7). The turbulent fluctuation near the floor was, as with Heikkinen et al., under-predicted. The comparison of predicted and measured concentration in the isothermal flow was good (fig. 3.9).

Skovgaard et al. [77] used a low Reynolds number $k-\epsilon$ turbulence model (fig. 3.8). It is stated that the low Reynolds number model demanded a fine grid be used in the inlet because of its location directly beneath the ceiling. Comparison of velocity and turbulence quantities are made with LDA measurements obtained in a scale model and with other simulations. At sections $X/H = 1.0$ and 2.0 the agreement with the measured velocity and turbulence levels is good. Generally, the velocity decay in the jet is slightly faster than the measurements suggest and hence the growth in the jet width is over-predicted. An important observation is that a small

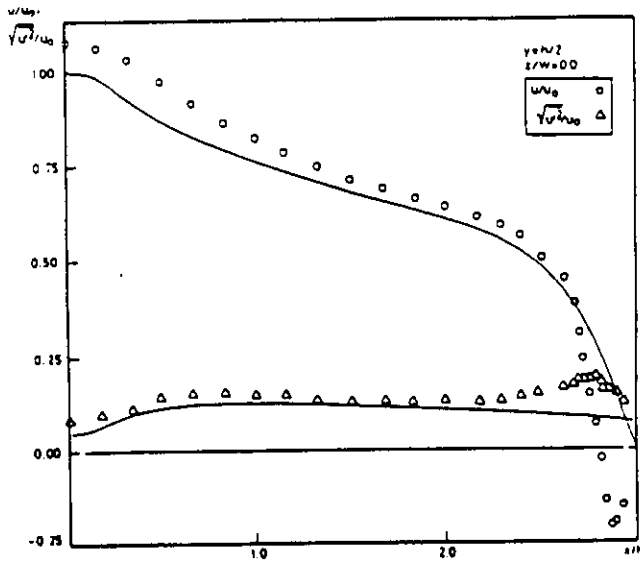


FIGURE 3.7
Test case 2D1: Lemaire
Comparison between
computed and measured
mean velocity and
turbulent intensity in
section $y = h/2$

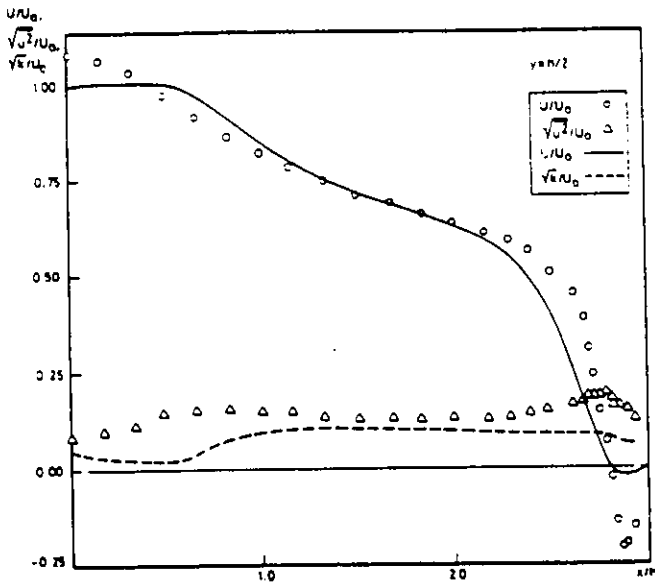


FIGURE 3.8
Test case 2D1:
Skovgaard et al.
Comparison between
computed and measured
mean velocity and
turbulent intensity in
section $y = h/2$

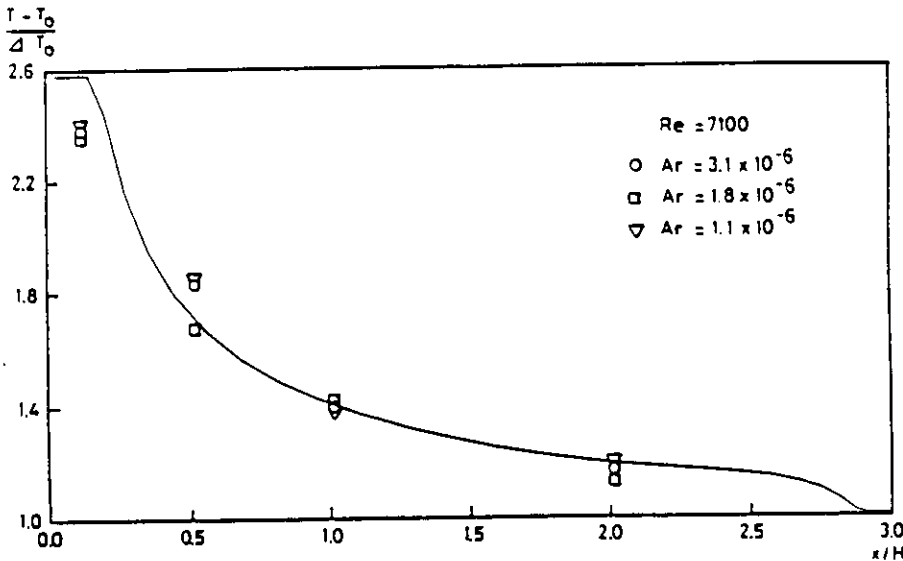


FIGURE 3.9
Test case 2D1: Lemaire
Comparison between
computed and measured
normalised
concentrations in section
 $y/H = 0.75$

recirculation is predicted at the corner of the room opposite the inlet, although the magnitude is very much smaller than the measured values. Recirculation at the opposite corner near the floor was not predicted. Some comparisons of other simulation results with measurement indicate that a one-equation turbulence model under-predicts the velocity in the wall jet beneath the ceiling. Other codes compared are a TEACH derivative and a vorticity-streamfunction code.

Chen [80] used a low Reynolds number turbulence model. In the isothermal case, results appear similar to those of others, the main features being that the velocity and turbulence trends are well represented but the corner recirculation are not predicted and turbulence levels are under-predicted. A good correspondence between predicted and measured concentration was achieved. It was suggested that the small discrepancies were due to Reynolds number differences.

Said [79]. A three-dimensional grid of 37 x 34 x 15 (18870 cells) was used. The trends of velocity and turbulence intensity were reproduced quite well, but as with other simulations corner recirculations were not predicted, and turbulence levels were under-predicted.

Test case 2D2: non-isothermal

Chen [80]. No intermediate jet penetration length could be found. The critical Archimedes number at which the flow patterns changed was 0.143 (fig. 3.10). Measurements reported by Nielsen [68] indicated a critical Archimedes number of 0.02. However, Chen points out that the ratio of slot height to room height and Reynolds number used in the experiment were different to those specified in the simulations.

Heikkinen et al.[84] found that jet penetration length was equivalent to the room length at Archimedes number of 0.12 or less, and almost zero at Archimedes number of 0.16 or more. Intermediate jet penetrations were not found except during the course of iteration. It was stated as very important to ensure that the equations are well converged before accepting a solution. Good practice is to periodically inspect the solution during convergence, site the monitor location in an intelligent way and to inspect the traces of residual errors.

Lemaire [83] found that the predicted flow pattern was dependent on initial conditions. A hysteresis effect was evident. Again, as with the Heikkinen data, no intermediate penetration lengths were observed. Starting from uniform initial fields the Archimedes number at which the flow pattern changed was 0.173 to 0.175.

Vogl et al.[81]. The simulations confirm previous simulation results by predicting an absence of intermediate jet penetration length. The critical Archimedes number, which was 0.15 to 0.16, was found to be independent of starting conditions.

Said [79]. In the simulations, some three-dimensional effects are evident in the flow field plots which indicate a reduction in penetration length as the Archimedes number is increased. The highest Archimedes number modelled was 0.143 which correspond to the critical Archimedes number found by Chen. At this condition evidence of reverse flow exists at two-thirds distance along the room, although three-dimensional effects were strong making it is difficult to interpret the flow field (fig. 3.11). However, this is an important observation which needs further investigation through three-dimensional simulation.

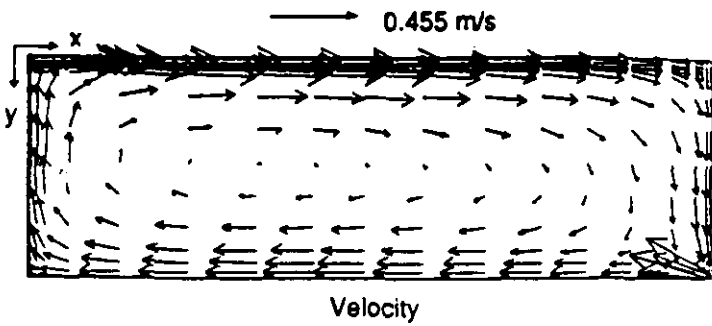


FIGURE 3.10a
Test case 2D2: Chen
Velocity and temperature
distributions if $Ar = 0.142$

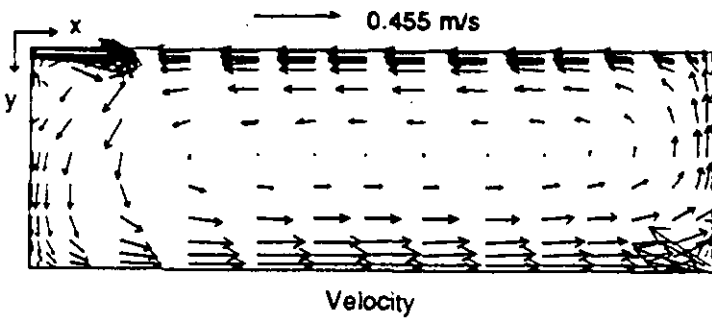
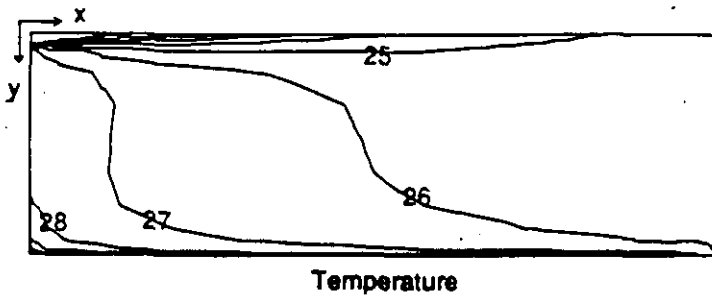


FIGURE 3.10b
Test case 2D2: Chen
Velocity and temperature
distributions if $Ar = 0.143$

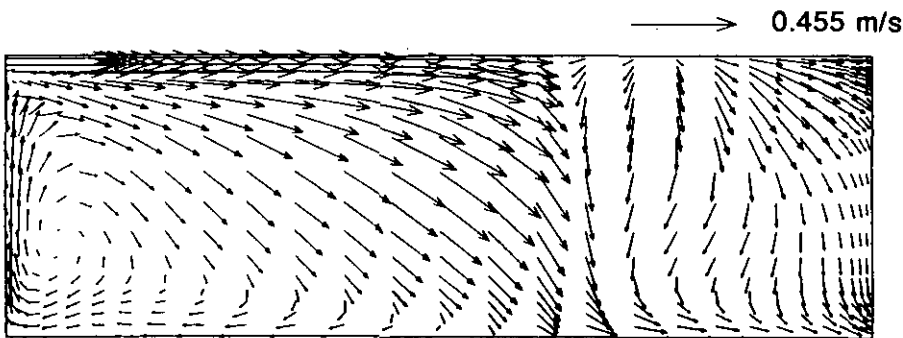
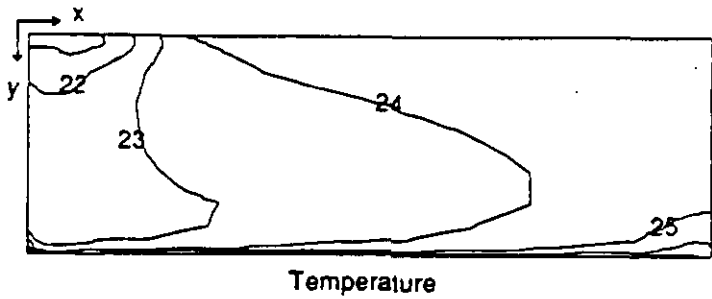


FIGURE 3.11 Test case 2D2 (3D-calc.): Said.
Velocity if $Ar = 0.143$.

3.3.3 Test case B (forced convection, isothermal)

Flow patterns

Air flow patterns for the isothermal case (B1, B2 and B3) are well predicted by the simulation models and encouraging agreement is obtained between air speeds. Some asymmetry effects are evident from measured data, which could not be investigated using the symmetry-plane assumptions imposed by the modellers.

Test case B1. A predicted air flow pattern on the room centre-line for test case B1 is shown in Figure 3.12 (Lemaire and Elkhuizen [44]). A prescribed velocity inlet model has been used. Velocities in the occupied zone are below 0.1m/s. Measured air speeds are shown in figure 3.13 (Lemaire and Crommelin [18]), and further predictions are shown in figure 3.14 (Skovgaard and Nielsen [85]). The measured air speed at floor level is 0.05m/s and the predicted is in the region of 0.06m/s, indicating very good agreement. However, it should be noted that the accuracy of measurement at these low velocities tends to degrade and that only one set of measured data exists.

Test case B2. Measured air speeds on the centre-line of the room for test case B2 are shown in figure 3.15 (Blomqvist [14]) and figure 3.16 (Heikkinen [16]). A selection of predicted flow patterns using different inlet models are shown in figure 3.17 (Fontaine [86]), figure 3.18 (Heikkinen and Piira [87]), figure 3.19 (Fürst [41]) and figure 3.20 (Johanson [88]). A uniformity of flow pattern is evident. Contours of air speed from simulations are shown in figure 3.21 (Lemaire and Elkhuizen [44]) and figure 3.22 (Vogl and Renz [89]). Predicted air speeds at near floor level are in the range 0.1 to 0.2m/s compared to measured speeds of 0.15m/s and slightly higher.

Test case B3. A comparison of measured and predicted air speed for test case B3 is shown in Figure 3.23 (Heikkinen [86]) and figure 3.24 (Skovgaard and Nielsen [85]). The predicted and measured air speeds at near floor level are up to 0.35m/s.

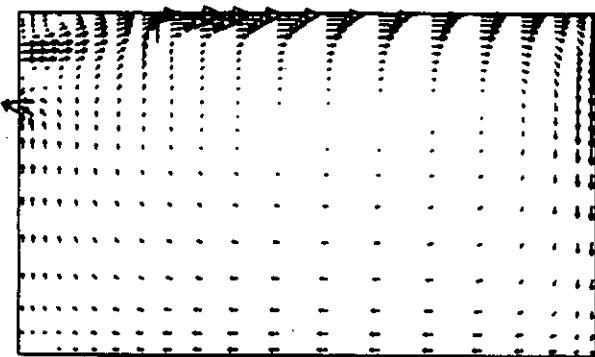


FIG 3.12 Case B1, simulated, $z = 0.0\text{m}$,
Lemaire, B1P001NL, flow pattern

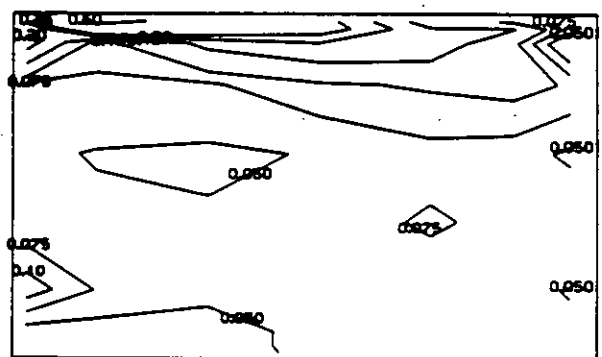


FIG 3.13 Case B1, measured, $z = 0\text{m}$,
Lemaire, B1M001NL, iso-vels

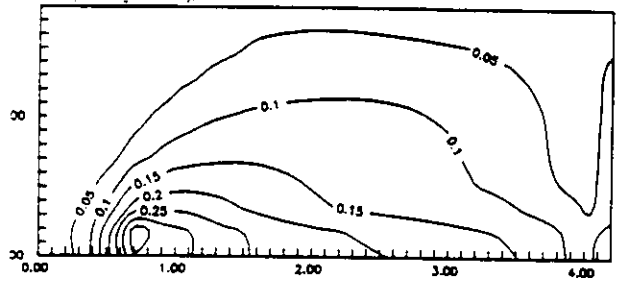
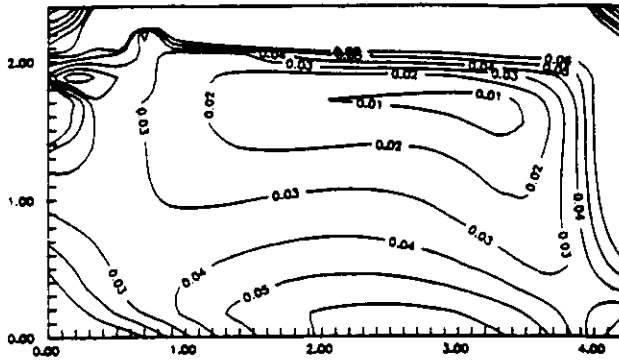


FIGURE 3.14 Case B1, simulated, $z = 0.0\text{m}$ (left) and $y = 2.36\text{m}$ (right), Skovgaard et al, B1004DK, iso-vels

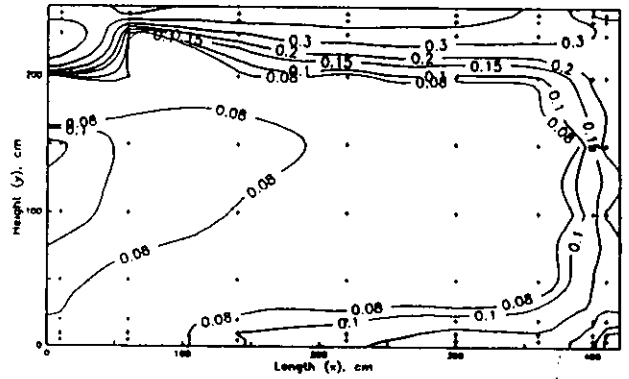
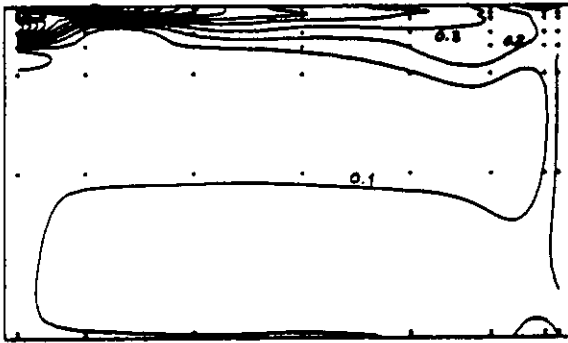


FIG 3.15 Case B2, measured, $z = 0.0\text{m}$, Blomqvist, B2T01SIB, iso-vels

FIG 3.16 Case B2, measured, $z = 0.0\text{m}$, Heikkinen, B2T03SF, iso-vels

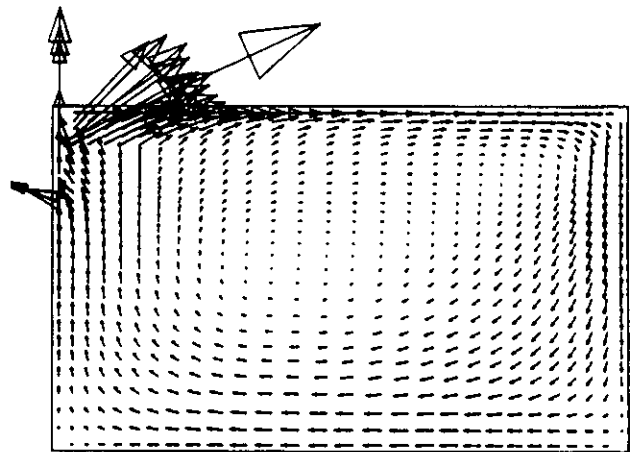
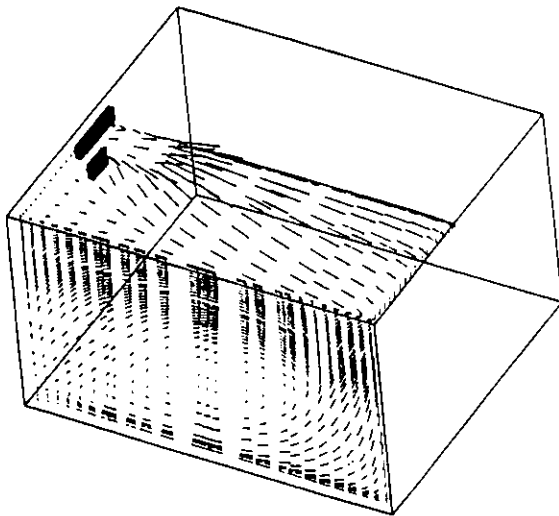


FIG 3.17 Case B2, simulated, $z = 0.0\text{m}$, Fontaine, B20F, flow pattern

FIG 3.18 Case B2, simulated, $z = 0.0\text{m}$, Heikkinen, B2C04SF1, flow pattern

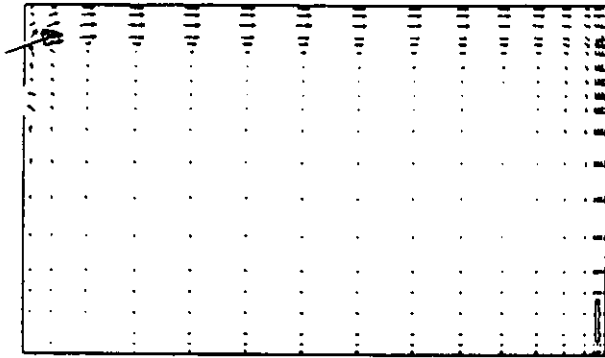


FIG 3.19 Case B2, simulated, $z = 0.0\text{m}$, Furst, B2GER, flow pattern

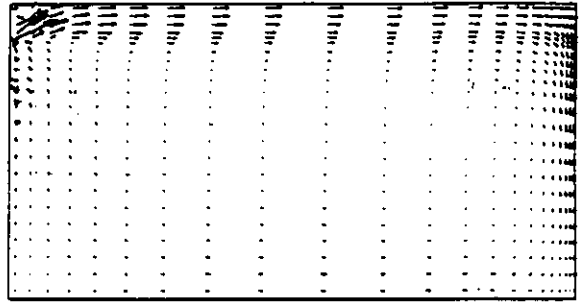


FIG 3.20 Case B2, simulated, $z = 0.0\text{m}$, Johanson, B2_CTH_C, flow pattern

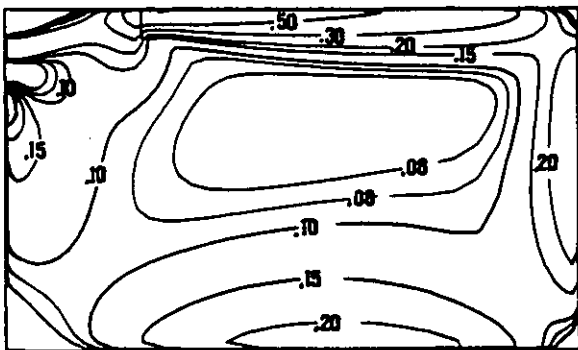


FIG 3.21 Case B2, simulated, $z = 0.0\text{m}$, Lemaire, B2P002NL, iso-vels

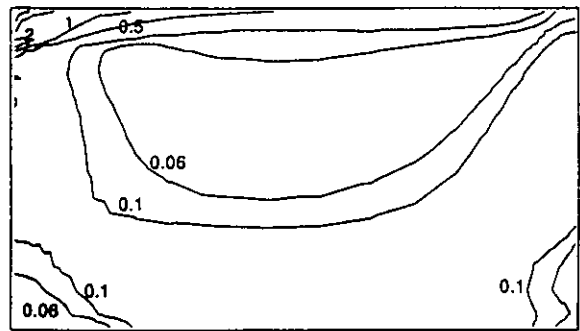


FIG 3.22 Case B2, simulated, $z = 0.0\text{m}$, Vogl, B2FRG, iso-vels

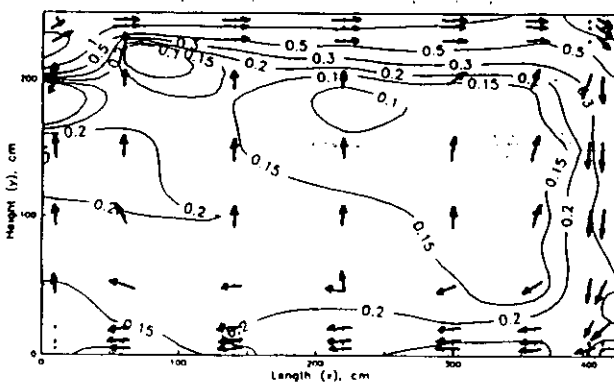


FIG 3.23 Case B3, measured, $z = 0.0\text{m}$, Heikkinen, B3T02SF1, iso-vels

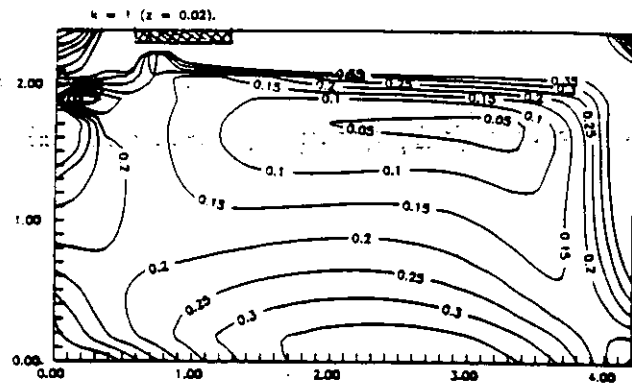


FIG 3.24 Case B3, simulated, $z = 0.0\text{m}$, Skovgaard, B3004DK, iso-vels

Flow visualisation

The flow in the water scale model (section 2.1.2) was visualized by Biolley [12] for test case B1, B2 and B3 with the diffuser. In addition, for case B2, the diffuser was replaced by a basic rectangle (180mmx62mm) and a wide slot (710mmx16mm), respectively. The aim was to verify the computed flow patterns based on these diffuser models (section 2.2.3).

Figure 3.25 and 3.26 show the observed flow patterns with the 'real' diffuser and the basic rectangle. The injected fluid forms a highly turbulent three-dimensional jet impinging with an angle on the ceiling. The jet widens as it flows along the ceiling to the end and side walls. When it reaches the end wall, the fluid spreads out to the sides. In short the jet wraps the test room. At the side walls near the end wall and the ceiling, two streams counteract each other: the one coming from the ceiling in the direction of the main jet and the one bound to the return of the fluid that reached the end wall. Two vertical columns are created in the corners opposite to the diffuser. Other local features are: (1) a small transverse vortex in the triangle enclosed by the jet, diffuser and ceiling, and (2) a circulation at the bottom corners of the rear wall.

The jet from the basic rectangle spreads more in the transverse directions and is thinner on the ceiling in the central plane. Its inertia, however, equals the inertia of the jet from the real diffuser, whereas the inertia of the jet from the wide slot is less. The length L_c of the two vertical columns in the opposite corners is indicated in figure 3.27 and figure 3.28 for case B1 and case B2, respectively. The shorter length L_c for case B1, compared with case B2 (and B3) demonstrates the presence of a low Reynolds number effect.

Key comfort parameters

Occupied zone data on mean velocity, turbulent velocity, modified velocity and maximum velocity are summarised in table 3.4.

Figure 3.29a shows the variation of maximum velocity in the occupied zone with air flow rate, from all measurements and predictions. Low Reynolds number effects are evident at the low flow rate end of the range. However, those who performed simulations using a high Reynolds number turbulence model (the majority) would not expect to predict this.

Figure 3.29b shows, as expected, that the mean velocities increase almost linearly with supply air flow rate. There are, though, simulation results where the predicted mean velocity is clearly too low and some which are high. It is unclear as yet whether this is due to the characteristics of the code used or related to assumptions made by the operator. The figures for modified velocity generally follow those for the mean velocity. It should be noted that certainly for case B1 and possibly case B2 the mean velocities are very low and hence difficult to measure with any reasonable accuracy.

Individual researchers have commented on measurements [45] and have discussed the physical effects and models [4,76].

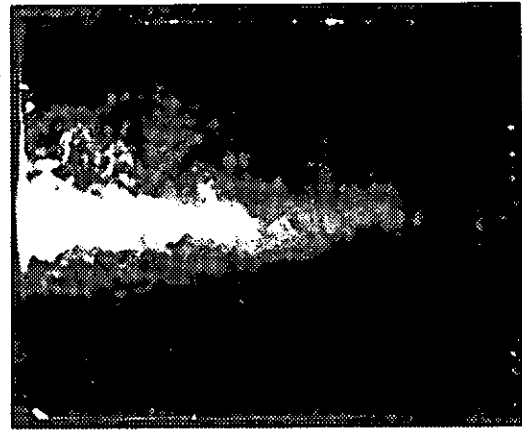
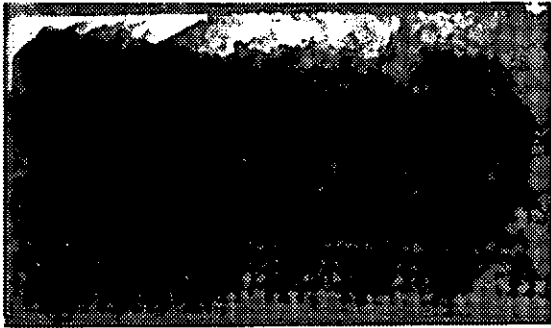


FIGURE 3.25 Case B2, observed, $z = 0.0\text{m}$ (left) and $y = 2.4\text{m}$ (right), Biolley, real diffuser

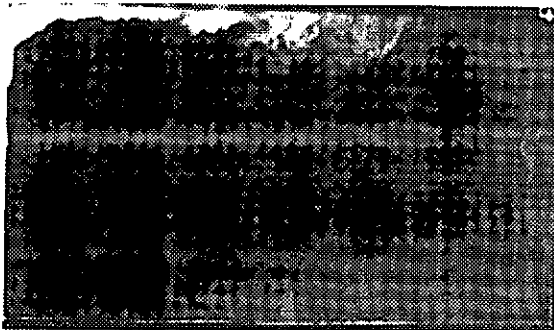


FIGURE 3.26 Case B2, observed, $z = 0.0\text{m}$ (left) and $y = 2.4\text{m}$ (right), Biolley, basic rectangle



FIG 3.27 Case B1, observed, $z = 1.7\text{m}$,
Biolley, real diffuser

FIG 3.28 Case B2, observed, $z = 1.7\text{m}$,
Biolley, real diffuser

TABLE 3.4 Test case B1, B2 and B3: occupied zone data

Ref.	M or S	Ave. Um	Ave. Ut	Ave. U*	Max Um	Max Temp	Ave. Temp	Min Temp
B1CH	S	0.020	0.007	0.022	0.038	-	-	-
B1_CTH_C	S	0.032	0.010	0.034	0.057	-	-	-
B1C01SF1	S	0.041	0.010	0.043	0.073	-	-	-
B1004DK	S	0.041	0.019	0.046	0.070	-	-	-
B1001DK	S	0.045	0.019	0.051	0.075	-	-	-
B1GER	S	0.049	0.022	0.055	0.090	-	-	-
B1C03SF1	S	0.053	0.014	0.055	0.093	-	-	-
B1M001NL	M	0.059	-	0.059	0.123	-	-	-
B1P001NL	S	0.060	0.016	0.063	0.104	-	-	-
B1FRG	S	0.083	0.038	0.093	0.151	-	-	-

Ref.	M or S	Ave. Um	Ave. Ut	Ave. U*	Max Um	Max Temp	Ave. Temp	Min Temp
B2CD	S	0.017	0.005	0.020	0.049	-	-	-
B2N2	S	0.027	0.107	0.114	0.073	-	-	-
B2_CTH-C	S	0.033	0.010	0.035	0.060	-	-	-
B2CH	S	0.048	0.019	0.052	0.086	-	-	-
B2T01SIB	M	0.082	0.031	0.089	0.189	22.30	21.08	20.20
B2C01SF1	S	0.092	0.024	0.097	0.161	-	-	-
B2T03SF1	M	0.100	0.023	0.103	0.178	18.40	18.07	17.75
B2C03SF1	S	0.108	0.029	0.113	0.189	-	-	-
B2B002NL	S	0.108	0.022	0.112	0.190	-	-	-
B2B001NL	S	0.109	0.019	0.112	0.192	-	-	-
B2GER	S	0.109	0.047	0.122	0.211	-	-	-
B2FRG	S	0.117	0.044	0.129	0.215	-	-	-
B2C04SF1	S	0.119	0.040	0.128	0.205	-	-	-
B2P001NL	S	0.123	0.034	0.129	0.213	-	-	-
B20F	S	0.130	0.055	0.146	0.221	-	-	-
B2004DK	S	0.131	0.054	0.145	0.222	-	-	-
B2P002NL	S	0.135	0.051	0.148	0.234	-	-	-
B2001DK	S	0.151	0.081	0.187	0.252	-	-	-

Ref.	M or S	Ave. Um	Ave. Ut	Ave. U*	Max Um	Max Temp	Ave. Temp	Min Temp
B3CH	S	0.033	0.053	0.063	0.070	-	-	-
B3_CTH_C	S	0.034	0.010	0.036	0.061	-	-	-
B3C01SF1	S	0.190	0.052	0.202	0.333	-	-	-
B3T02SF1	M	0.205	0.055	0.213	0.418	18.85	18.40	17.97
B3C03SF1	S	0.218	0.061	0.229	0.381	-	-	-
B3GER	S	0.221	0.095	0.247	0.434	-	-	-
B3FRG	S	0.242	0.092	0.265	0.440	-	-	-
B3P001NL	S	0.251	0.070	0.264	0.438	-	-	-
B3004DK	S	0.253	0.104	0.280	0.428	-	-	-
B3001DK	S	0.314	0.123	0.347	0.527	-	-	-

M= measured, S= simulated

Ave. Um= averaged velocity (speed) (m/s) in occupied zone.

Ave. Ut= averaged turbulent velocity (speed) (m/s) in occupied zone.

Ave. U*= averaged modified velocity (speed) (m/s) in occupied zone.

Temperatures (°C) refer to occupied zone.

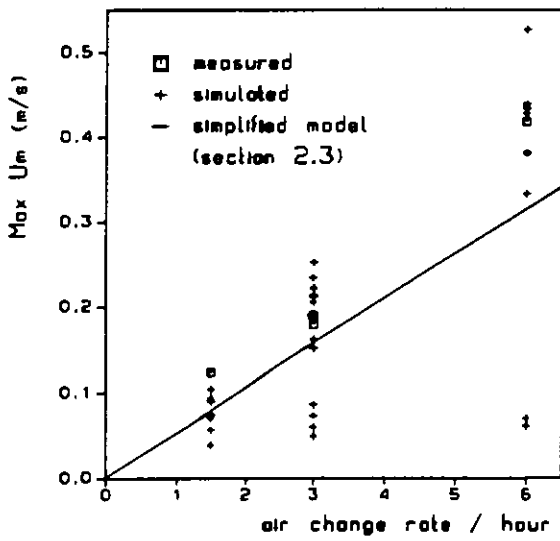


FIG 3.29a Case B1, B2, B3 : maximum velocity U_m in occupied zone

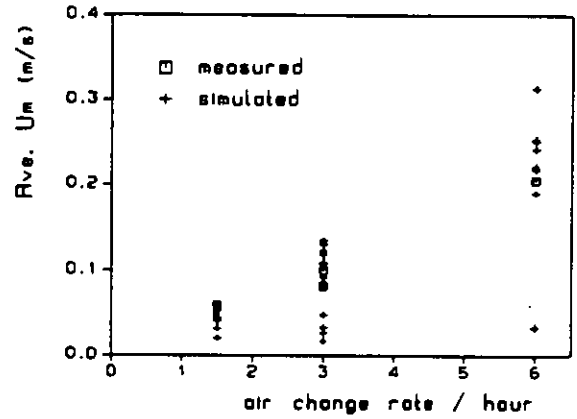


FIG 3.29b Case B1, B2, B3 : average velocity U_m in occupied zone

Profiles/graphs

An example of profiles of mean velocity and turbulent velocity along the three lines (fig 3.1) is shown for simulations and measurements in the scale model by Fontaine et al (figure 3.30). Figure 3.31 shows the measured and simulated velocity decay along the jet centre-line and figure 3.32 measured air speed profiles above the floor.

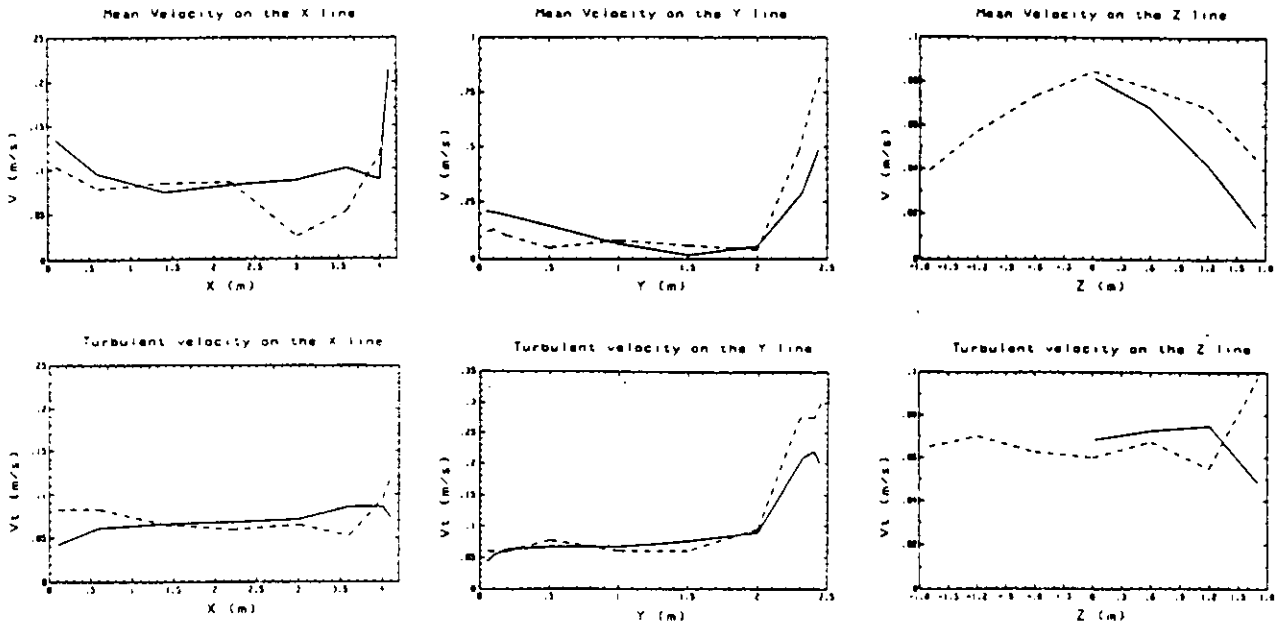
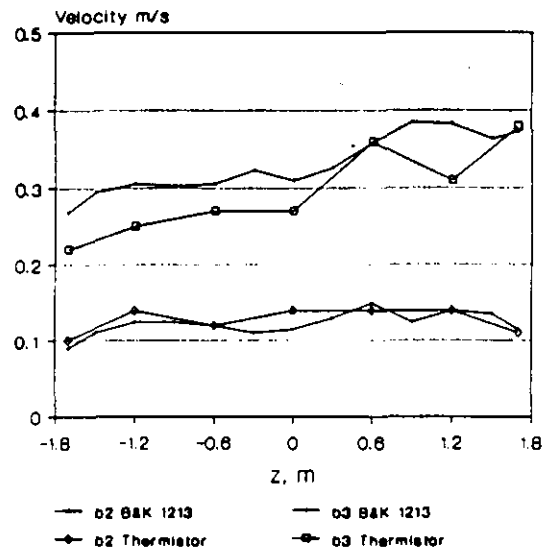
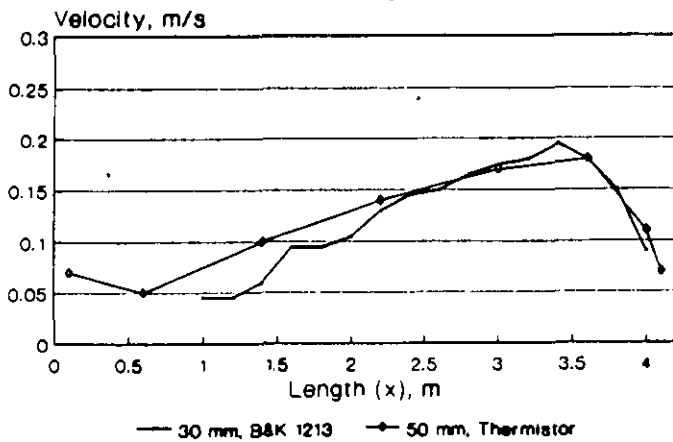
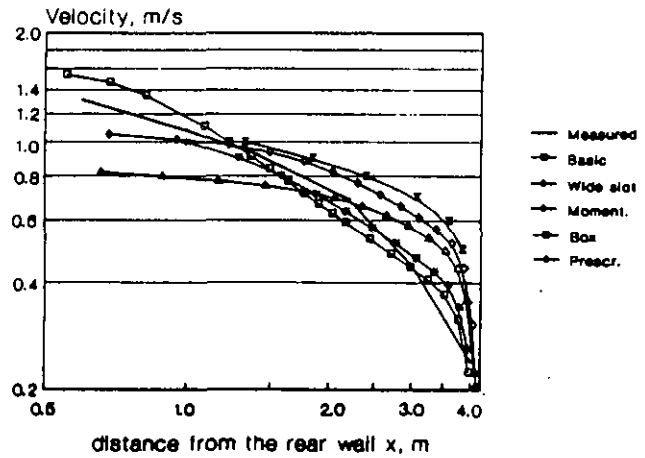
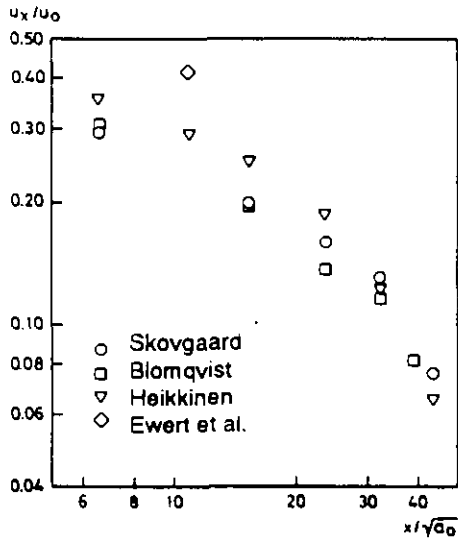


FIGURE 3.30 Test case B2: profiles of mean velocity and turbulent velocity along the three lines: predicted (solid) and measured (dotted) in scale model by Fontaine et al.



Turbulence parameters near the supply air diffuser

Ewert et al. [24,25] measured velocity components and turbulence quantities on an imaginary box, sized 1.0m x 1.0m x 0.4m height, surrounding the supply air diffuser. The test room dimensions were slightly different from the basic test room. The results are compared with numerical predictions with FLUENT based on the 'basic model' of the supply. Figure 3.33 shows profiles at the symmetry plane of the imaginary box.

Measurements yield higher velocities than simulations with PLDS and QUICK scheme. PLDS results in a lower maximum velocity due to its higher numerical diffusion. The measured turbulent kinetic energy is ten times higher than calculations with PLDS and two times higher than those with the QUICK scheme. It is concluded that the comparison of the dissipation rate is quite difficult, because measured data are evaluated with simplifying models ('internal length scale' and 'wave number spectrum'). The resulting values from the two models differ by more than one order of magnitude, but both curves indicate the same tendency. Results from numerical simulations are completely different. The profiles from the QUICK scheme are again closer to measurements. Additional k-and ϵ -profiles calculated with equation (2.3) (normally used if only velocities are available) are included in the figure for a turbulence intensity $Tu = 0.1$.

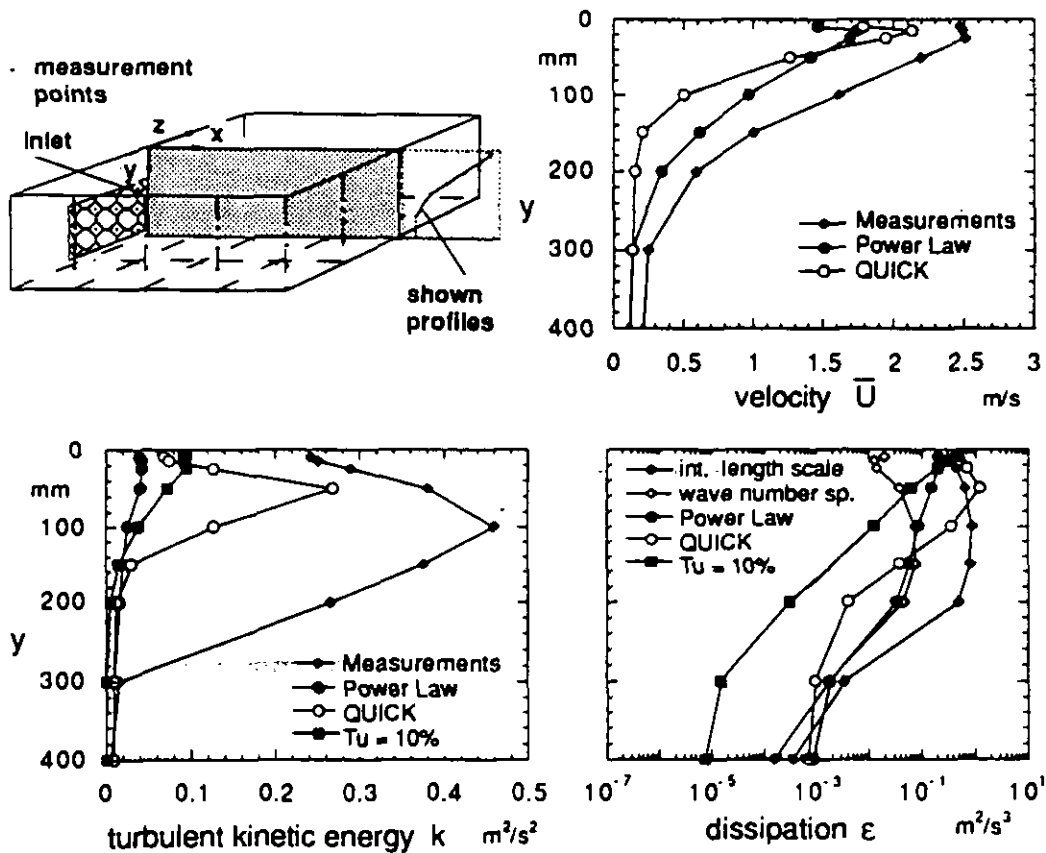


FIGURE 3.33 Test case B3: comparison between LDA-measurements and simulations at the symmetry plane of the imaginary box made by Ewert et al. [24,25].

Turbulence characteristics in the room

Sandberg et al. [92] measured instantaneous velocities with a constant temperature hot film anemometer in order to extend the knowledge of turbulence in a real room situation. In particular the idea was to investigate the effect of the deflection of the jet that occurs at the corners of the room. The mean velocity, standard deviation and turbulent integral length scale (from autocorrelation function) were determined for flow rates $n = 1.0, 1.5, 2.0, 3.0, 4.0, 5.0$ and 6.0 ach^{-1} . The last value corresponds to supply velocity $u_0 = 6.63 \text{ m/s}$ and nozzle discharge Reynolds number $Re_d = 6,652$.

From measurements at a fixed distance $x = 2.2 \text{ m}$ ($x/\sqrt{a_0} = 22.6$) along a vertical line it is concluded that the streamwise velocity and turbulence intensities become independent of Re_d for $Re_d > 2,220$. ($n > 2.0 \text{ ach}^{-1}$). The integral length scale becomes independent of Re_d from $Re_d \sim 3,300$ ($n \sim 3 \text{ ach}^{-1}$).

Measurements near the wall showed that both the mean velocity and the turbulent fluctuations were Reynolds number dependent for $y^+ > 10$. A wall function with coefficient 3.45 in front of $\log y^+$ was derived, instead of the "universally" adopted value of 5.5. The difference may be due to one or a combination of the following factors: (1) error in the measured wall shear stress, (2) curve fitted over a too short region and (3) developing flow.

Measurements carried out on the jet centre-line (location of maximum velocity) along the perimeter of the room ($n = 3.0 \text{ ach}^{-1}$) showed: (1) the decay of the velocity of the jet does not coincide with any classical formula for a jet in an infinite quiescent ambient, (2) the turbulence length scale when close to the terminal becomes equal to the characteristic dimension of the terminal, (3) under the ceiling the turbulent length scale is 0.076 times the distance from the terminal, (4) the turbulent length scale becomes twice the characteristic dimension of the terminal in the occupied zone. The evolution of the integral scale is shown in figure 3.34. The general behaviour of the jet can be described such that the jet restarts after it has decelerated and been deflected at the corner.

The general conclusion is that in the case where the jet is supplied into a finite ambient and in particular where the jet is constrained to change direction at room corners the jet behaviour is strongly influenced. This room influence must be considered in testing procedures of supply air terminals in order to have confidence of successful application at the design stage.

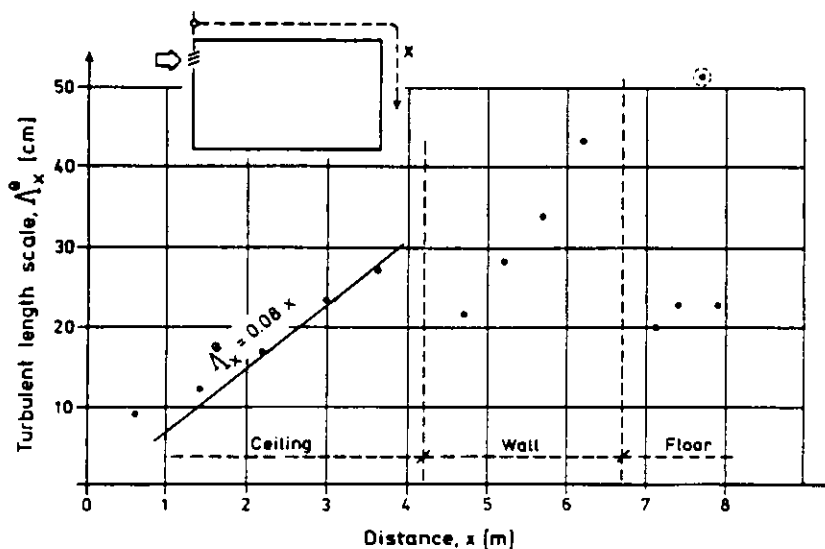


FIGURE 3.34 Testcase B2: the integral scale Λ_x on the jet centre-line (Sandberg et al).

3.3.4 Test case E (mixed convection, summer cooling)

Flow patterns and isotherms

Test case E1. Figure 3.35 (Blomqvist [15]) and figure 3.36 (Fossdal [16]) show measured speed and temperature contours for case E1. The indications are that the supply jet is detaching at one-quarter to one-third the distance along the ceiling and deflecting down into the occupied zone. Measurements in the jet region in the occupied zone show velocities of 0.2 to 0.3m/s from Blomqvist, and 0.1 to 0.2m/s from Fossdal. The temperature in this region is 20°C from both sets of measurements. Simulation data from Heikkinen and Piira [65] is shown in figure 3.37. The velocities and temperatures in the detaching jet are generally consistent with those from measurement (velocities of 0.2 to 0.3m/s and temperature of 20°C). Lemaire [93] (figure 3.38) indicates a slightly longer projection whilst Johansson [94] under-predicts the throw but appears to generate consistent velocities (figure 3.39).

Test case E2. Measured velocity and temperature data for test case E2 is available from Blomqvist [15] (fig.3.40), Heikkinen [16] (fig.3.41) and Fossdal [17]. The supply jet appears to detach at approximately two-thirds distance along the ceiling. Occupied zone velocities are 0.1 to 0.2m/s and the temperatures approximately 21°C. Simulations by, Said [95] and Tjelflaat [96] are shown in figures 3.42 and 3.43. Generally consistent flow patterns are obtained although some under-prediction of velocity (Said, Tjelflaat) is occurring. Lemaire [93]; in figure 3.44, demonstrates that flow reversal can occur at the window (change in penetration length) dependent on the inlet model used. Vogl and Renz [97] show the influence of differencing scheme on air speed contours, by comparing PLDS and QUICK, in figure 3.45.

Test case E3. Measured velocity and temperature data for test case E3 is available from Blomqvist [15] (fig.3.46), Heikkinen [16] (fig.3.47) and Fossdal [17]. The jet does not appear to detach from the ceiling. Velocities higher than 0.3m/s are generated at near floor level on the centre-plane, and temperatures of 20 to 21°C. Examples of predictions are shown in figure 3.48 (Chen [98]). Consistent with measurements, the jet remains attached to the ceiling and projects down the window.

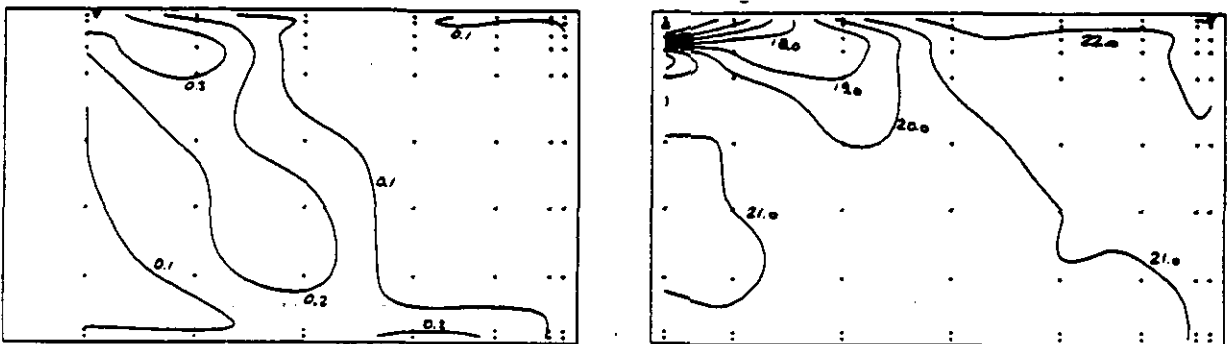


FIGURE 3.35 Case E1, measured, $z = 0.0\text{m}$, iso-vels (left) and isotherms (right), Blomqvist, E1T02SIB

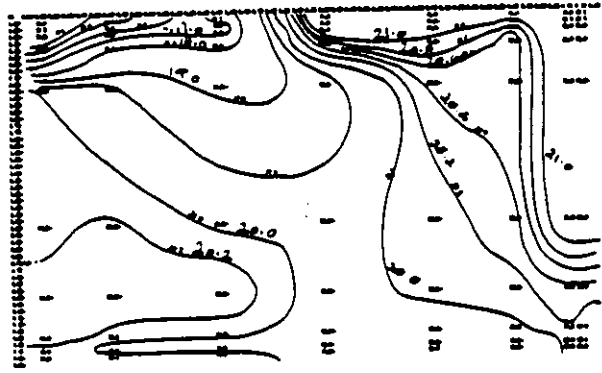
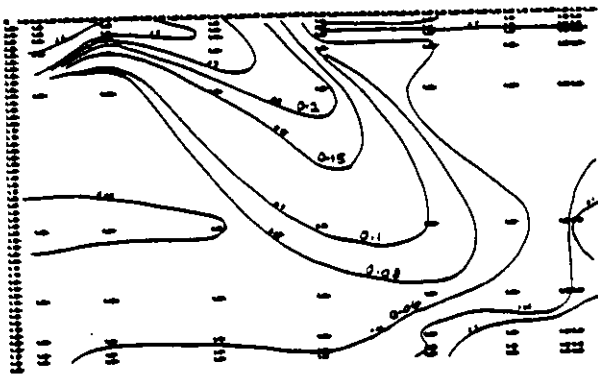


FIGURE 3.36 Case E1, measured, $z = 0.0\text{m}$, iso-vels (left) and isotherms (right), Fossdal, E1N

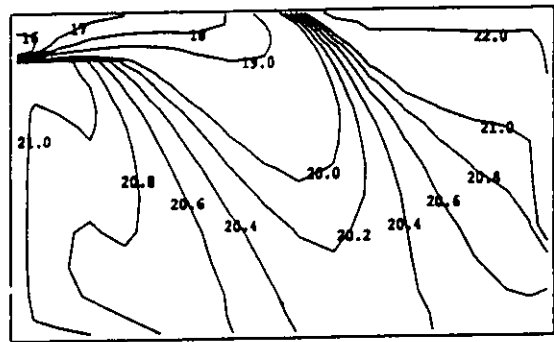
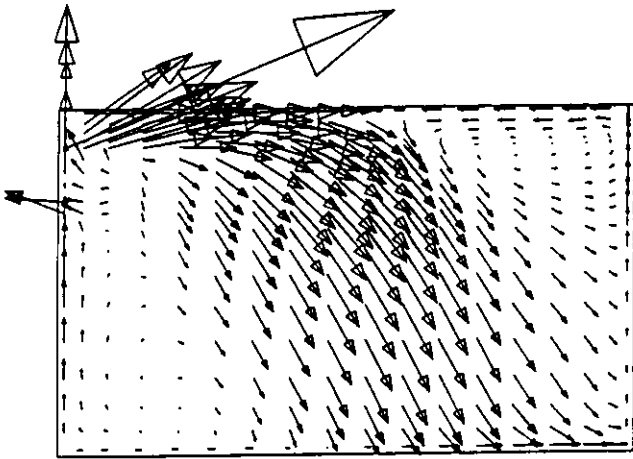


FIGURE 3.37 Case E1, simulated, $z = 0.0\text{m}$, flow pattern (left) and isotherms (right), Heikkinen, E1CO2SF1

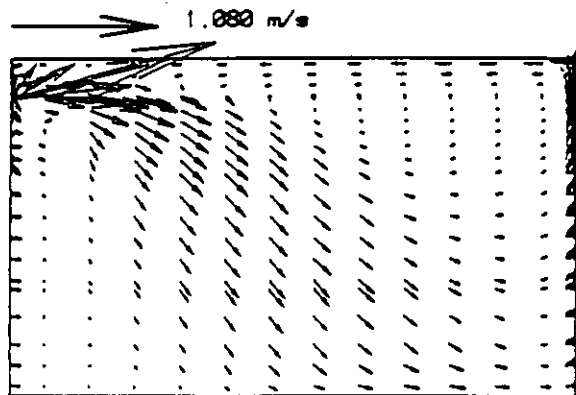
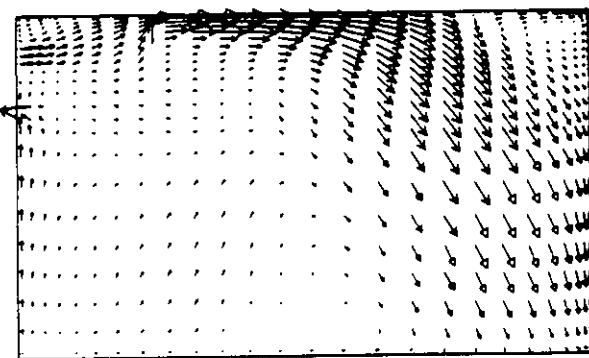


FIG 3.38 Case E1, simulated, $z = 0.0\text{m}$, Lemaire, E1P001NL, flow pattern

FIG 3.39 Case E1, simulated, $z = 0.0\text{m}$, Johanson, flow pattern

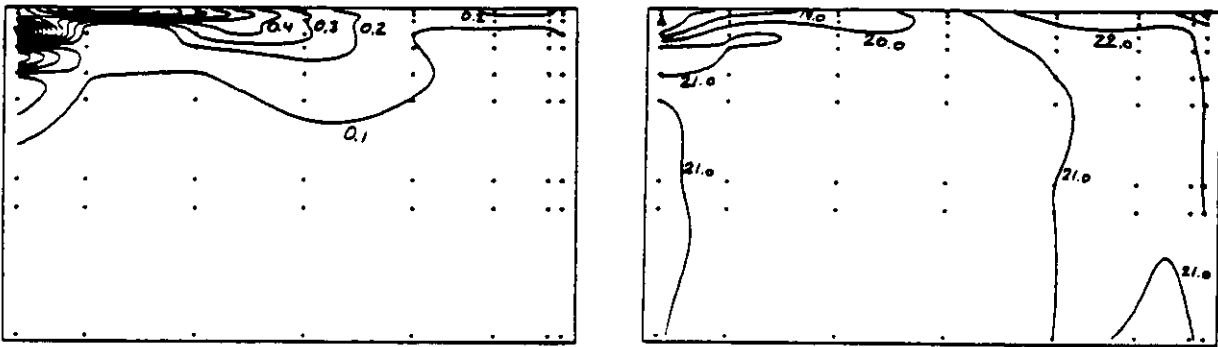


FIGURE 3.40 Case E2, measured, $z = 0.0\text{m}$, iso-vels (left) and isotherms (right), Blomqvist, E2T01SIB.

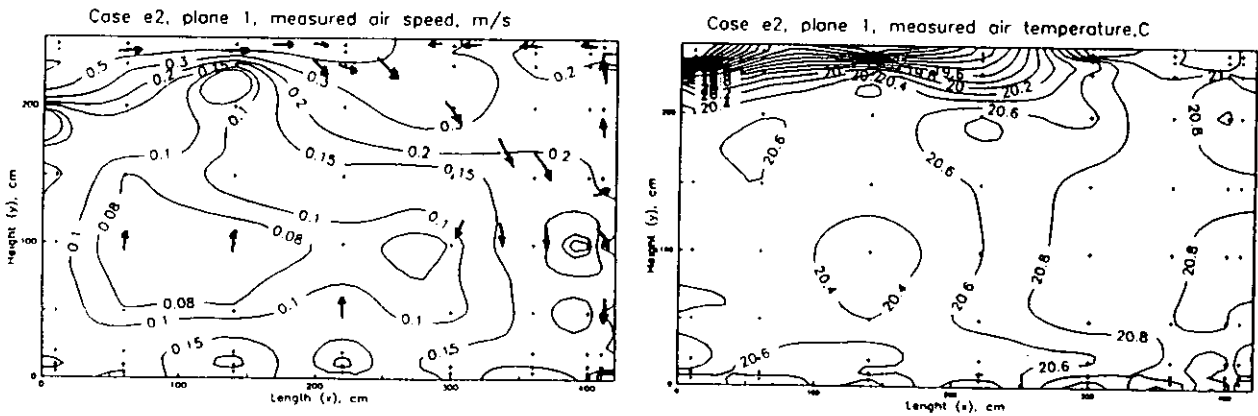


FIGURE 3.41 Case E2, measured, $z = 0.0\text{m}$, iso-vels (left) and isotherms (right), Heikkinen, E2CO2SF1

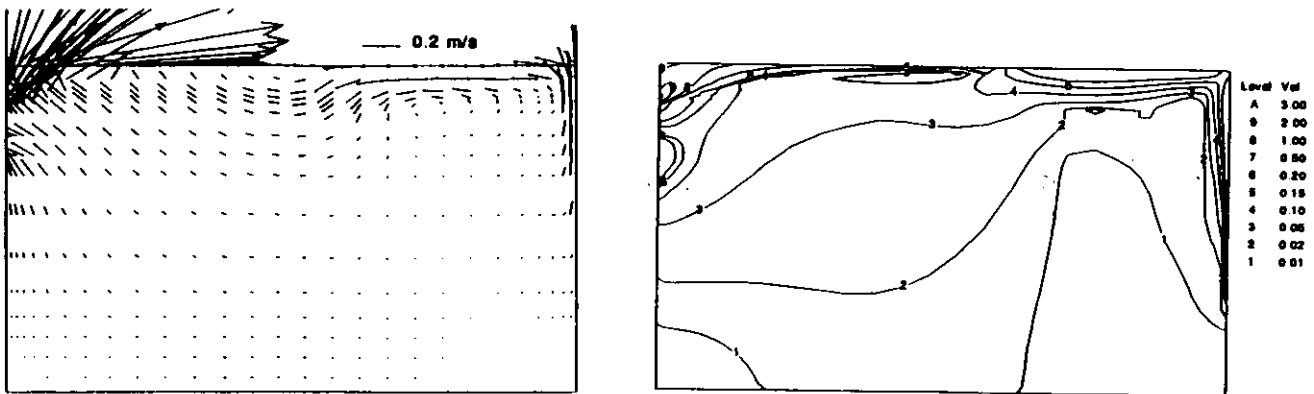


FIGURE 3.42 Case E2, simulated, $z = 0.0\text{m}$, flow pattern (left) and isovels (right), Said, E2CD

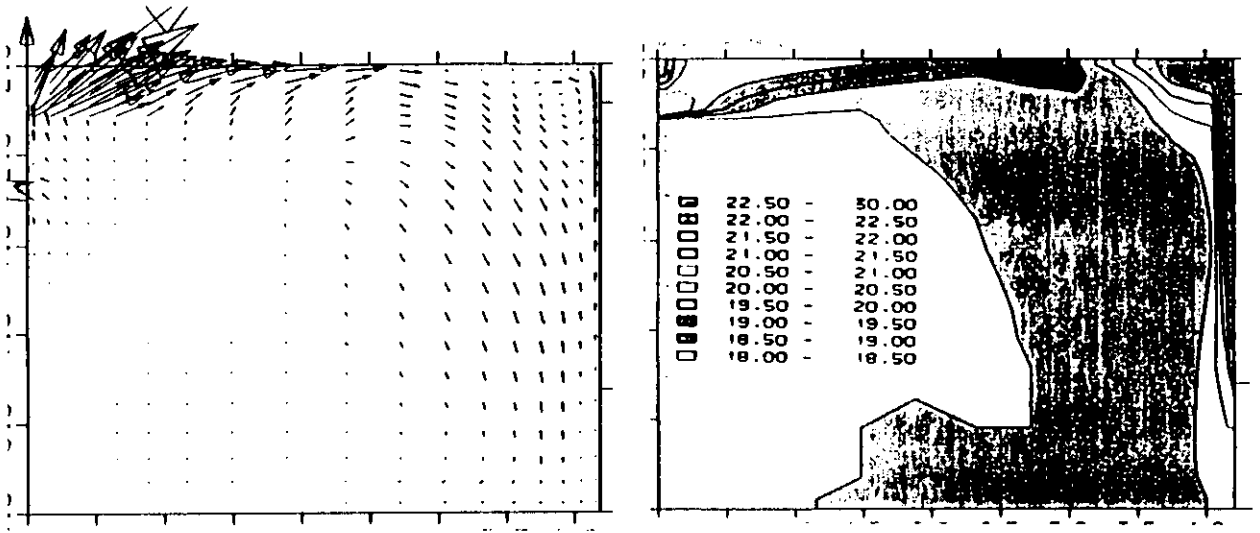


FIGURE 3.43 Case E2, simulated, $z = 0.0\text{m}$, flow pattern (left) and isotherms (right), Tjelflaat, E2N2

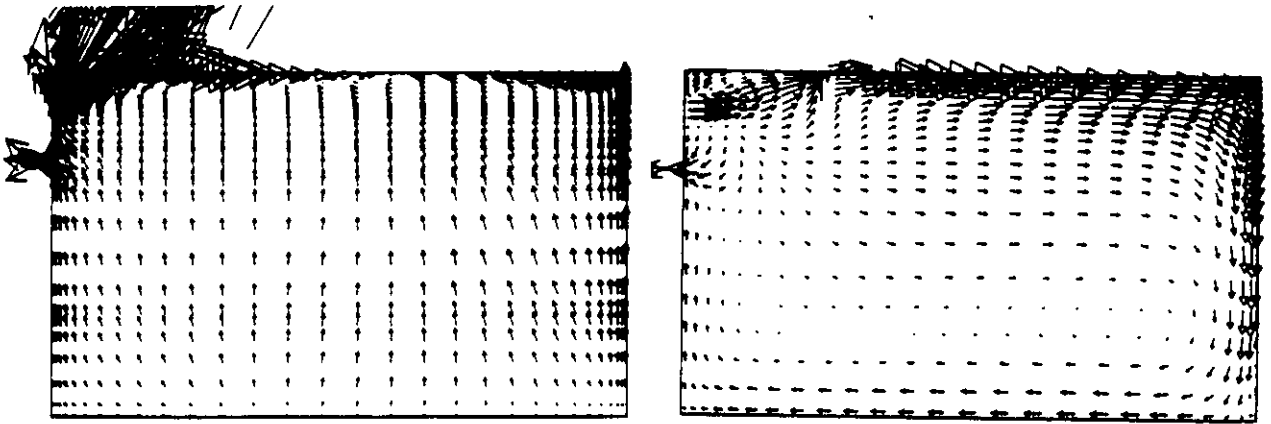


FIGURE 3.44 Case E2, simulated, $z = 0.0\text{m}$, 'basio model' (left) and 'prescribed velocity model' (right), Lemaire, E2B002NL (left) and E2P001NL (right)

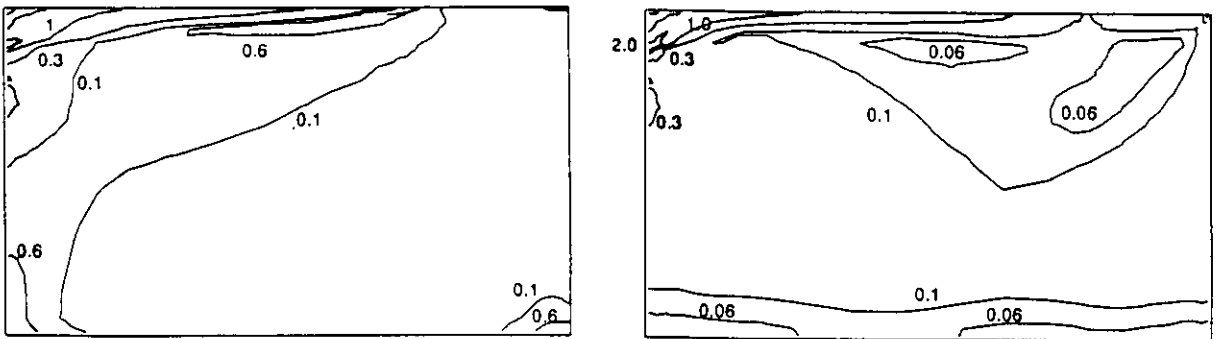


FIGURE 3.45 Case E2, simulated, $z = 0.0\text{m}$, PLDS (left) and QUICK (right) scheme, Vogl et al., E2FRG (left) and E2FRGXQ (right), iso-vels.

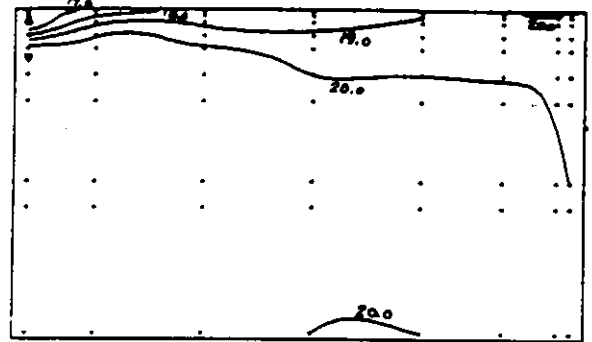
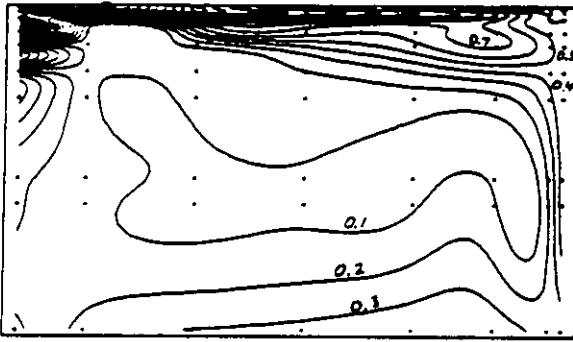


FIGURE 3.46 Case E3, measured, $z = 0.0\text{m}$, iso-vels (left) and isotherms (right), Blomqvist, E3T01SIB

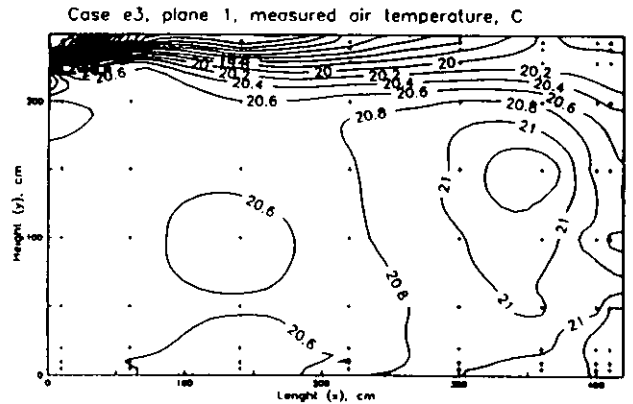
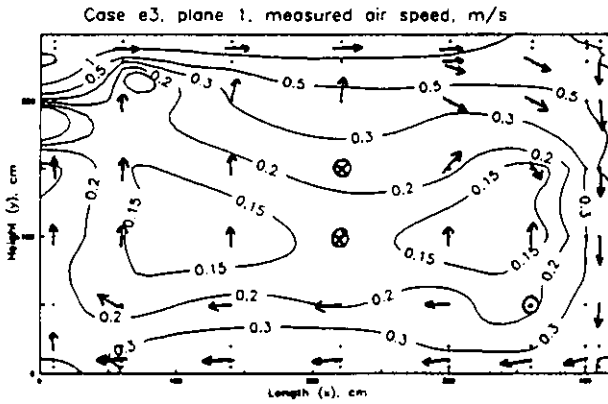


FIGURE 3.47 Case E3, measured, $z = 0.0\text{m}$, iso-vels (left) and isotherms (right), Helkkinen, E3T02SF1

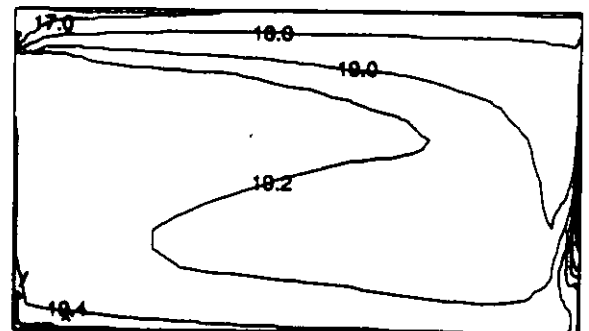
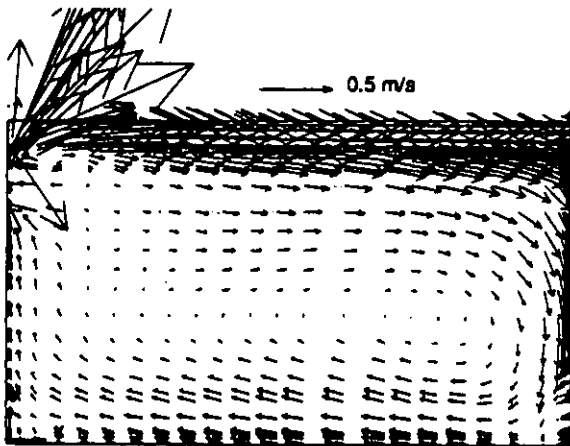


FIGURE 3.48 Case E3, simulated, $z = 0.0\text{m}$, flow pattern (left) and isotherms (right), Chen, E3CH

Penetration depth of the jet

Figure 3.49 and figure 3.50 show, as expected, a sensitivity of the penetration length of the jet to the Archimedes number for measurement data sets (Blomqvist [28] and Heikkinen [21]) and simulation (Heikkinen [21] and Renz [31]). The measured data from Heikkinen indicates a varying jet penetration length across the room. This test case represents a particularly onerous one to simulate. However, whilst some differences exist between the simulated results and measurement at high Archimedes number the nature of the flow is quite well represented in terms of flow patterns, mean velocities, penetration length and occupied zone temperatures.

Lemaire [93], in simulations with the prescribed velocity inlet model found that for the higher flow rate cases (E2 and E3) the supply air jet dominates the flow pattern, causing a down-flow at the window. However, at the lowest flow rate (E1) the warm air rising from the window deflects the jet down from the ceiling. At this high Archimedes number the prescribed velocity model fails and flow instabilities were found which caused difficulties in achieving convergence to a steady-state solution. Simulations with the basic inlet model were easier to converge although some reduction in penetration length was observed.

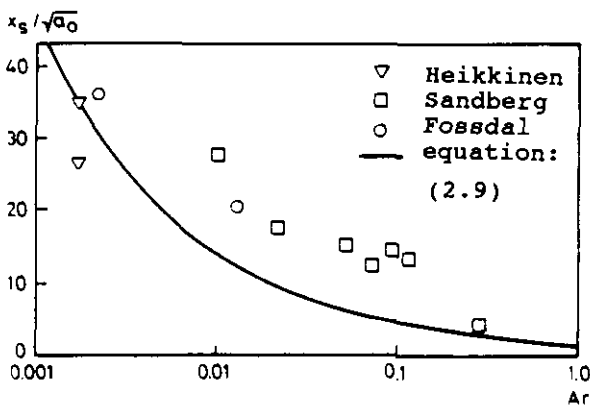


FIG 3.49 Case E1, E2, E3 : measured jet penetration depth x_s

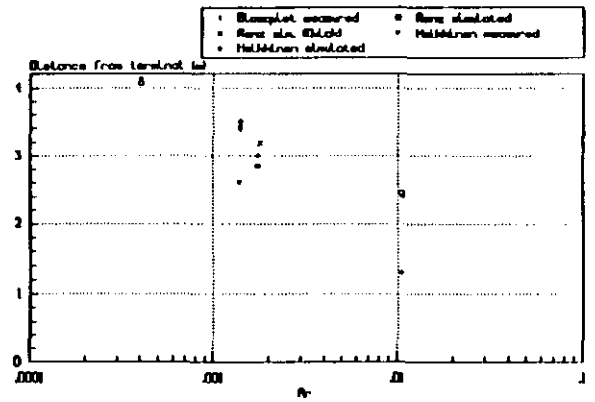


FIG 3.50 Case E1, E2, E3 : simulated jet penetration depth x_s

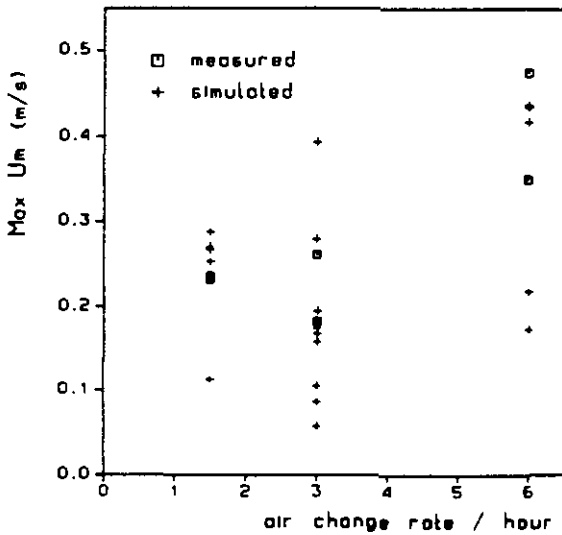


FIG 3.51a Case E1, E2, E3 : maximum velocity U_m in occupied zone

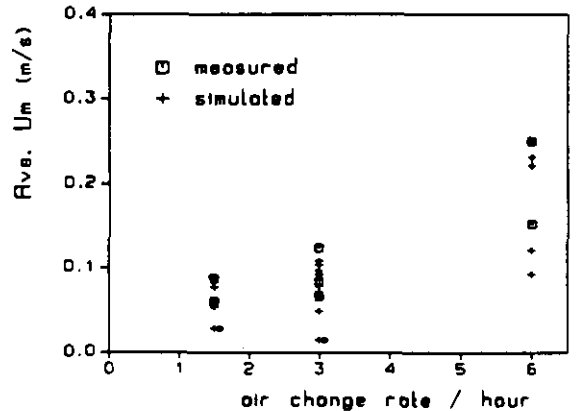


FIG 3.51b Case E1, E2, E3 : average velocity U_m in occupied zone

Key comfort parameters

Table 3.5 summarises the occupied zone velocity and temperature data. The variation of maximum and average velocity in the occupied zone with air flow rate is shown in figure 3.51.

In general, the measured data for the summer cooling case indicates the difficulty in reproducing the test conditions accurately.

TABLE 3.5 Test case E1, E2 and E3: occupied zone data

Ref.	M or S	Ave. Um	Ave. Ut	Ave. U*	Max Um	Max Temp	Ave. Temp	Min Temp
E1FRG	S	0.029	0.040	0.052	0.112	18.90	18.56	18.10
E1CH	S	0.054	0.023	0.061	0.252	19.11	18.70	17.80
E1N	M	0.060	0.016	0.064	0.230	20.50	19.98	18.90
E1P001NL	S	0.060	0.031	0.069	0.266	20.09	19.81	19.07
E1CO2SF1	S	0.077	0.044	0.090	0.287	21.00	20.65	19.82
E1TO2SIB	M	0.087	0.039	0.096	0.234	21.80	20.85	20.00
E1GER	S	0.089	0.041	0.101	0.289	19.31	19.07	18.48

Ref.	M or S	Ave. Um	Ave. Ut	Ave. U*	Max Um	Max Temp	Ave. Temp	Min Temp
E2CD	S	0.015	0.005	0.019	0.056	20.00	20.00	19.99
E2FRG	S	0.049	0.052	0.074	0.085	19.40	19.15	19.10
E2FRGXQ	S	0.049	0.057	0.078	0.105	20.10	19.82	19.70
E2TO1SIB	M	0.066	0.034	0.075	0.181	22.00	21.19	20.50
E2N2	S	0.067	0.029	0.075	0.393	20.15	19.98	19.78
E2CH	S	0.068	0.038	0.080	0.279	19.50	19.18	18.50
E2B002NL	S	0.078	0.017	0.081	0.157	19.70	19.54	19.45
E2B001NL	S	0.078	0.019	0.081	0.167	19.46	19.35	19.26
E2N	M	0.083	0.021	0.086	0.260	21.40	20.95	20.20
E2POO1NL	S	0.092	0.051	0.107	0.177	20.51	20.39	20.30
E2GER	S	0.096	0.048	0.109	0.181	19.75	19.63	19.46
E2CO1SF1	S	0.103	0.036	0.112	0.173	19.58	19.26	19.17
E2CO2SF1	S	0.108	0.048	0.122	0.194	21.09	20.75	20.60
E2T02SF1	M	0.123	0.036	0.129	0.260	21.35	20.86	20.28

Ref.	M or S	Ave. Um	Ave. Ut	Ave. U*	Max Um	Max Temp	Ave. Temp	Min Temp
E3CH	S	0.092	0.051	0.109	0.172	19.60	19.24	19.07
E3FRG	S	0.121	0.100	0.153	0.217	19.40	19.06	18.90
E3N	M	0.152	0.030	0.155	0.350	21.20	20.51	20.10
E3GER	S	0.221	0.100	0.249	0.436	18.68	18.59	18.37
E3CO2SF1	S	0.231	0.065	0.243	0.417	20.21	19.83	19.63
E3POO1NL	S	0.249	0.088	0.270	0.434	20.31	20.08	19.83
E3T02SF1	M	0.250	0.065	0.260	0.474	22.07	20.88	20.46

M= measured, S= simulated

Ave. Um= averaged velocity (speed) (m/s) in occupied zone.

Ave. Ut= averaged turbulent velocity (speed) (m/s) in occupied zone.

Ave. U*= averaged modified velocity (speed) (m/s) in occupied zone.

Temperatures (°C) refer to occupied zone.

3.3.5 Test case D (free convection with radiator)

Flow patterns and isotherms

In simulations, Lemaire [51] found that the flow pattern remained similar for the three cases, with the pattern driven by the buoyant flow from the radiator upwards over the cold window. Prescribed heat fluxes were used for the radiator and the window. Previous simulations had demonstrated that the logarithmic wall functions under-predict (or in some cases over-predict) the surface convection coefficients, depending on the distance of the first gridnode to the wall.

Test case D1. Figure 3.52 shows an example of the flow pattern, air speeds and temperature distribution for test case D1. No measurements were available.

Test case D2. Figure 3.54 shows observed flow patterns, measured air speeds and temperatures for the centre-plane for test case D2 (Lemaire [19]). The experiments indicate a cold downward flow along the window colliding with the hot rising jet from the radiator. In general most simulations predicted a hot rising flow along the window. Unfortunately only one set of measurements is available, contrary to the objective of this evaluation. A second experiment is still needed for stronger confirmation. Predictions are shown in figure 3.53 (Lemaire [51]). The predicted temperatures are slightly higher than measured but still indicative of very low speed air movement. Figure 3.55 shows predicted air flow patterns and air speed contours from Vogl and Renz [49]. Low velocities broadly consistent with measurement are generated. Chen [47], predicted an air flow pattern and temperature distribution consistent with measurements and other simulations. Furst [49] demonstrated that a downward (reverse) flow over the radiator could be generated if the heat transfer from the radiator was incorrectly calculated (from the wall functions used). Heikkinen and Piira [52] (figure 3.57) also demonstrated that a downflow can be generated behind the radiator if the window convective heat flow is prescribed to be high enough.

Test case D3. Figure 3.58 shows the centre-plane, air speeds and temperatures for test case D3. The flow pattern looks similar to the predicted patterns of test case D1 and D2. No measurement data is available, though the simulation results appear plausible and consistent with test case D1 and D2 results, but not with the case D2 experiment.

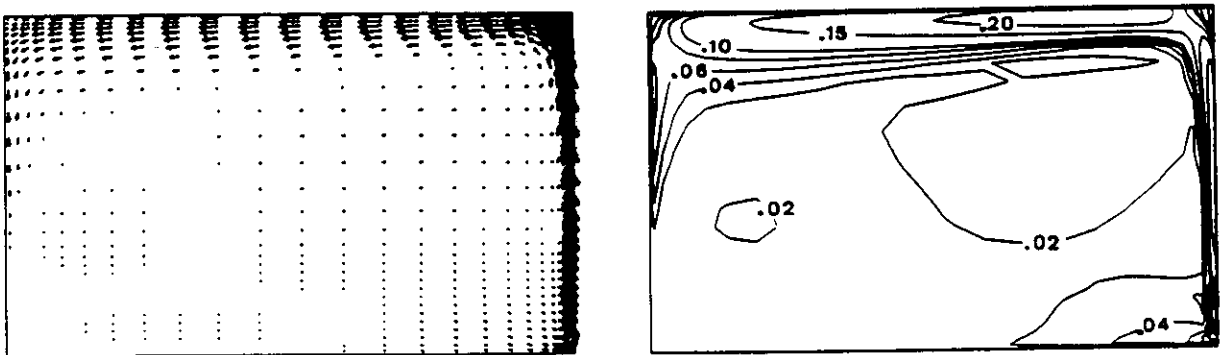


FIGURE 3.52a Case D1, simulated, $z = 0.0\text{m}$, flow pattern (left) and iso-vels (right), Lemaire, D1Q001NL

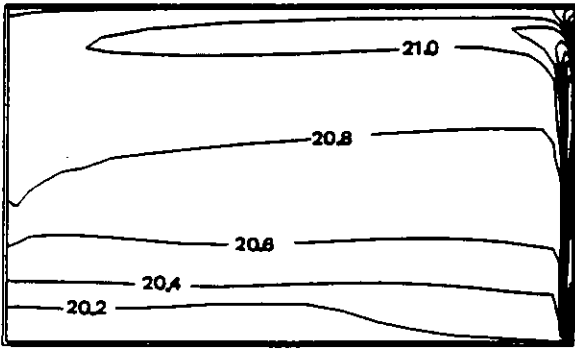


FIG 3.52b Case D1, simulated, $z = 0.0m$, Lemaire, D1Q001NL, Isotherms

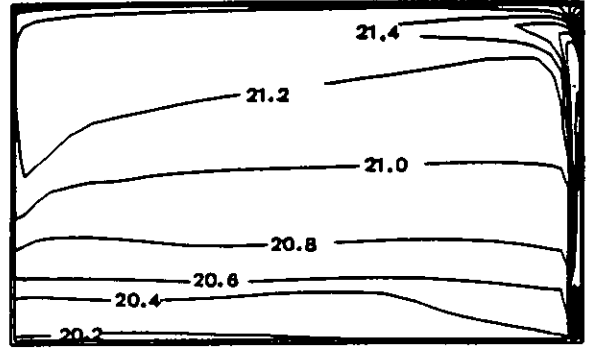


FIG 3.53b Case D2, simulated, $z = 0.0m$, Lemaire, D2Q001NL, Isotherms

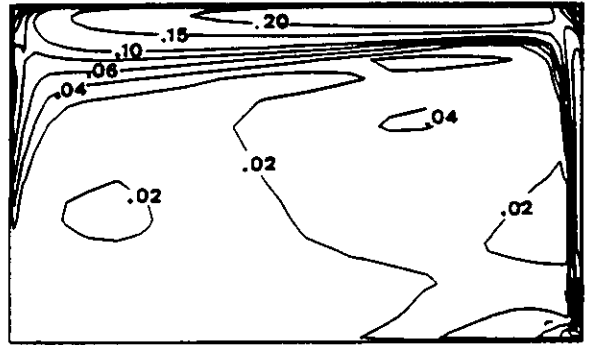
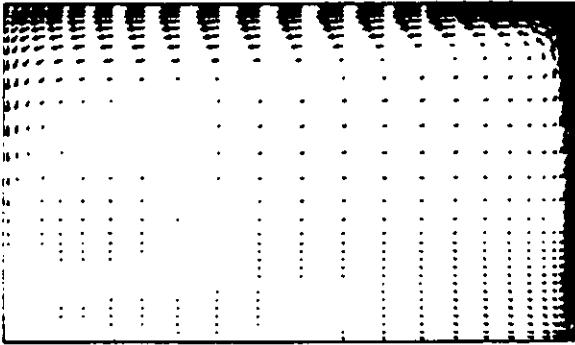


FIGURE 3.53a Case D1, simulated, $z = 0.0m$, flow pattern (left) and Iso-vels (right), Lemaire, D2Q001NL

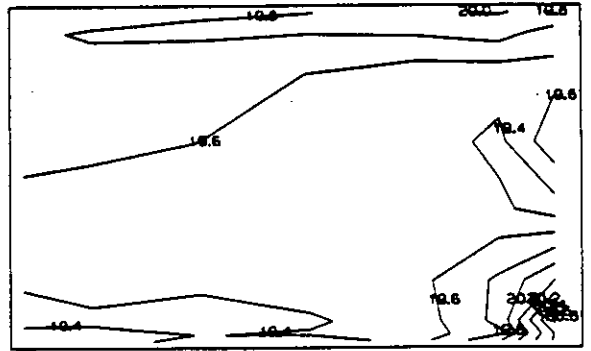
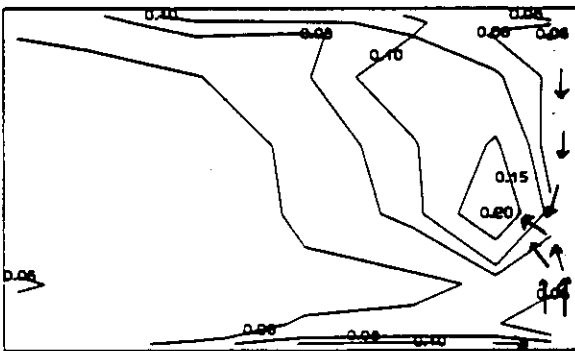


FIGURE 3.54 Case D2, measured, $z = 0.0m$, Iso-vels (left) and isotherms (right), Lemaire, D2M001NL

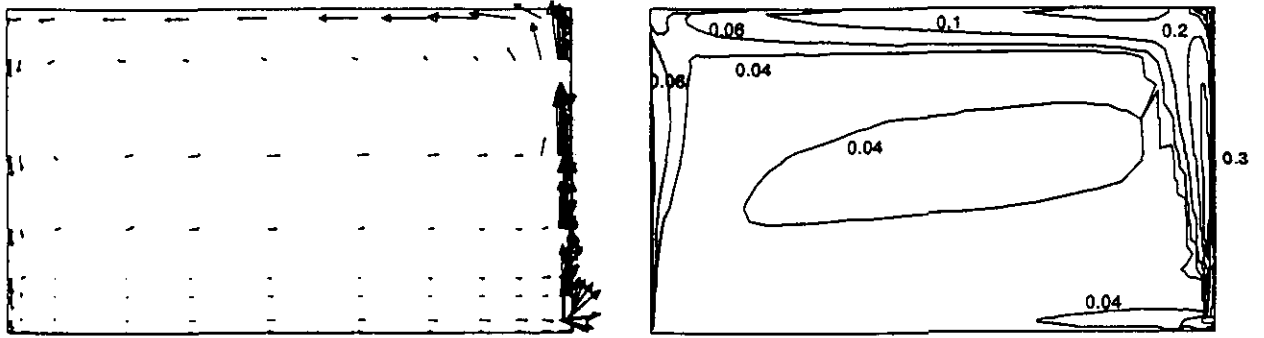


FIGURE 3.55 Case D2, simulated, $z = 0.0\text{m}$, flow pattern (left) and iso-vels (right), Vogl et al., D2FRG

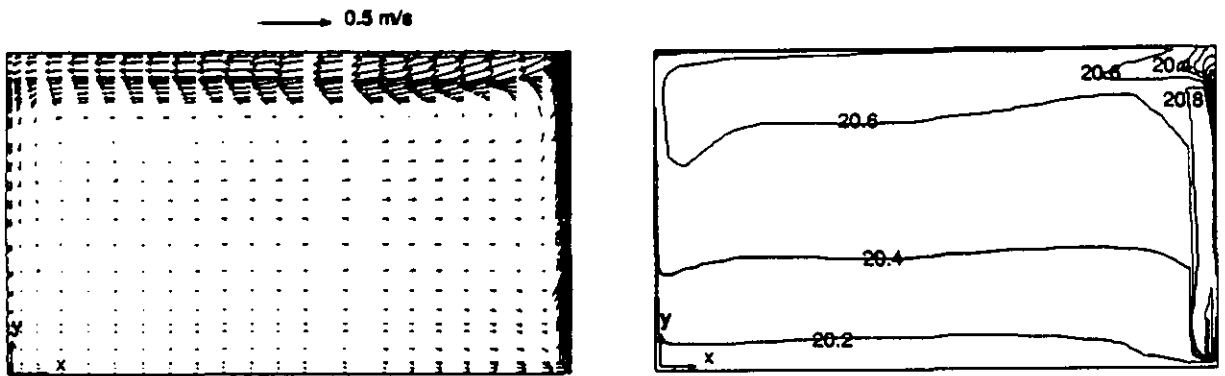


FIGURE 3.56 Case D2, simulated, $z = 0.0\text{m}$, flow pattern (left) and isotherms (right), Chen, D2CH

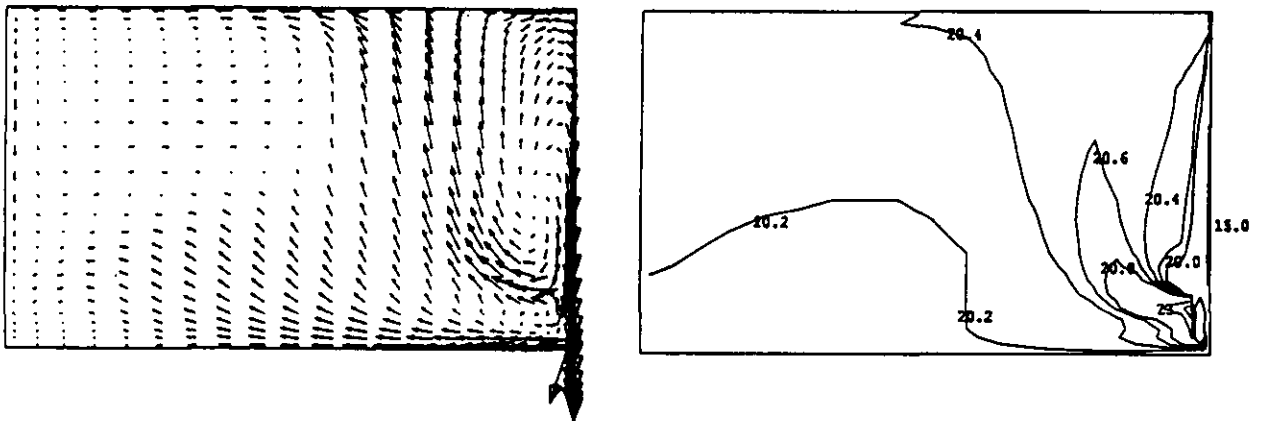


FIGURE 3.57 Case D2, simulated, $z = 0.0\text{m}$, flow pattern (left) and isotherms (right), Heikkinen et al., D2C02SF1

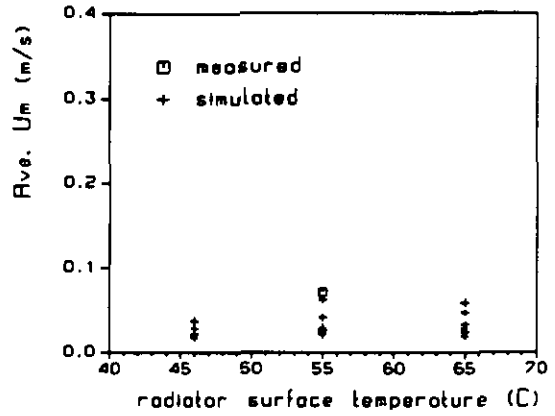
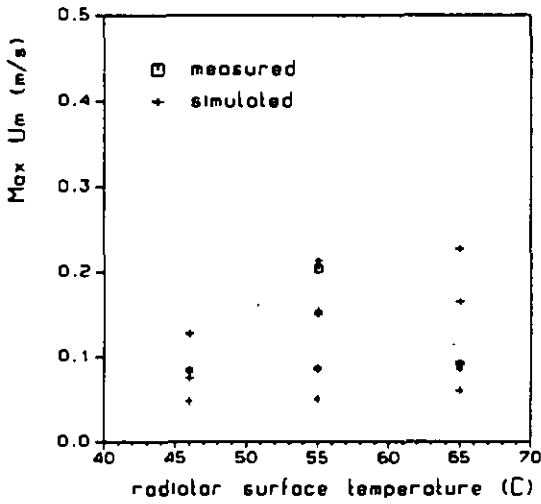


FIGURE 3.58 Case D3, simulated, $z = 0.0\text{m}$, iso-vels (left) and isotherms (right), Lemaire, D2Q003NL

Key comfort parameters

Table 3.6 summarises the occupied zone velocity and temperature data. The variation of maximum and average velocity in the occupied zone with radiator surface temperature (and corresponding window surface temperature) is shown in figure 3.59.

Most of the predicted air velocities in the occupied zone are low, and the average temperature is in almost all cases between 20°C and 21°C . It is unfortunate that measured data is limited; the only set indicates an occupied zone air speed higher than most of the simulation data and a temperature slightly lower.

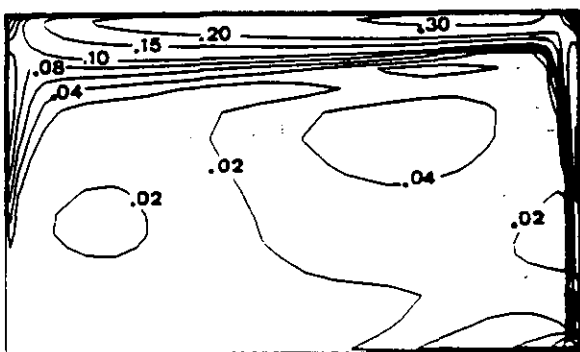


FIG 3.59a Case D1, D2, D3 : maximum velocity in occupied zone

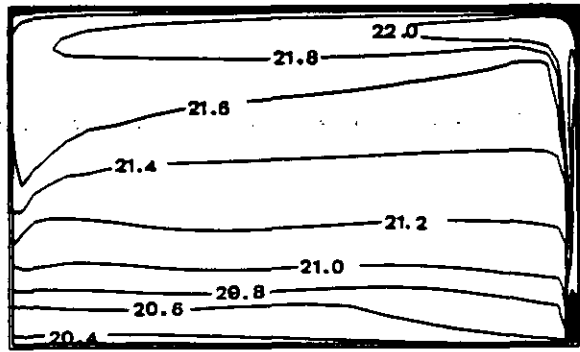


FIG 3.59b Case D1, D2, D3 : average velocity in occupied zone

TABLE 3.6 Test case D1, D2 and D3: occupied zone data

Ref.	M or S	Ave. Um	Ave. Ut	Ave. U*	Max Um	Max Temp	Ave. Temp	Min Temp
D2CH	S	0.021	0.010	0.025	0.084	20.57	20.29	20.07
D2Q001NL	S	0.022	0.006	0.024	0.087	21.17	20.58	20.11
D2FRG	S	0.024	0.016	0.030	0.049	21.30	20.61	20.10
D2CO1SF1	S	0.026	0.012	0.029	0.154	20.58	20.18	19.98
D21GER	S	0.029	0.008	0.031	0.085	21.56	20.85	20.23
D2CO2SF1	S	0.041	0.022	0.047	0.150	21.06	20.20	19.96
D2GER	S	0.062	0.036	0.074	0.213	20.28	20.10	19.93
D2M001NL	M	0.071	-	0.071	0.203	20.16	19.52	19.23

Ref.	M or S	Ave. Um	Ave. Ut	Ave. U*	Max Um	Max Temp	Ave. Temp	Min Temp
D1CH	S	0.017	0.009	0.020	0.074	20.54	20.28	20.08
D1Q001NL	S	0.020	0.005	0.021	0.081	20.89	20.40	20.06
D1FRG	S	0.022	0.014	0.028	0.046	21.10	20.52	20.10
D11GER	S	0.028	0.007	0.030	0.085	21.76	20.93	20.23
D1CO2SF1	S	0.036	0.020	0.042	0.127	20.66	20.15	19.89
D1GER	S	0.037	0.019	0.042	0.128	20.38	20.11	20.01

Ref.	M or S	Ave. Um	Ave. Ut	Ave. U*	Max Um	Max Temp	Ave. Temp	Min Temp
D3CH	S	0.019	0.008	0.021	0.085	20.76	20.38	20.09
D3Q001NL	S	0.024	0.006	0.025	0.090	21.57	20.84	20.21
D3FRG	S	0.028	0.018	0.035	0.059	21.60	20.83	20.10
D31GER	S	0.033	0.009	0.035	0.093	21.95	21.12	20.32
D3CO2SF1	S	0.047	0.026	0.055	0.165	20.71	20.23	19.88
D3GER	S	0.058	0.033	0.070	0.227	20.40	20.11	19.91

M= measured, S= simulated

Ave. Um= averaged velocity (speed) (m/s) in occupied zone.

Ave. Ut= averaged turbulent velocity (speed) (m/s) in occupied zone.

Ave. U*= averaged modified velocity (speed) (m/s) in occupied zone.

Temperatures (°C) refer to occupied zone.

Zonal models

Zonal model results have been generated by Inard and Buty [9] for comparison with measurements and CFD simulations. It is found for case D2 and for assumed constant heat transfer coefficients, that a single-zone model yields the same mean air temperature of 20.3°C as a five-zone model. However, a similar two-zone model gives an increase in mean temperature of about 0.6°C, whilst the assumption of variable convection coefficients in a five-zone model reduces the mean air temperature by approximately 0.6°C. The predicted temperature difference in the height varies from 0.4°C (five-zone, variable convection coefficients) to 1.2°C (two-zone, constant convection coefficients). The measured difference is about 0.5°C in case D2. Similar findings apply for cases D1 and D3.

Figure 3.60 shows computed air temperature profiles for case D2 and case D3 based on the various models.

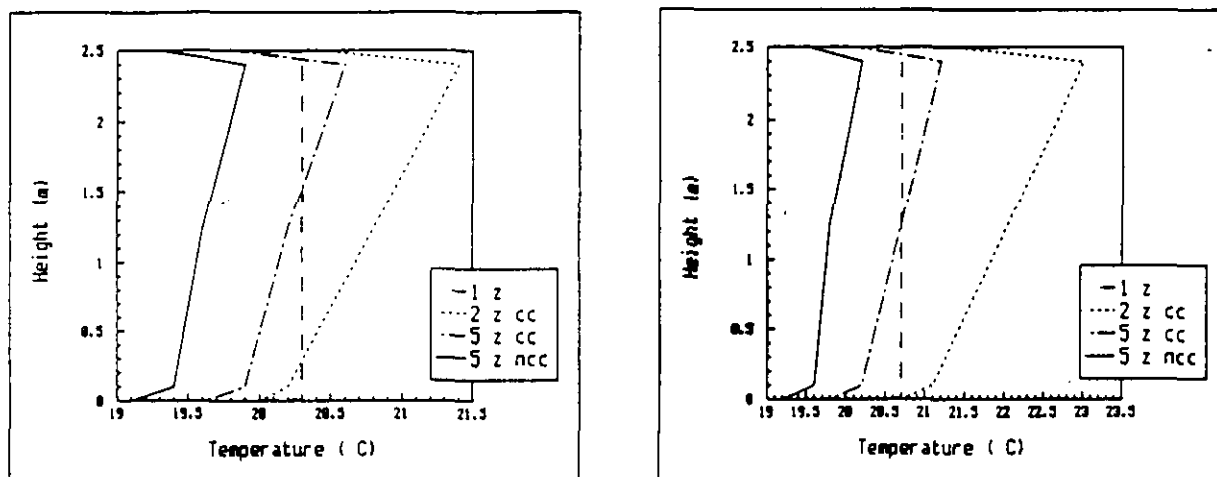


FIGURE 3.60 Case D2 (left) and case D3 (right): air temperature profiles based on zonal modelling by Inard et al.

Note: z = zone, cc = constant coefficients, ncc = variable coefficients

3.3.6 Test case F (forced convection with contaminant)

Measurements

Heiselberg [22] reported results of measurements of test cases F1, F2 and F3. Lemaire et al. [23] measured test case F2. Measurements were made on the centre-plane ($Z = 0.0\text{m}$) only and reported as dimensionless mean values with standard deviation. The concentration values are normalised relative to the mean concentration in the exhaust.

As expected, in all tests the minimum concentration occurred in the supply jet closest to the inlet opening (figure 3.61 to 3.64), although evidence exists of entrainment of the contaminant into the supply jet giving locally higher values at the ceiling. All tests were undertaken at nominally isothermal conditions with measured temperature differences of 0.2°C , 0.7°C and 0.3°C in the three tests by Heiselberg. The air change rate was 1.5 ach^{-1} as in case B1 suggesting that low Reynolds number effects would be present.

Test case F1 (Heiselberg): In this test, with a contaminant density of 0.8kg/m^3 , the maximum recorded concentration was 2.38 at $(X,Y) = (2.9\text{m}, 0.6\text{m})$, with a standard deviation of 0.42. The contaminant was being convected upwards and entrained into the supply jet. High values also occur beneath the source. Near to the geometric centre of the room (the release point) the maximum concentration was 2.07 at $(X,Y) = (2.2\text{m}, 1.3\text{m})$, with a standard deviation of 0.43. Measurement at distances $X = 2.2\text{m}$ and $X = 3.8\text{m}$ were repeated, with a significant variability found at $X = 2.2\text{m}$. For example, in the first measurements at $X = 2.2\text{m}$ the maximum value of 2.05 occurred at $Y = 0.9\text{m}$, where the corresponding value in the second measurements was 1.71. The standard deviations were 0.44 and 0.50, respectively. The maximum value in the second measurements was 2.07 at $Y = 1.3\text{m}$, where in the first set the value was 1.64. The standard deviations were 0.43 and 0.39 in the second and first measurements, respectively.

Test case F2 (Heiselberg). In this test, with a contaminant density of 1.2 kg/m^3 , the maximum recorded concentration was 2.65 (std. dev. 0.15) at $(X,Y) = (2.9\text{m}, 0.6\text{m})$. In the upper part of the room the contaminant is mixed with the recirculating room air, but high concentrations exist in the occupied zone. At $(X,Y) = (2.5\text{m}, 0.6\text{m})$ a near-maximum concentration of 2.62 (std. dev. 0.29) occurred. Measurements repeated at $X = 0.4\text{m}$ indicated a maximum concentration of 2.08 (std. dev. 0.10) and 1.45 (std. dev. 0.06) is the first and second tests, respectively, at $Y = 0.08\text{m}$ (height). Measurements repeated at $X = 2.2\text{m}$ showed maximum values of 2.25 (std. dev. 0.14) and 2.10 (std. dev. 0.29), respectively, at a height of $Y = 0.9\text{m}$.

Test case F2 (Lemaire et al.). Figure 3.64 shows mean concentrations of contaminant on the symmetry plane for test case F2 (Lemaire and Crommelin [70]). High concentrations were evident near the floor consistent with the measurements by Heiselberg. The concentrations near the source and the floor, however, are significantly greater.

Test case F3 (Heiselberg). In this test, with a contaminant density of 1.8kg/m^3 , the maximum concentration was 4.10 (std. dev. 0.14) at $(X,Y) = (1.9\text{m}, 0.6\text{m})$. The contaminant (of high density) streams towards the floor. The supply jet is not able to penetrate into the lower part of the room, and hence high concentrations develop. Measurements repeated at $X = 2.2\text{m}$ indicated maximum values of 3.63 (std. dev. 0.16) and 3.88 (std. dev. 0.23) at $Y = 0.3\text{m}$ height.

Simulations

Test case F2 (Lemaire). Lemaire [99] simulated test case F2 using the WISH3D code and standard $k-\epsilon$ model. A grid of $20 \times 22 \times 21$ (9240 cells) was used for the half room and a prescribed velocity inlet model near the inlet was imposed. The contaminant was modelled as a neutral source within the computational cell located in the middle of the room. The velocity field generated was visually similar to that from run B1P001NL by Lemaire and Elkhuizen [51]. As expected from a simulation, the maximum concentration occurred at the release point (figure 3.65) with contours of equal concentration showing the contaminant convected with the main flow. The minimum concentration occurred, of course, in the supply jet.

Test case F2 (Heikkinen et al.) The WISH3D code has also been used by Heikkinen and Piira [100] to model the transport of a neutral contaminant, in test case F2. A half-room has been simulated using a grid of $26 \times 26 \times 16$ (10816 cells) and a 'basic model' for the supply. Figure 3.66 shows contours of concentration normalised by reference to the value at the exhaust. The shape and values of the contours compare quite well with those from Lemaire. However, the flow field is slightly different such that there is a downward component to the convection of contaminant whereas Lemaire indicates an upward component superimposed on the otherwise horizontal flow towards the wall containing the diffuser.

Evaluation (test case F2)

The contaminant concentrations on the symmetry plane from both simulations are similar to those measured by Heiselberg although higher measured values than simulated were observable at low level. The maximum measured concentration appears at $(X,Y) = (2.9\text{m}, 0.6\text{m})$. This location differs from the release point at $(X,Y) = (2.1\text{m}, 1.2\text{m})$, indicating that the flow is not fully turbulent as is supposed in the simulations.

Figure 3.67 shows the measured average ventilation effectiveness, defined as the concentration in the exhaust divided by the average concentration in the room. According to Heiselberg the result is typical for ventilation systems with both supply and exhaust at ceiling level and a low air change rate. The simulations, however, yield an average ventilation effectiveness of 1.04 compared to the measured value around 0.8.

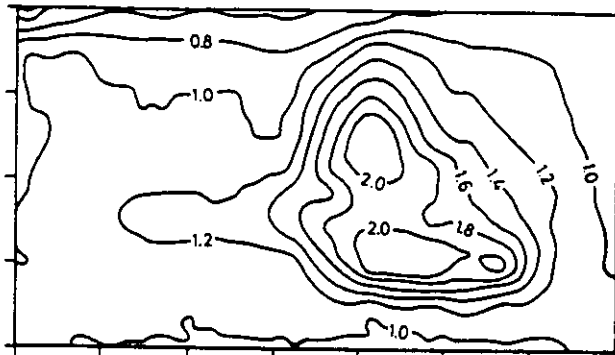


FIG 3.61 Case F1, measured, $z = 0.0\text{m}$, Helsingberg (density 0.8 kg/m^3)

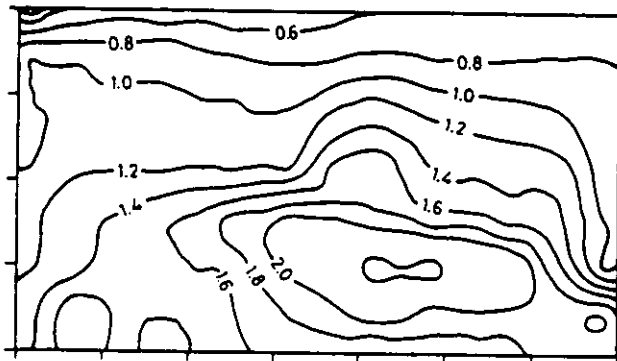


FIG 3.62 Case F2, measured, $z = 0.0\text{m}$, Helsingberg (density 1.2 kg/m^3)

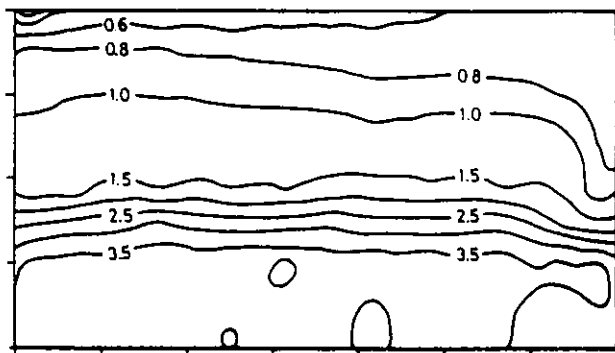


FIG 3.63 Case F3, measured, $z = 0.0\text{m}$, Helsingberg (density 1.8 kg/m^3)

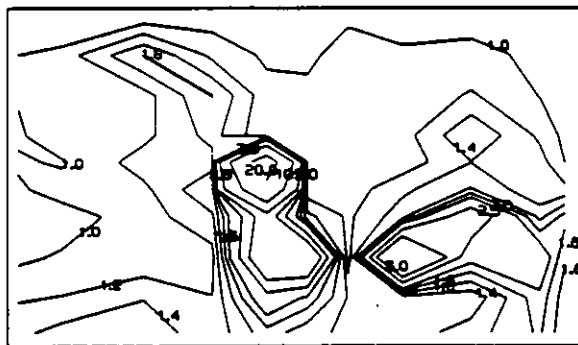


FIG 3.64 Case F2, measured, $z = 0.0\text{m}$, Lemaire (density 1.2 kg/m^3)

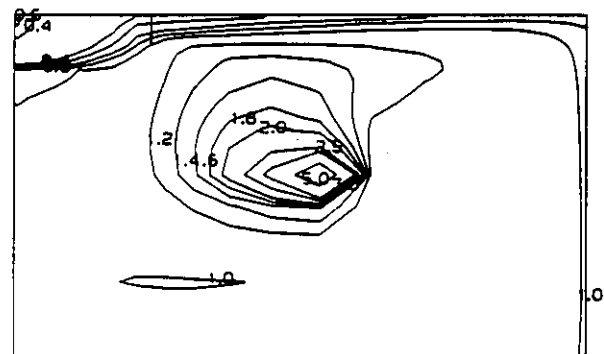


FIG 3.65 Case F2, simulated, $z = 0.0\text{m}$, Lemaire (density 1.2 kg/m^3)

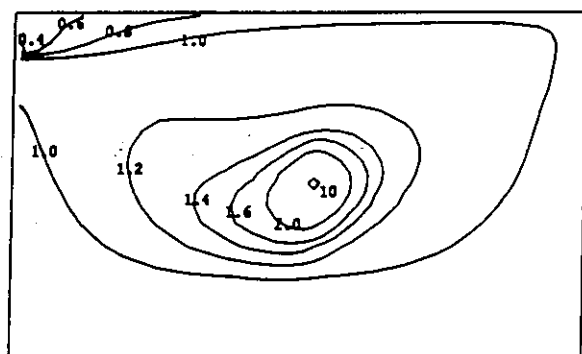


FIG 3.66 Case F2, simulated, $z = 0.0\text{m}$, Heikkinen (density 1.2 kg/m^3)

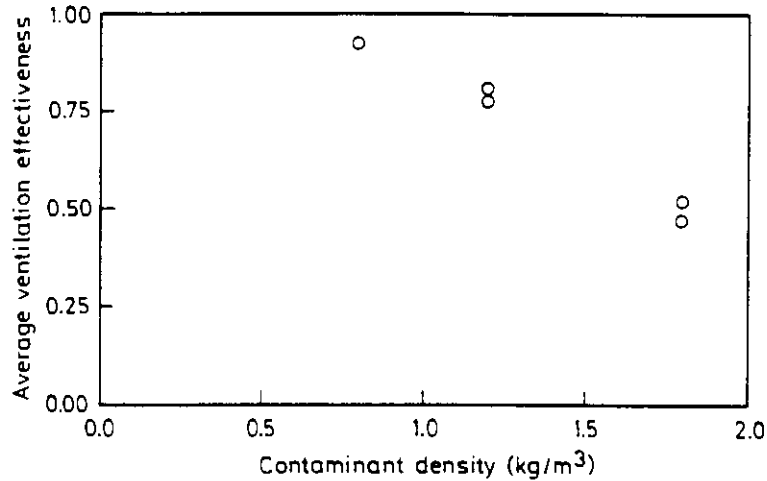


FIGURE 3.67 Case F1, F2 and F3, measured, Helselberg, average ventilation effectiveness.

3.3.7 Test case G (displacement ventilation)

Flow patterns and isotherms

Figure 3.68 (Lemaire et al. [20]) and figure 3.69 (Blomqvist [101]) show measured speed and temperature contours for case G1. The figures show the cold flow from the jet spreading over the floor. The contour of 0.1 m/s has the same shape and ends at about half way along the room. The contour corresponds with the measured isotherm of 22°C (Lemaire) or 21°C (Blomqvist). The simulations by Lemaire [102] (figure 3.70) show similar speed contours near the floor, and the isotherm corresponding with the 0.1m/s contour is 19.5°C. The measurements focused on the behaviour of the cold jet near the floor, in order to provide a dataset which can be used to evaluate analytical models which can predict this behaviour.

The simulations also show entrainment of air by the electric bulb. This, however, is not supported by the measurements. Probably too little measuring points were located near the bulb, or the assumed 25W convective heat source was in reality lower. The simulations were performed with a 'discrete transfer' radiation model coupled to the flow program. The temperature of the window was prescribed and the electric bulb was represented by a black cubed with edges of 100mm. A uniform heat flux through its sides was specified (75% radiation and 25% convection). The diffuser was represented by a box of 105mm x 210mm enveloping the cylindrical low velocity air diffuser. A horizontal and radial directed velocity of 0.262 m/s was prescribed on the sides of the box. Supply turbulence characteristics were: $Tu = 0.05$, $k_0 = 0.0095 \text{ J/kg}$ and $\epsilon_0 = 0.468 \text{ J/kg.s}$.

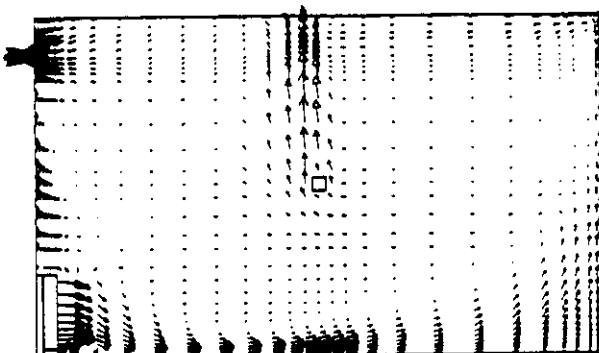


FIG 3.70a Case G1, simulated, $z = 0.0\text{m}$, flowpattern, Lemaire, G1P001NL

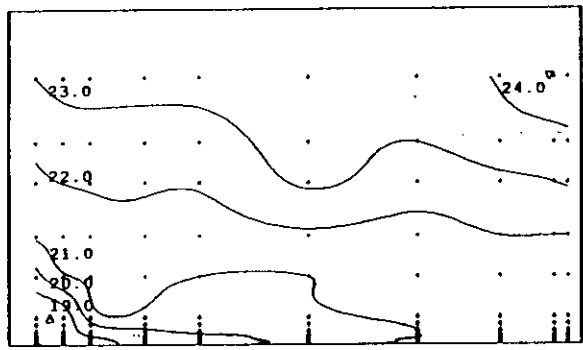
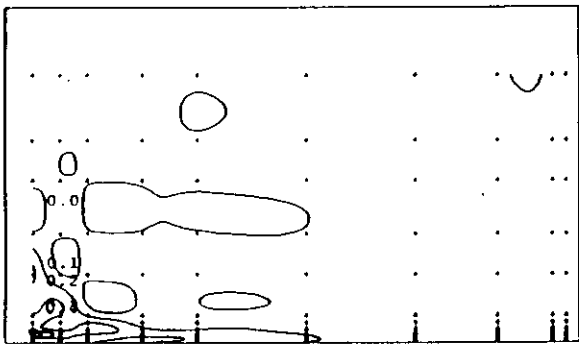


FIGURE 3.68 Case G1, measured, $z = 0.0$ m, iso-vels (left) and isotherms (right)
Blomqvist, G1T01SB

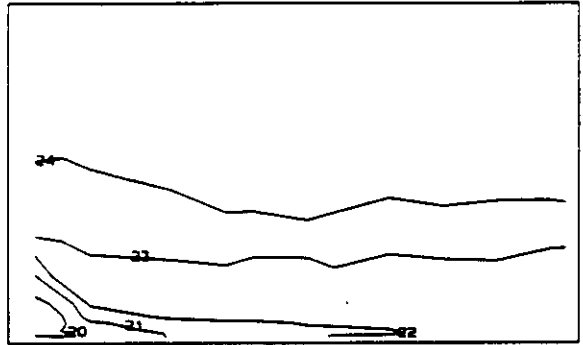
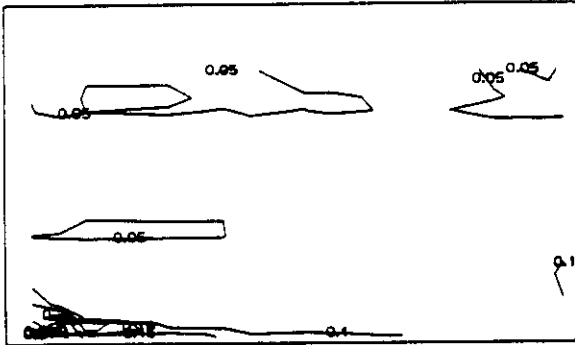


FIGURE 3.69 Case G1, measured, $z = 0.0$ m, iso-vels (left) and isotherms (right)
Lemaire, G1M001NL

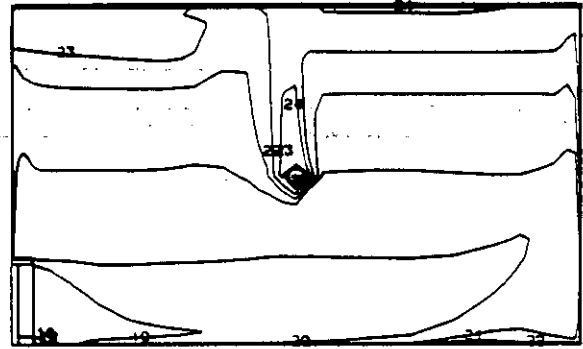
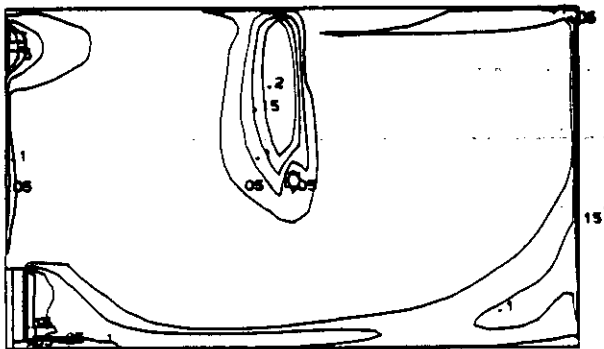


FIGURE 3.70b Case G1, simulated, $z = 0.0$ m, iso-vels (left) and isotherms (right)
Lemaire, G1P001NL

Key comfort parameters

Table 3.7 summarises the occupied zone velocity and temperature data. The maximum velocities in the occupied zone occur at $X = 0.6\text{m}$, where the cold flow enters the occupied zone. The data from Blomqvist show a deeper penetration of the cold flow into the occupied zone than the data from Lemaire. The lowest velocities occur in the simulations. More data will be available soon from measurements and predictions made by Nielsen [105].

TABLE 3.7 Test case G1: occupied zone data

Ref.	M or S	Ave. U_m	Ave. U_t	Ave. U^*	Max U_m	Max Temp	Ave. Temp	Min Temp
G1T01SIB	M				0.316	22.9		18.7
G1P001NL	S	0.046	0.009	0.047	0.151	22.6	20.1	18.3
G1M001NL	M	0.063	-	0.063	0.194	24.6	23.5	20.1

M= measured, S= simulated

Ave. U_m = averaged velocity (speed) (m/s) in occupied zone.

Ave. U_t = averaged turbulent velocity (speed) (m/s) in occupied zone.

Ave. U^* = averaged modified velocity (speed) (m/s) in occupied zone.

Temperatures ($^{\circ}\text{C}$) refer to occupied zone.

Graphs/profiles

The measured vertical temperature difference in the middle of the room was approx. 3.5°C for in both measurements and approx. 3.8°C in the simulation.

Contaminant transport

Figure 3.72 shows normalised concentration contours predicted by Lemaire. The average ventilation effectiveness in the whole room with source A and source B was 10:8 and 4.5 respectively. The ventilation effectiveness in the occupied zone was 17.0 (source A) and 34.5 (source B). Measured values will become available soon [105].

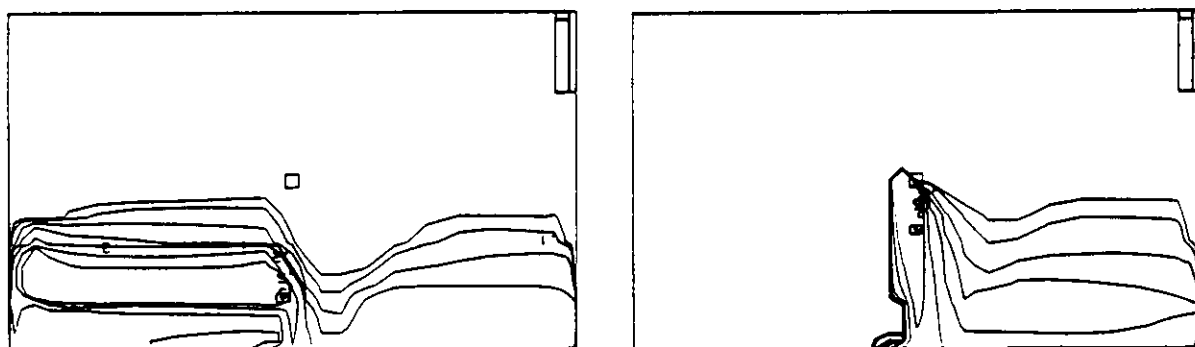


FIGURE 3.71 Case G1, simulated, $z = 0.0\text{ m}$, source A (left) and source B (right), Lemaire, G1P001NL, normalised concentration contours

3.4 Application of existing computational fluid dynamics models

3.4.1 Flow asymmetries

In almost all simulations a symmetry plane has been assumed, in order to save computing time. However, some evidence of flow asymmetries exists, from the experimental data.

In measurements of case E3, Fossdal [17] found that the jet deflected 150 to 200mm to one side of the symmetry plane. The reason for this was unknown although an inaccurate adjustment of the nozzles was suggested. Heikkinen [16] found less asymmetries in the jet region, but strong asymmetry near the floor. Skovgaard et al.[45] reported the measurement of asymmetric velocity profiles near the floor at an air change rate of 8 ach^{-1} (a slightly higher flow rate than case B3), despite the jet region being symmetric.

Fontaine et al [12] , computed asymmetric flow fields in the whole room for test case B2. The flow predicted with the 'basic model' was much more asymmetric than the flow predicted with the 'box method'. The fully converged results were confirmed by flow visualisations in the water scale model. It was suggested that the solutions of the flow equations are non unique and that the solution algorithms picked up one of the two asymmetric solutions. Imposing a symmetry condition $Z = 0$ leads to an averaging process.

3.4.2 Representation of boundary conditions at the supply opening: inlet models

Within the scope of Annex-20, a number of inlet models were investigated and in additional studies results were compared with measurements. Skovgaard et al.[43], Heikkinen [7], Ewert et al [24] and Fontaine et al [12] studied isothermal flow and Chen [8] non-isothermal flow. Tjelflaat[96] and Lemaire[44,93] used defined inlet models in the benchmarks only. The modelling is discussed in section 2.2.3.

Skovgaard et al.[43] concludes that in isothermal flow the 'prescribed velocity method' is the best choice compared with the basic model. In particular, if low Reynolds number effects are present, the model will incorporate these from the supply and from the resulting flow up to the border of the volume at a certain distance from the supply.

Heikkinen [7], (i.e. fig.3.33) suggests that a simple opening (basic model) can produce good results for regions remote from the initial jet development. The numerical diffusion in the initial section of the jet resembles the diffusion properties of the diffuser and helps to make better predictions. Numerical diffusion, however, is difficult to control. The prescribed velocity model and the momentum method were also studied and were found encouraging. Though the size of the opening used with the momentum method influences the results and with the particular specification used caused too much mixing in the initial development of the jet. Local grid refinement could be a way of allowing better modelling of the initial jet development.

Ewert et al. [24] simulated test case B2 in a room with slightly different dimensions (4.8m x 3.0m x 2.5m height). The basic model with k and ϵ from (2.3) and the box method were applied. Measured velocity-profiles (see section 3.3.3) and turbulence quantities (ϵ calculated in two different ways) were prescribed on the faces of the box. In addition k and ϵ from (2.3) were used, instead of measured values. It is concluded that the influence of the turbulence boundary condition is small compared with the influence of the box method versus the basic model. The basic model yields turbulent kinetic energies in the occupied zone two times larger than those resulting from the box method. The difference in these results significantly effects the PPD value (predicted percentage of dissatisfied) introduced by Fanger.

Fontaine et al [12] used the prescribed velocity model in test case B2 and found a fair agreement between their experimental results and numerical predictions. (See e.g. fig. 3.31). The required velocity profiles were computed with equation (2.6), instead of using measured data near the inlet, which proved to be inaccurate.

Chen [8], used the momentum method and simple rectangular slot models (case E2). The latter model with one (basic model), 12 and 84 slots. As an example figure 3.72 shows a comparison between measured and predicted velocities. It is concluded that the momentum method and the method using 84 simple rectangular slots predict air velocity and temperature distributions in the room similar to those from the experiments. The computing costs with the 84-slots method are extremely high. Hence in practice the momentum method is suggested to be used to simulate a complex diffuser.

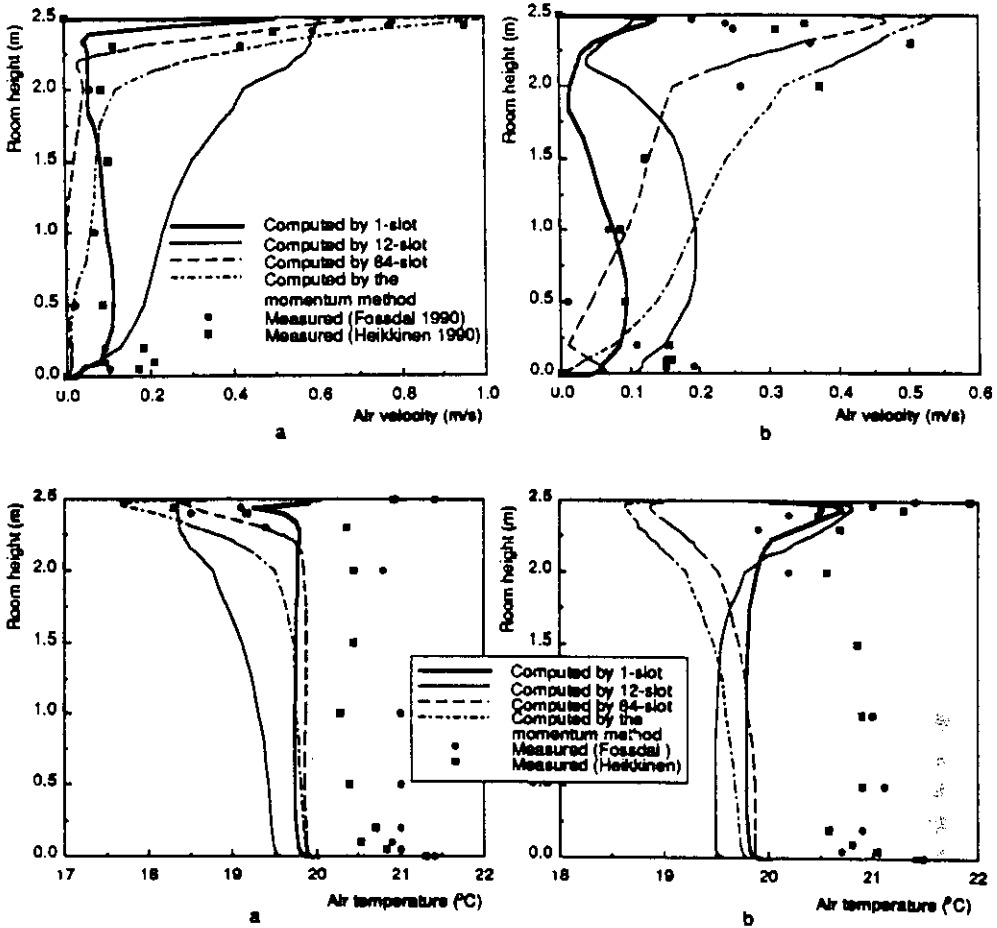


FIGURE 3.72 Test case E2: Measurements and computations with different inlet models, velocities and temperatures on $z = 0.0\text{m}$, (a) at $x = 1.4\text{m}$ and (b) at $x = 3.0\text{m}$. Chen [8].

Lemaire [93] found for test case E that it was easier to get a converged solution when using the basic inlet model than when prescribing the velocity on a plane a specified distance from the diffuser. The prescribed velocity method (with zero gravity), seems to underestimate the buoyant force near the inlet. For test cases B, Lemaire et al. [44] found that convergence was more difficult when using the basic inlet model, possibly due to large velocity gradients near the inlet. The use of the prescribed velocity model was recommended for the isothermal simulations.

Tjelflaat [96] modelled case E2 with a basic inlet model and with a porosity model. The latter comprised a porous opening equivalent to the diffuser dimensions to achieve the correct mass and momentum flux. It was found that the porosity model caused a high generation of turbulence energy leading to excessive diffusion of momentum and premature detaching of the jet.

3.4.3 Wall functions

Vogl and Renz [89,97] implemented the standard logarithmic wall functions for test cases B and E. The necessity, though, was that the first grid line should be in the turbulent regime. This meant that at the end of each simulation, checks had to be made and grid lines adjusted if necessary. For test cases D [48] the distance between the radiator and the wall was too small to meet this requirement. Here, the low Reynolds number model of Lam and Bremhorst [30], described by Chen [76] was used allowing (and requiring) grid lines to be located in the laminar sublayer.

For test cases D, Frst [49] used the temperature wall functions of Reynolds [103] to predict the heat flux from the radiator, but found fixing the heat transfer coefficient based on empirical data to be more realistic. In test cases E [42], it was also found that the same temperature wall functions used resulted in a poorer prediction of window heat transfer than was reported by Chen [98].

In test cases E, using a prescribed velocity inlet model, Lemaire [93] fixed the convective heat flux at the window - based on a surface temperature and an empirical convective heat transfer coefficient. It was argued that standard thermal wall functions predict surface heat transfer with insufficient accuracy. However, in further simulations of test case E2 with the basic inlet model, a prescribed surface temperature boundary condition was used. The simulations with a fixed convective heat flux resulted in boundary layers consistent with forced (not free) convection, and back-calculated window temperatures which were too low (case E1) or too high (case E3). In contrast, the simulations with the basic inlet model and fixed temperature indicated free convection at the window. Similarly, for test cases D, Lemaire [51] found that when using standard temperature wall functions the predicted convective heat transfer coefficients for the radiator were 50% of the empirical values and for the window were 75%.

The results confirm clearly that the logarithmic wall function is not suitable for computing free convection boundary layers, as already stated in e.g. [5]. The computed heat transfer coefficient depends on the distance of the first grid point to the wall. So, in fact the heat transfer coefficient is prescribed.

3.4.4 Turbulence models

Most participants have used the standard high-Reynolds number, buoyancy-extended k-epsilon turbulence model. Chen [76] used a low Reynolds number model from Lam and Bremhorst [30]. The low Reynolds number model used by Tjelflaat [91] did not include the buoyancy-extension terms to allow for the generation and suppression of turbulence energy due to temperature gradient.

In measurements, Skovgaard et al [6] found low Reynolds number effects occurring below air change rates of 3 to 4, equivalent to test conditions B1 and B2. The influence of the lower turbulence levels is to reduce the room velocities. Fontaine et al [12] also shows the presence of low Reynolds number effects in the water scale model (see fig. 3.27 and 3.28). Another indication are the differences between measured and predicted concentration profiles in case F2.

3.4.5 Difference scheme

The difference schemes used include Upwind (UDS), Hybrid (HDS), Power Law (PLDS) and QUICK.

Vogl and Renz [81] studied, in two-dimensional simulations based on case B2, the use of the PLDS and QUICK as implemented in FLUENT. Grids of 23x25 and 46x50 were used. Because of the jet projecting across the grid at an angle in the region of the inlet the predicted flow is expected to be influenced by numerical diffusion resulting in a smearing of the momentum and a reduced projection of the jet. The calculation with PLDS on the coarser grid indicates a broad jet. Using PLDS on the finer grid, the jet profile was similar to that generated using QUICK on the coarser grid. As expected the best results were obtained with QUICK on the finer grid. However, it was found that QUICK was less stable than PLDS and so needed greater under-relaxation and increased run-times.

A comparison was also made between PLDS and QUICK on test case E2 (on the same grid) [81]. Although an inspection of the velocity vector plots indicates some differences in the flow field in the occupied zone, table 3.5 suggests that averaged velocities, turbulence level and temperatures are similar in both cases. The run-time using QUICK was substantially longer.

Heikkinen and Piira [87] found that when using QUICK differencing rather than PLDS (in FLUENT 2.99), run-times increased by a factor of two. It was stated that the differencing scheme is particularly important in the initial jet development region where the jet is projecting at an angle across the grid. Here, the QUICK scheme is believed to generate more accurate results than the first-order schemes.

3.4.6 Grid refinement

A number of grid resolutions have been employed ranging from 18x17x12 (3672 cells) to 40x44x21 (36960 cells) for half-room simulations. Generally, it is expected that the finer the grid the more accurate becomes the solution, although clearly many other factors are important.

Lemaire [93], in test case E2, when using a standard thermal wall function found that refining a grid from 20x22x14 (6160 cells) to 30x33x21 (20790 cells) increased the heat gain through the window by 35%, whilst the main flow pattern, velocities and temperatures remained largely unchanged. The turbulent velocity, however, increased by 40%.

Lemaire et al. [44] for cases B, found that air velocities near the ceiling decreased with grid resolution possibly due to over-prediction of shear stress. Near the floor the velocities increased with increasing grid resolution. On the finer grid the turbulence energy was predicted to be almost twice the coarse grid values.

Heikkinen et al. [87] found that with the power law scheme the maximum velocity in the occupied zone for cases B increased with grid refinement, as the numerical diffusion in the jet region decreased. However, with the QUICK scheme the opposite occurred possibly due to the influence of the wall functions as the distance from the first grid node to the wall became smaller. Compared to measurements, almost all the computations over-predicted the maximum velocity in the occupied zone. The fine grid QUICK scheme results (22800 cells for the half room) appeared the most accurate, but were believed still not grid independent.

In two-dimensional simulations based on case B2, Vogl and Renz [81] used two grids, of 23x25 and 46x50 cells, and two differencing schemes. Predicted velocity profiles in the jet showed that some differences between the coarser and finer grid simulations. Grid independence could not be confirmed.

3.4.7 Computer resources

A wide range of computing platforms have been used from 386 PC's and engineering workstations up to CRAY X-MP.

Said [90,95] used a 33MHz 386/387 PC and has reported execution times of 225 CPU-hours for cases B2 and E2 using a mesh of 26496 cells. The code used, EXACT3, needed 21800 iterations to achieve convergence. EXACT3 uses an explicit and time-dependent formulation.

Chen [76], using PHOENICS on a CYBER 855 mainframe, recorded run times of 16 to 20 CPU-hours for each simulation of cases B on a mesh of 12180 cells. For each simulation of cases D [64], 18 to 27 CPU-hours and 2000 to 3000 iterations were required. A similar but slightly improved performance was found for test cases E [98], where 17 to 20 CPU-hours and 2000 iterations were needed. A combination of steady-state under-relaxation and false time step relaxation were used to procure convergence.

Using SIMULAR-AIR on a VAXstation 3200, Furst [41] recorded 30 to 40 CPU-hours of execution time and 1600 to 2200 iterations of time-dependent computation to achieve solutions for each condition of test cases B. The mesh sizes were 3672 to 4536 cells. For test cases D and E, execution times were typically 40 CPU-hours for 2300 to 2500 iterations [56,49]. In each run the simulation time period was 300s, and time steps of 0.02s (at the start of the simulation) and 0.2s were used.

Vogi and Renz [48,89,97] used FLUENT 2.99 on an 8Mbyte VAXstation 3200. They recorded 17 to 47 CPU-hours for 950 to 2650 iterations for each condition of test cases B, and 74 to 170 CPU-hours for 2700 to 6450 iterations for each condition of test cases D. For test cases E1 and E3, 59 CPU-hours and 2100 iterations each were needed. On test case E2, using QUICK differencing rather than the power law scheme caused the run-time to increase from 76 to 219 CPU-hours and the iteration count to increase from 2700 to 7300. The claim with QUICK differencing is that of greater numerical accuracy (on the same mesh) than can be achieved with first order schemes, although as reported, a decrease in stability of the calculation manifests. The mesh size for these computations was 9360 cells.

Lemaire [93], using WISH3D, reported run times of 16 CPU-hours on an IRIS-personal workstation for test cases E2 and E3. This corresponded to 8000 iterations. For test case E1 the run time was approximately doubled because of an oscillation of a flow separation point at the ceiling. On a coarse grid (6160 cells) using the basic inlet model the run-time for test case E2 was 5 CPU-hours for 5000 iterations. A fine grid (20790 cells) simulation was then started from linearly interpolated coarse grid results. A further 6000 iterations were necessary to achieve convergence, taking approximately 24 CPU-hours. For test cases D [26], solutions were reported as relatively easy to obtain, taking 12 CPU-hours for 5000 iterations

On test case B2, Heikkinen and Piira [87] reported execution times of 0.37, 0.52 and 2.22 CPU-hours on a CRAY X-MP for 6300, 7875 and 22800 cells, respectively. The iteration counts were 900, 1000 and 1470 for the three grids, where finer grid solutions require more iterations. The FLUENT 2.99 code implementing power law differencing was used. Using QUICK differencing, the run times increased to 0.86 CPU-hours for 6300 cells and 4.9 CPU-hours for 22800 cells.

Fontaine [86], using EOL3D on a SUN Sparc 1 recorded 33 CPU-hours for case B2. A total of 1785 iterations were performed on a grid of 29952 cells.

Lemaire [99] found that when calculating contaminant concentration, only a few CPU-minutes were needed on an IRIS workstation. The contaminant concentration field was obtained by post-processing previously computed velocity field data where the latter took 6000 iterations and 18

CPU-hours. A prescribed velocity inlet was modelled and the hybrid differencing scheme used.

Said [79] used a 3-D grid to model the essentially 2D test cases using a 37 x 34 x 15 (18870 cells) grid. For the isothermal simulation 8 CPU-hours (25000 iterations) were required on an IBM 3090 mainframe.

4. CONCLUSIONS AND RECOMMENDATIONS FOR FUTURE WORK

4.1 Application of simulation models as design tools

The work of IEA Annex 20, subtask 1 lead to the following conclusions, regarding the application of the simulation models as design tools.

- (1) CFD-simulations are useful when values of difficult-to-measure variables are needed in all points of the flow field.
- (2) CFD-simulations are useful to study the sensitivity of flow patterns to small changes of conditions (trends).
- (3) CFD-simulations are useful to predict air flow patterns for critical projects, i.e., when neither similar experience nor measured data exist (large spaces, unconventional ventilating systems, strong buoyancy effects).
- (4) Simplified methods are useful to estimate the throw of supply air jets, the maximum velocity in the occupied zone, or the thermal plume in a radiator-window configuration.
- (5) A catalogue of pre-calculated cases (section 2.3.3) is useful to get a quick overview of flow patterns that may develop in standard office rooms under various conditions.

In general, CFD-codes can make a valuable contribution to understanding air movement in spaces and can predict room air movement with sufficient realism to be of use to design practice. It is necessary, however, that CFD-codes are used with care and, most importantly, with the exercise of sound engineering judgement. The codes are difficult to use, time consuming and demanding in computer resources - many hours of computing are required even on relatively fast machines. Skill and experience are still required to get the best of the codes (section 3.4) and many technical problems exist, as identified during the project (section 4.3).

In spite of these difficulties, the subtask-1 work indicates that CFD-methods are now ready to be used as design tools. Initial use will be by specialists, but further developments of methods and improvements of the user-interface will lead to wide acceptance in the not-so-distant future.

Above conclusions are based on the evaluation of the benchmark exercises (Whittle [3]) and the discussions during the Annex-meetings (Moser [10]).

4.2 Performance of models in prediction of flow parameters

Two- and three-dimensional measurements and simulations have been performed under isothermal and buoyant conditions encompassing forced and free convection. CFD codes and zonal models have been used.

The task of comparing and evaluating the results of these benchmark exercises appeared to be an ambitious one. Difficulties existed, both associated with the computer predictions (section 4.1, 4.3) and in interpreting and rationalising real measurement data. For example: measured data sets differ internally and most of the predictions are made with some knowledge of previous measurements or simulations.

Nevertheless, the following general conclusions can be stated, concerning the performance of the models in prediction of flow parameters.

- (1) Almost all the *CFD models and modelling* approaches can predict the *Isothermal* air flow pattern and velocity decay with an acceptable degree of realism. In many cases the predicted occupied zone velocities are within a band indicating general compliance with expectation. However, in some cases velocities are under-predicted, but it is not clear for what reason. The *two-dimensional* test results indicated very good agreement for velocity decay and for the general trend of turbulence energy, although the latter was generally under-predicted. Small recirculation areas in the corners of the room were usually not predicted although their impact is believed small. In the one case where corner recirculation was reproduced a *low Reynolds number* model was used.
- (2) In *buoyant* flow, it has been shown that CFD models can predict flow pattern, velocity and temperature distribution, although with a reliability reduced from that demonstrated for isothermal flow. In the *two-dimensional* case the codes generated plausible and consistent results although no intermediate jet penetration length was found as suggested by measurement data. *Three-dimensional* computation, however indicated the existence of such intermediate length. It was hard to obtain converged and grid-independent results.
- (3) *Zonal models* have been shown capable of predicting with reasonable accuracy the temperature in a room heated by a radiator. The models appear simple and quick to use, though they are limited in range of application and provide no (or limited) information on flow velocities.

More detailed information on the findings of the benchmark exercises can be found in participants' individual reports referenced in this report.

4.3 Technical problems of CFD models

The benchmark exercises, clearly show the areas where technical problems of CFD-models exists. The areas as pointed out by Whittle [3] and in a slightly different formulation by Moser [1] are:

- (1) *Turbulence model at existing range of Reynolds numbers and near walls.*
No turbulence models other than the widely-used $k-\epsilon$ closure have been tested. Even so, a range of results is found for predictions of turbulence under similar conditions, particularly in buoyant flow. This can have implications for thermal comfort. Experts have agreed that so-called-low-Reynolds-number corrections are needed near walls and at low turbulence levels. Such a model has been used by some participants, and measurements have indicated this to be an important factor. Further and more detailed work is needed to evaluate this approach.
- (2) *Modelling of the supply jet characteristics.*
This proved to be particularly difficult in the Annex-20 test cases. A number of models (approaches) of the inlet have been used. It would be helpful if the manufacturers of air diffusers would publish some near field data (e.g. profiles in front of the device) with their technical specifications.
- (3) *Natural and mixed convection at cold or warm surfaces.*
Three methods of dealing with heat transfer have been tried: (1) to prescribe wall temperature and have the program compute the heat flux; (2) to prescribe wall temperature and empirical local heat transfer coefficients and (3) to estimate the local heat flux by empirical formulas and apply it in the simulation as a heat source (or sink)

over the surface. The first method is the most desirable one and needs thermal wall functions. Using these methods, temperature differences, in the occupied zone, from measurements and simulations were generally quite similar. But some simulations identified serious shortcomings in predicting surface convection coefficients. Differences in surface convection assumptions can radically change the flow pattern.

(4) *Number, size and type of computational grid.*

- All computations were done with cartesian grids, which have the disadvantage that grid refinements extend from wall to wall and into regions where a fine resolution is not needed (and cells with undesirable large aspect ratios may appear). "Local grid refinement" (e.g. to better model the initial jet development) or "boundary fitted coordinates" (e.g. for better representing of oblique-entry flows) can overcome these problems, but were not applied in this Annex.
- It was not explicitly proved that the numerical results were grid-independent. Accurate and robust convection discretisation to better model the recirculating flows appearing in HVAC can help to avoid grid-dependency.
- The method to compute only a half room under symmetrical boundary conditions, is not always valid. The benchmark exercises indicate that geometric symmetry may not result in flow symmetry (section 3.4.1). This should be investigated further.
- It should be recognised that two-dimensional flows are rare and that three-dimensional simulations may be needed to investigate characteristics of interest.

(5) *Numerical procedure to reach solution of system.*

- Convergence of flow fields with buoyancy effects in general is poor. Monitoring of convergence during the iteration process and adjustment of relaxation factors during the solution process is needed. Non-segregated methods combined with multigrid techniques, can provide faster convergence. These methods have not been tested in Annex-20 and should be investigated further.
- Experimental and numerical results suggest unsteady air motion under certain conditions at high Rayleigh number. However, this must still be verified. If in fact, steady solutions do not exist under some circumstances, time dependent simulation would be appropriate.

Information on some of these topics is also provided in chapter 2 of this report.

4.4 General conclusions

The work for Annex 20 has been done with great enthusiasm and the commitment of all participants to common goals made the project a success.

General conclusions regarding the performed work are (Moser [10]):

- (1) The experimental verification of proposed design methods has shown that complete *validation* is an impossible task. Experiments are never perfect and *all* potential applications of a method cannot be foreseen. Therefore, the performance of a design tool may only be *evaluated* for certain specific uses. Annex experience shows that independent, parallel experiments should be conducted if possible.
- (2) Attention has been focused on technical *problems*, which have been described and analyzed. Future progress is only possible by concentrating on these problems and not by ignoring them.

- (3) The technical results are in a form that can be implemented in practice, as well as in future projects.

Main project conclusions, regarding subtask 1 are (Moser [10]):

- (1) On the whole, project objectives have been met within the planned 42 project months. In some Research Items much more has been done than intended, in others emphasis has shifted a little and working objectives been reformulated. This is a consequence of a dynamic approach, where the direction of a new step is based on previous results. In some instances, the availability of staff and facilities had an influence.
- (2) The whole collaborative achievement amounts to more than the sum of individual national efforts. Some results would have been impossible without international cooperation, as for instance, the verification of a theory developed in one country by test data from another.
- (3) Cooperation with the IEA Air Infiltration and Ventilation Centre, AIVC, was excellent.
- (4) In a task-sharing Annex, such as this one, project leaders have no financial incentives to control productivity of participants. In spite of this, all participants acted responsibly and were well motivated to deliver promised work of high quality.

4.5 Recommendations for future work

It is recommended to work further at solving the technical problems indicated in section 4.3.

The exercise in undertaking measurements in similar test rooms and computations using different codes (and modelling assumptions) has provided substantial amounts of data and results which will continue to be of value in the future. More work could profitably be done in further evaluating the data and in undertaking additional simulations to extend the value of the work completed.

New proposals for IEA Energy Conservation-in-Buildings-and-Community-Systems projects, which will make use of the products of Annex 20 are: "Energy-Efficient Ventilation of Large Enclosures" and "Residential Ventilation Systems".

In general, international projects should have immediate impact on conservation of energy and environment (Moser [10]). Their results should be in a form easily implemented in engineering practice. On the other hand, such projects are ideally suited to study the physics of energy systems. Therefore, objectives should reflect a sound balance between fundamental and applied products.

REFERENCES

1. Nielsen P.V., "Air flow simulation techniques, -progress and trends", 10th AIVC Conference, Espoo, Finland, Sep. 25-28, 1989.
2. International Energy Agency, IEA, "Air flow patterns within buildings, -Annex XX of the IEA Implementing Agreement on Energy Conservation in Buildings and Community Systems.' Legal text with description of project objectives, means and responsibilities, etc., drafted by the IEA R&D staff, reviewed by the IEA Office of the legal Counsel, and adopted by the executive Committee. No.0633R/13.6.89.
3. Whittle G.E., "Evaluation of measured and computed test case results from Annex 20, Subtask 1", IEA Annex 20, Research Item 1.35, 12th AIVC Conference, Ottawa, Canada, Sep. 24-27, 1991.
4. Moser A., "Low Reynolds number effects in single room air flow", IEA Annex 20, Research Item 1.1, Working Report, ETH, Zürich, Switzerland, Nov. 1988.
5. Chen Q., Moser A., Huber A., "Prediction of buoyant, turbulent flow by a low-Reynolds-number k-epsilon model", ASHRAE Transactions, Vol. 96, Part 1, 1990. Paper AT-90-2-2(3366) of ASHRAE Atlanta Winter Meeting, Feb.1990.
6. Skovgaard M., Nielsen P.V., "Numerical investigation of low Reynolds number effects", IEA Annex 20, Research Item 1.1, 12th AIVC Conference, Ottawa, Canada, Sep. 24-27, 1991.
7. Heikkinen J., "Modelling of supply air terminal for room air flow simulation, IEA Annex 20, Research Item 1.24, 12th AIVC Conference, Ottawa, Canada, Sep. 24-27, 1991.
8. Chen Q., Moser A., "Simulation of multiple-nozzle diffuser", IEA Annex 20, Research Item 1.20, 12th AIVC Conference, Ottawa, Canada, Sep. 24-27, 1991.
9. Inard C., Buty D., "Simulation of Thermal Coupling Between a Radiator and a Room with Zonal Models", IEA Annex 20, Research Item 1.26, 12th AIVC Conference, Ottawa, Canada, Sep. 24-27, 1991.
10. Moser A., "The message of Annex 20: Air flow patterns within buildings", 12th AIVC Conference, Ottawa, Canada, Sep. 24-27, 1991.
11. Lemaire A.D., "Specification of test case D (free convection with radiator)", IEA Annex 20, Research Item 1.15, Working Report, TNO, Delft, The Netherlands, May 1989.
12. Fontaine J., Biolley F., Rapp R., Serieys J., "Ventilation Flow Analyses-Flow Visualization & LDA Measurements in Water Scale Models, Validation of Numerical Results", IEA Annex 20, Research Item 1.19 and 1.36, 12th AIVC Conference, Ottawa, Canada, Sep. 24-27, 1991.
13. Crommelin, R.D., Dubbeld M., "Modified anemometers for indoor climate research, Journal of Physics E; Scientific Instruments 1976; Volume 9, United Kingdom, 1976.
14. Blomqvist C., "Measurement of test case B (forced convection, isothermal)", IEA Annex 20, Research Item 1.16, Technical Report, NSIBR, Gavle, Sweden, March 1991.
15. Blomqvist C., "Measurement of test case E (mixed convection, summer cooling)", IEA Annex 20, Research Item 1.17, Technical Report, NSIBR, Gavle, Sweden, March 1991.
16. Heikkinen J., "Measurements of test cases B2, B3, E2 and E3 (isothermal and summer cooling cases)", IEA Annex 20, Research Item 1.16 and 1.17, Technical Report, Technical Research Centre, Espoo, Finland, May 1991.
17. Fossdal S., "Measurement of test case E (mixed convection, summer cooling)", IEA Annex 20, Research Item 1.17, Preliminary Report, NBRI, Oslo, Norway, June 1990.
18. Lemaire A.D., Crommelin R.D., "Measurement of test case B1 (forced convection, isothermal)", IEA Annex 20, Research Item 1.16, Technical Report, TNO, Delft, The Netherlands, Aug. 1991.
19. Lemaire A.D., Crommelin R.D., "Measurement of test case D (free convection with radiator)", IEA Annex 20, Research Item 1.18, Technical Report, TNO, Delft, The Netherlands, Aug. 1991.

20. Lemaire A.D., Crommelin R.D., "Measurement of test case G (displacement ventilation)", IEA Annex 20, Research Item 1.49, Technical Report, TNO, Delft, The Netherlands, Aug. 1991.
21. Heiselberg P., "Concentration Distributions in a Ventilated Room under Isothermal Conditions", IEA Annex 20, Research Item 1.32, 12th AIVC Conference, Ottawa, Canada, Sep. 24-27, 1991.
22. Heiselberg P., "Measurements of test case F (forced convection with contaminants)", IEA Annex 20, Research Item 1.32, Technical Report, The University of Aalborg, Aalborg, Denmark, Sep. 1991.
23. Lemaire A.D., Crommelin R.D., "Measurement of test case F2 (forced convection with contaminants)", IEA Annex 20, Research Item 1.32, Technical Report, TNO, Delft, The Netherlands, Aug. 1991.
24. Ewert M., Renz U., Vogel N., Zeller M., "Definition of the Flow Parameters at the Room Inlet Device - Measurements & Calculations", IEA Annex 20, Research Item 1.43, 12th AIVC Conference, Ottawa, Canada, Sep. 24-27, 1991.
25. Ewert M., Zeller M., "Turbulence Parameters at Supply Opening (Measurements)", IEA Annex 20, Research Item 1.43, RWTH, Aachen, Germany, March 1991.
26. Liddament M.W., "A review of building air flow simulation", IEA, Air Infiltration and Ventilation Centre, Technical Note AIVC TN 33, March 1991.
27. Said M.N., "Two and three-dimensional computer codes developed for applications other than room air flows", IEA Annex 20, Research Item 1.10, Working Report, IRC-NRC, Ottawa, Canada, Nov. 1988.
28. Baker A.J., Kelso R.M., "Computational fluid dynamics procedures applied to prediction of room air motion", Contract Technical Report, ASHRAE TR on 464-RP, Report CFDL/89-2, Dept. Engineering Science and Mechanics, University of Tennessee, Knoxville, USA, June 1989.
29. Launder B.E., Spalding D.B., "The numerical computation of turbulent flows", *Computer Methods in Applied Mechanics and Energy*, Vol.3, 00.269-289, 1974.
30. Lam C.K.G., Bremhorst K., "A modified form of the k- ϵ model for predicting wall turbulence", *ASME Transactions*, Vol 103, pp. 456-460, USA, Sep.1981.
31. Minkowics W.J., Sparrow E.M, Schneider G.E., Pletcher R.H., "Handbook of Numerical Heat Transfer", John Wiley & Sons Inc, New York, 1988.
32. Patankar, S.V., Spalding, D.B., "A Calculation Procedure for Heat Mass and Momentum Transfer in Three-Dimensional Parabolic Flows", *Int. J. Heat Mass Transfer*, Vol. 15, pp. 1787-1806, 1972
33. Rhie C.M., Chow W.L., "Numerical study of the turbulent flow past an airfoil with trailing edge separation, *AIAA J1*, 21, pp. 1527-1532, 1982.
34. Burns A.D., Wilkes N.S., Jones I.P., Kighley J.R., UKAEA Harwell, Computer Science and Systems, Division, June 1986.
35. Raithby G.D., "Some Recent Advances in Computational Fluid Dynamics", COBEM87-IX Congresso Brasileiro de Engenharia Mecanica, Florianapolis, SC, Dec 1987, pp. 33-38.
36. Thompson C.P., Leaf G.K., Vanka S.P., "Application of a multigrid method to a buoyancy induced flow problem", Argonne National Laboratory, USA, 1988.
37. Vanka S.P., Misegades K.P., "Vectorized multigrid fluid flow calculations on a Cray XMP/48", *Int. Journal for Numerical Methods in Fluids*, Vol 7, 1987, pp. 634-648.
38. Nielsen P.V., "Representation of boundary conditions at supply opening", IEA Annex 20, Research Item 1.11, Technical Report, The University of Aalborg, Aalborg, Denmark, Feb. 1989.
39. Lemaire A.D., "Modelling of boundary conditions near the radiator", IEA Annex 20, Research Item 1.12, Technical Report, TNO, Delft, The Netherlands, May 1989.
40. Skovgaard M., Lemaire, A.D. "Basic model", Technical Note on "Representation of boundary conditions at supply opening", IEA Annex 20, Research Item 1.11, TNO, Delft, The Netherlands, Feb 1990.

41. Fürst J., "Simulation of test case B (forced convection, isothermal)", IEA Annex 20, Research Item 1.19, Technical Report, ROM, Hamburg, Germany, March 1990.
42. Fürst J. "Simulation of test case E (mixed convection, summer cooling)", IEA Annex 20, Research Item 1.20, Technical Report, ROM, Hamburg, Germany, May 1990.
43. Skovgaard M, Nielsen P.V, "Modelling Complex Inlet Geometries in CFD-Applied to Air Flows in Ventilated Rooms", 12th AIVC Conference, Ottawa, Canada, Sep. 24-27, 1991.
44. Lemaire A.D., Elkhuizen P.A., "Simulation of test case B (forced convection, isothermal)", IEA Annex 20, Research Item 1.19, Technical Report, TNO, Delft, The Netherlands, Oct. 1990.
45. Skovgaard M, Hyltdgard C.E., Nielsen P.V., "High and Low Reynolds Number Measurements in a Room with an Impinging Jet, Roomvent'90, Oslo, Norway, 1990.
46. Lemaire A.D., "Modelling of boundary conditions near the radiator", IEA Annex 20, Research Item 1.12, Working Report, TNO, Delft, The Netherlands, May 1989.
47. Chen Q., "Simulation of test case D (free convection with radiator)", IEA Annex 20, Research Item 1.21, Technical Report, ETH, Zürich, Switzerland, Jan. 1990.
48. Vogl N. Renz U., "Simulation of test case D (free convection with radiator)", IEA Annex 20, Research Item 1.21, Technical Report, RWTH, Aachen, Germany, March 1991.
49. Fürst J, "Simulation of test case D (free convection with radiator)", IEA Annex 20, Research Item 1.21, Technical Report, ROM, Hamburg, Germany, May 1990.
50. Lemaire A.D., Technical Note on: "Specification of test case D (free convection with radiator)", IEA Annex 20, Research Item 1.15, TNO, Delft, The Netherlands, July 1990.
51. Lemaire A.D., "Simulation of test case D (free convection with radiator)", IEA Annex 20, Research Item 1.21, Technical Report, TNO, Delft, The Netherlands, March 1991.
52. Heikkinen J., Piira K., "Simulation of test case D (free convection with radiator)", IEA Annex 20, Research Item 1.21, Technical Report, Technical Research Centre, Espoo, Finland, Dec. 1990.
53. Nielsen P.V., "Models for the prediction of room air distribution", 12th AIVC Conference, Ottawa, Canada, Sep. 24-27, 1991.
54. Grititlin M., "Zuluftverteilung in Räumen", Luft- und Kältetechnik, nr 5, 1970.
55. Hestad T., "A Design Method for Diffusers Based on Theory, Full-Scale Experiments and Practical Experience" (in Norwegian), Tekniska Meddelanded nr. 83, Institutionen för Uppvärmnings- och Ventilationsteknik, KTH, Stockholm, 1975.
56. Inard C., Buty D., "Simulation of testcase D with zonal models; approach with simplified models", IEA Annex 20, Research Item 1.26, Technical Report, INSA, Lyon, France, March 1991.
57. Inard C., "Contribution à l'étude du couplage thermique entre une source de chaleur et un local", Thèse Doct.: INSA, Lyon, 1988
58. Howarth A.T., "Temperature distribution and air movements in rooms heated with a convective heat source", PhD Doct.: University of Manchester, 1980
59. Chen Q., Moser A., Suter P., "A Data Base for Assessing Indoor Air Flow, Air Quality, and Draught Risk - Volume One: The fundamentals", IEA Annex 20, Research Item 1.23, Draft not for sale, ETH, Zürich, Switzerland, Jan. 1991.
60. Chen Q., Moser A., Suter P., "A Data Base for Assessing Indoor Air Flow, Air Quality, and Draught Risk - Volume Two: An Atlas for a Displacement and a Well-Mixed Ventilation System", Research Item 1.23, Draft not for sale, ETH, Zürich, Switzerland, Jan. 1991.
61. Chen Q., "Simplification Principle and Data Base Structure", IEA Annex-20, Research Item 1.23, Technical Report, ETH, Zürich, Switzerland, Nov. 1989.
62. Moser A., "Simplified model with data base of computed flow fields: Interpolation in data base of pre-calculated cases", IEA Annex 20, Report Research Item 1.23, Technical Report, ETH, Zürich, Oct. 1989.
63. Whittle G.E., "Evaluation of cases B, D, E, F and 2D", IEA Annex 20, Research Item 1.22, 1.35, 1.40", Technical Report, Arup Research and Development, London, United Kingdom, Sep. 1991.

64. Heikkinen, J., "Specification of testcase B (forced convection, isothermal)", IEA Annex 20, Research Item 1.13, Technical Report, Technical Research Centre, Espoo, Finland, April 1989.
65. Heikkinen, J., "Specification of testcase E (mixed convection, summer cooling)", IEA Annex 20, Research Item 1.14, Technical Report, Technical Research Centre, Espoo, Finland, April 1989.
66. Skaaret, E., "Specification of testcase F (forced convection, isothermal with contaminants)", IEA Annex 20, Research Item 1.31, NBRI, Oslo, Norway, Oct 1989.
67. Lemaire A.D., "Specification of test case G (displacement ventilation)", IEA Annex 20, Research Item 1.47, Technical Report, TNO, Delft, The Netherlands, May 1991.
68. Nielsen, P V., "Specification of a two-dimensional test case", IEA Annex 20, Research Item 1.45, Technical Report, The University of Aalborg, Aalborg, Denmark, Nov. 1990.
69. Nielsen, P V., Restivo, A., Whitelaw, J H., "The velocity characteristics of ventilated rooms", Journal of Fluids Engineering, Vol 100, pp 291-298, Sep. 1978.
70. Ruddick K., Whittle G.E., "A proposed specification for a common data format", IEA Annex 20, Research Item 1.22, Working Report, Arup Research and Development, London, United Kingdom, May 1989.
71. Nielsen P.V., "Selection of Air Terminal device", IEA Annex 20, Research Item 1.02, Technical Report, The University of Aalborg, Aalborg, Denmark, Dec.1988.
72. Ruddick K., Whittle G.E., "A proposed specification for a common data format", IEA Annex 20, Research Item 1.22, Working Report, Arup Research and Development, London, United Kingdom, May 1989.
73. Whittle, G E., Ruddick, K., "A proposal for data processing, evaluation and presentation", IEA Annex 20, Research Item 1.22, Technical Report, Arup Research and Development, London, United Kingdom, Nov. 1989.
74. ASHRAE Standard 55-1981. "Thermal Environmental Conditions for Human Occupancy", 1981.
75. ISO Standard 7730. "Moderate thermal environments - determination of the PMV and PPD indices and specification of the conditions for thermal comfort", 1985.
76. Chen Q., "Simulation of test case B (forced convection, isothermal)", IEA Annex 20, Research Item 1.21, Technical Report, ETH, Zürich, Switzerland, Jan. 1990.
77. Skovgaard M., Nielsen P.V., "Simulation of simple test case, Case 2D1", The University of Aalborg, Aalborg, Denmark, Sep. 1991.
78. Jones W.P., Launder B.E., "The prediction of Laminarisation with a two-equation model of turbulence", Int. Journal of Heat and Mass Transfer, Vol 15, pp 301-314, 1972.
79. Said N., "Simulation of a Two-Dimensional Benchmark Test case", IEA Annex 20, Research Item 1.46, Technical Report, NRC, Ottawa, Canada, March 1991.
80. Chen Q., "Simulation of simple test cases (2D1, 2D2)", IEA Annex 20, Research Item 1.46, Technical Report, ETH, Zürich, Switzerland, March 1991.
81. Vogl N., Renz U., "Simulation of Simple Two-Dimensional Test Cases: 2D1, 2D2", IEA Annex 20, Research Item 1.46, Technical Report, RWTH, Aachen, Germany, March 1991.
82. Lemaire A.D., "Testrooms, identical testrooms", IEA Annex 20, Research Item 1.3, Technical Report, TNO, Delft, The Netherlands, May 1989.
83. Lemaire A.D., "Simulation of simple test cases 2D1, 2D2", IEA Annex 20, Research Item 1.46, Technical Report, TNO, Delft, The Netherlands, May 1991.
84. Heikkinen, "Simulation of simple (two-dimensional) test cases", IEA Annex 20, Research Item 1.46, Technical Report, Technical Research Centre, Espoo, Finland, May 1991.
85. Skovgaard M., Nielsen P.V., "Simulation of test case B (forced convection, isothermal)", IEA Annex 20, Research Item 1.19, Technical Report, The University of Aalborg, Aalborg, Denmark, Sep. 1991.
86. Fontaine J., "Simulation of test case B (forced convection, isothermal)", IEA Annex 20, Research Item 1.19, Technical Report, INRS, Vandoeuvre, France.

87. Heikkinen J. Piira K., "Simulation of test case B (forced convection, isothermal)", IEA Annex 20, Research Item 1.19, Technical Report, Technical Research Centre, Espoo, Finland, Dec.1990.
88. Johanson S.H., Davidson L., Olson E., "Simulation of test case B (forced convection, isothermal)", IEA Annex20, Research Item 1.19, Technical Report, Chalmers University of Technology, Gotenburg, Sweden, June 1991.
89. Vogl N., Renz U., "Simulation of test case B (forced convection, isothermal)", IEA Annex 20, Research Item 1.19, Technical report, RWTH, Aachen, Germany, March 1991.
90. Said N., "Simulation of test case B2 (forced convection, isothermal)", IEA Annex 20, Research Item 1.19, Technical report, NRC, Ottawa, Canada, Feb. 1991.
91. Tjelflaat P.O., Frydenlund F., "Simulation of test case B (forced convection, isothermal)", IEA Annex 20, Research Item 1.19, Technical report, SINTEF, Trondheim, Norway, June 1990.
92. Sandberg M., Blomqvist C., Matson M., "Turbulence Characteristics in Rooms Ventilated with a High Velocity Jet", IEA Annex 20, Research Item 1.34, 12th AIVC Conference, Ottawa, Canada, Sep. 24-27, 1991.
93. Lemaire A.D., "Simulation of test case E (mixed convection summer cooling)", IEA Annex 20, Research Item 1.20, Technical report, TNO, Delft, The Netherlands, March 1991.
94. Johanson S.H., Davidson L., Olson E., "Simulation of test case E (mixed convection summer cooling)", IEA Annex 20, Research Item 1.20, Technical report, June 1991.
95. Said N., "Simulation of test case E2 (mixed convection summer cooling)", IEA Annex 20, Research Item 1.20, Technical report, NRC, Ottawa, Canada, Feb. 1991.
96. Tjelflaat P.O., Frydenlund F., "Simulation of test case E (mixed convection summer cooling)", IEA Annex 20, Research Item 1.20, Technical report, SINTEF, Trondheim, Norway, June 1990.
97. Vogl N., Renz U., "Simulation of test case E (mixed convection summer cooling)", IEA Annex 20, Research Item 1.20, Technical report, RWTH Aachen, Germany, March 1991.
98. Chen Q., "Simulation of test case E (mixed convection summer cooling)", IEA Annex 20, Research Item 1.20, Technical report, ETH Zürich, Switzerland, Jan. 1990.
99. Lemaire, A D., "Simulation of test case F2 (forced convection, isothermal with contaminants)", IEA Annex 20, Research Item 1.33, Technical report, TNO, Delft, The Netherlands, July 1991.
100. Heikkinen, J., Piira, K., "Simulation of test case F (isothermal with contaminants)", IEA Annex 20, Research Item 1.33, Technical report, Technical Research Centre, Espoo, Finland, Dec. 1990.
101. Blomqvist et al, "Measurement of test case G (displacement ventilation)", IEA Annex 20, Research Item 1.49, Technical Report, NSIBR, Gavle, Sweden
102. Lemaire, "Simulation of test case G (displacement ventilation)", IEA Annex 20, Research Item 1.48, Technical Report, TNO, Delft, The Netherlands, Aug. 1991.
103. Reynolds, A.J. "Turbulent flow in engineering", Wiley, London, 1974
104. ISO standard 7726, "Thermal environments - Instruments and methods for measuring physical quantities", 1985.
105. Nielsen P.V., "Velocity distribution in rooms with displacement ventilation and low level diffusers", IEA Annex 20, Research Item 1.50, Technical Report, The University of Aalborg, Aalborg, Denmark, Sep. 1992.

APPENDIX A : List of contributing investigators, organisations and countries

INVESTIGATOR	ORGANISATION	COUNTRY	ABBR.
Dr. N. Said	NRC, Ottawa	CANADA	C
Dr. A. Moser/ Dr. Q. Chen	ETH, Zurich	SWITZERLAND	CH
Prof. Dr. P. Nielsen/ Mr. M. Skovgaard	Univ. of Aalborg	DENMARK	DK
Dr. P. Heiselberg/ Dipl.Ing. J. Heikkinen	VTT, Espoo	FINLAND	SF
Dr.-Ing. J. Fürst	ROM, Hamburg	GERMANY	D1
Prof.Dr.-Ing. U. Renz/ Prof.Dr. M. Zeller/ Dipl.Ing. M. Ewert	RWTH, Aachen	GERMANY	D2
Dr. N. Vogl Dr. C. Inard/ Dr. F. Allard	INSA, Lyon	FRANCE	F1
Ing. D. Buty	CSTB, Marne la Vallee	FRANCE	F2
Dr. F. Biolley/ Dr. J. Fontaine	INRS, Vandoeuvre	FRANCE	F2
Ing. P. Oliaro	Politecnico di Torino	ITALY	I
Ir. A.D. Lemaire	TNO, Delft	NETHERLANDS	NL
Dr.Ing. S. Fossdal/ Dr. E. Skaaret	NBRI, Oslo	NORWAY	N1
Dr. P. Tjelflaat Prof. E. Olsson/ Dr. L. Davidson/ Mr. S.H. Johanson	SINTEF, Trondheim Chalmers Univ., Goteborg	NORWAY SWEDEN	N2 S1
Dipl.Ing. C. Blomqvist/ Dr. Sandberg	NSIBR, Gavle	SWEDEN	S2
Dr. M. W. Liddament	AIVC, Coventry	UNITED KINGDOM	UK
Dr. G.E. Whittle/ Mr. K. Ruddick	Ove Arup, London	UNITED KINGDOM	UK

APPENDIX B : Names and addresses of participating organisations

National Research Council of Canada, NRC - IRC
Institute for Research in Constructions
Montreal Road, M-24
Ottawa K1A 0R6, Canada

University of Aalborg
Department of Building Technology and Structural Engineering
Sohngaardsholmsvej 57
DK-9000 Aalborg, Denmark

VTT, Technical Research Centre of Finland
Laboratory of Heating and Ventilation
P.O. Box 206
SF-02151 Espoo, Finland

Service Génie Energétique et Climatique, C.S.T.B.
Champs-sur-Marne
B.P. no. 2, Cedex 2
F-77421 Marne-la-Vallee, France

INRS, Institut National de Recherche et de Sécurité
Centre de Recherche
Ave. de Bourgogne, B.P. 27
F-54501 Vandoeuvre Cedex, France

INSA de Lyon
Centre de Thermique, Bât. 307
20 Avenue Albert Einstein
F-69621 Villeurbanne Cedex, France

Lehrstuhl für Wärmeübertragung und Klimatechnik
RWTH Aachen
Eilfschornsteinstr. 18
D-5100 Aachen, Germany

Rud. Otto Meyer
Zentralbereich, Systementwicklung
ROM-Zentrale, Tilsiterstr. 162
D-2000 Hamburg 70, Germany

Dip. di Energetica
Politecnico di Torino
Corso Duca degli Abruzzi, 24
I-10129 Torino, Italy

TNO Building and Construction Research
Department of Indoor Environment, Building Physics and Systems
P.O. Box 29
2600 AA Delft, The Netherlands

The Norwegian Building Research Institute
Forskningsveien 3B
P.O. Box 123, Blindern
N-3014 Oslo 3, Norway

Department of Heating and Ventilating
University of Trondheim
N-7034 Trondheim - NTH, Norway

The National Swedish Institute for Building Research
Box 785
S-801 29 Gävle, Sweden

Chalmers University of Technology
Department of Thermo- and Fluid Dynamics
S-41296 Gothenburg, Sweden

Institute für Energietechnik ML
Lab. für Energiesysteme
ETH - Zentrum
CH-8092 Zürich, Switzerland

Air Infiltration and Ventilation Centre
Barclays Venture Centre,
Sir Williams Lyons Road
Coventry CV4 7EZ, United Kingdom

Ove Arup & Partners
Arup Research & Development
13 Fitzroy Street
London W1P 6BQ, United Kingdom

ecbcs bookshop

ANN 20 1993: 1